TAMPERE UNIVERSITY OF TECHNOLOGY

OSSI NIEMIMÄKI

IMPROVED QUASI 3D MODELLING AND SIMULATION OF AXIAL FLUX MACHINES

Master of Science Thesis

Examiner: Professor Stefan Kurz
Examiner and subject approved
at the meeting of Faculty of Computing and Electrical Engineering Council on 11 January 2012

TIIVISTELMÄ

TAMPEREEN TEKNILLINEN YLIOPISTO
Sähkötekniikan koulutusohjelma
OSSI NIEMIMÄKI: Aksiaalivuokoneen mallinnus ja simulointi parannetulla kvasi-3D -menetelmällä
Diplomityö, 122 sivua, 9 liitesivua
Syyskuu 2012
Pääaine: Sähköfysiikka
Tarkastaja: professori Stefan Kurz
Avainsanat: Sähkömagneettinen mallintaminen, laskennallinen sähkömagnetiikka, aksiaalivuokone, kvasi-3D, dimension tiputus, sovellettu differentiaaligeometria

Kestomagnetoidut aksiaalivuokoneet ovat yleistyneet viime vuosikymmenien aikana. Vaikka aksiaalivuokoneiden perusrakenne on ollut tiedossa jo 1800-luvulta lähtien, on niiden sähkömagneettinen suunnitelu vielä kehitysvaiheessa. Eräs ehdotetuista suunnittelumenetelmistä on niin sanottu kvasi-3D -menetelmä, jossa koneen kolmiulotteinen geometria siivutetaan erillisiksi kaksiulotteisiksi pinnoiksi. Tällä siivutuksella pyritään yksinkertaistamaan koneen sähkömagneettista mallintamista.
Moderni sähkömagneettinen mallintaminen ei ole mahdollista ilman vahvaa matemaattista pohjaa. Tässä opinnäytetyössä kvasi-3D -menetelmää käsitellään muodollisesti ja matemaattisella kurinalaisuudella. Aksiaalivuokoneille luonnollinen kolmiulotteinen sähkömagneettinen kenttätehtävä kirjoitetaan differentiaaligeometrian kielellä ja edelleen hajotetaan joukoksi (2+1)-ulotteisia tehtäviä käyttäen hyväksi niin sanottua havainnoija-rakennetta. Kvasi-3D -menetelmän taustalla olevan dimension tiputuksen mahdollistavat oletukset nostetaan esille ja niiden käyttöperusteita selvennetään. Dimension tiputuksesta seuraavat kaksiulotteiset tehtävät sovitetaan edelleen laskentamalleiksi, ja nämä mallit toteutetaan kaupallisella ohjelmistolla. Laskentatuloksia verrataan jo teollisessa käytössä olevan malliin.
Näemme, että muodollinen lähestymistapa vahventaa mallinnusmenelmän teoreettista pohjaa, tehden siitä tarkemman ja luotettavamman. Jo käytössä olevien laskentamallien epätarkkuudet tulevat lisäksi selvemmin esille kun niitä verrataan teoriasta johdettujen mallien tuloksiin.

ABSTRACT

TAMPERE UNIVERSITY OF TECHNOLOGY
Master's Degree Programme in Electrical Engineering
OSSI NIEMIMÄKI: Improved Quasi 3D Modelling and Simulation of Axial Flux Machines
Master of Science Thesis, 122 pages, 9 Appendix pages
September 2012
Major: Electromagnetism
Examiner: Professor Stefan Kurz
Keywords: Electromagnetic modelling, computational electromagnetics, axial flux machines, quasi 3D, dimensional reduction, applied differential geometry

Permanent magnet axial flux machines have become to enjoy increasingly widespread usage during the past two decades. While the basic type of axial flux machines has been known for over a century, the electromagnetic design of these machines is still in its development. Several design methods have been proposed; one of them being the so-called quasi 3D method, in which the inherently 3D machine geometry is sliced into separate 2D surfaces in order to simplify the modelling of the electromagnetic behaviour of the machine.

In modern electromagnetic modelling, solid mathematical framework is crucial. In this thesis, the quasi 3D method is given a formal and mathematically rigorous treatment. The 3D electromagnetic field problem concerning axial flux machines is formulated using the tools of differential geometry, and geometrically decomposed to a set of (2+1)D problems with the aid of an observer structure. The assumptions leading to the dimensional reduction underlying the quasi 3D method are pointed out, and their justification is discussed. Following the dimensional reduction, the resulting 2D problems are reformulated to models suitable for computation, and these models are then implemented with a commercial software and compared to an already existing industry-used model.

The formal approach is shown to make the modelling method more accurate and reliable, as the theoretical foundation is strengthened. Furthermore, the implementation of the derived models clarifies the effect of the prevailing inaccuracies in the already existing models.

PREFACE

The thesis you hold in your hands or glance at on the computer screen is a result of the collaboration between KONE Corporation and the research unit of Electromagnetics at TUT. This document is distilled from over a year of work,[1] countless cups of coffee and innumerable hours of Tom Waits. Financial support from KONE is gratefully acknowledged.

I wish to thank the people from both parties involved: Jussi Huppunen, Tuukka Korhonen, Andrej Burakov and Eero Keskinen from KONE, and Stefan Kurz and Lauri Kettunen from TUT. This work would be nowhere near what it is without Stefan's excellent supervision and quite substantial help. I am grateful for Lauri, Timo Tarhasaari, Saku Suuriniemi and Antti Stenvall from TUT for their aid in building an intuition for the electromagnetic theory and an understanding of the mathematical nuances involved. Lasse Söderlund and Maija-Liisa Paasonen deserve credit for helping with all the practical issues I might have had at hand. Hails to the rest of the Electromagnetics crew for the unique work atmosphere and weird coffee break conversations.

I am much obliged to my parents, brothers and sisters for supporting me through these years and just for being there. I tip my hat to Arto Hiltunen for being such a great comrade through all these years of study at TUT. I owe you a pint, mate!

This thesis deals with mathematical modelling and its engineering motivated applications. While these are significant and interesting topics, they fall short in providing to what makes life truly worthy. *The single most important thing in the world is Love.* From the Heart of my Being, I greet and thank all those beautiful souls who have helped me to understand this. May your days be long and filled with *eudaimonia.*

Gobi Desert Canoe Club Blues Bar, Tampere, 9 August 2012

Ossi Niemimäki

[1] 'I love deadlines. I love the whooshing noise they make as they go by.' – Douglas Adams

CONTENTS

SYMBOLS AND ABBREVIATIONS

Abbreviations

AFM	Axial flux machine
BVP	Boundary value problem
FEA	Finite element analysis
PDE	Partial differential equation
RFM	Radial flux machine

Symbols

$\mathcal{A}$	atlas
$\vec{A}$	magnetic vector potential
A	magnetic potential, one-form
a	point in a manifold
A^u	component of $\vec{A}$ w.r.t. coordinate u
A_u	component of A w.r.t. coordinate u
$\vec{B}$	magnetic flux density, vector field
B	magnetic flux, two-form
b	point in a manifold
B^u	component of $\vec{B}$ w.r.t. coordinate u
H^u	component of $\vec{H}$ w.r.t. coordinate u
$\operatorname{cod}()$	codomain
$\mathcal{C}_p/\sim$	equivalence classes of smooth curves through a point p
$\mathcal{C}_p$	set of smooth curves through a point p
curl	rotor operator
c	smooth curve (also a scalar function)
C^k	set of k times differentiable functions
$\det f$	determinant of a matrix f
$\operatorname{diag}(x_1, \ldots, x_n)$	diagonal matrix with elements $x_1, \ldots, x_n$
D	metric
div	divergence operator
d	exterior derivative
$\mathrm{d}x_i$	basis vector for a cotangent space
$\hat{\mathrm{d}}$	horizontal exterior derivative
$\mathcal{D}$	differentiable structure
$\partial\mathcal{M}$	boundary of a manifold $\mathcal{M}$
∂_t	differentiation w.r.t. t
∂_{x_i}	basis vector for a tangent space
$\vec{D}$	electric flux density, vector field
D	electric flux, two-form

$\vec{E}$	electric field intensity, vector field
$\vec{e}_u$	normalized vector field w.r.t. coordinate u
E	electric field, one-form
f^*	pullback of a mapping f
f_*, df	pushforward, or differential of a mapping f
f	mapping
F_r	axial force density on a cylindrical slice with radius r
grad	gradient operator
$g_{x_1 \cdots x_n}$	component representation of a metric tensor g under the coordinates $\{x_i\}$
g, g_p	metric tensor (at a point p)
G	metric tensor matrix
$\mathcal{H}^1$	first cohomology group
$\vec{H}$	magnetic field intensity, vector field
H	magnetic field, one-form
h	mapping
h_z	differential of a mapping h w.r.t. coordinate z
$\mathcal{I}$	index set
j	extension operator (also an index)
$\vec{J}$	current density, vector field
$\vec{J}_c$	circuit (source) current density, vector field
$\vec{J}_e$	eddy current density, vector field
$\vec{J}_m$	magnetization (source) current density, vector field
J	current, two-form
J^u	component of $\vec{J}$ w.r.t. coordinate u
J_c	circuit (source) current, two-form
J_e	eddy current, two-form
J_m	magnetization (source) current, two-form
J_u	component of J w.r.t. coordinate u
J_{tot}	total current, two-form
$\hat{K}$	surface current amplitude
ker ()	kernel of a function
K	surface current
ℓ	length of a curve
$\mathcal{L}$	Lie derivative
$\{\mathcal{L}_i\}$	leaves of a foliation
$\mathcal{M}, (\mathcal{M}, \mathcal{D})$	differentiable manifold
$\vec{M}$	remanence flux density, vector field
M	remanence flux, two-form

M^u	component of $\vec{M}$ w.r.t. coordinate u
M_u	component of M w.r.t. coordinate u
$\mathcal{N}$	(sub)manifold
$\mathcal{O}_r$	radial observer
$\mathcal{O}_\varphi$	angular observer
$\{\mathcal{O}_p\}$	family of tangent space orientations at a point p
P	splitting w.r.t. an observer
p	point in a manifold
$\mathbb{R}^n$	real coordinate space
$\mathcal{R}$	residual
R	radius
r	radial coordinate
$\mathcal{S}$	(sub)manifold
span ()	vector span
${}^*T^k_{\mathcal{M}}$	k-cotangent bundle
${}^*T^k_p\mathcal{M}$	k-cotangent space
$\left(\vec{t},\tau\right),\left(\vec{t},\mathrm{d}s\right)$	(holonomic) observer structure
$T_{\mathcal{M}}$	tangent bundle of a manifold $\mathcal{M}$
$T_p\mathcal{M}$	tangent space of a manifold $\mathcal{M}$ at a point p
T	torque
T_r	torque density on a cylindrical slice with radius r
(u_i)	vector space basis
P_r	density of dissipated power on a cylindrical slice with radius r
U	set
u	tangent vector
(v_i)	vector space basis
${}^*V$	covector space
$\vec{v}$	vector field
vol	volume form
V	set (also a vector space)
v	tangent vector
$\mathcal{X}_{\mathcal{M}}$	space of vector fields on a manifold $\mathcal{M}$
X	set
x	variable
y	variable
z	variable
α	variable
ϵ	permittivity
η_s	norm of a observer-related one-form $\mathrm{d}s$

ε	variable
Γ	a generator of a homology group (also a curve)
γ	flow on a manifold, a smooth curve
ι	contraction operator
λ	conformal factor
μ	permeability
ν	reluctivity
Ω	(manifold) domain
ω, ω_p	differential form (at a point p), covector
χ_{cyl}	cylindrical chart
χ_{rot}	rotational chart
χ_{tr}	translational chart
ϕ	scalar potential, zero-form
Ψ	mapping defining a motion
$\psi, (U, \psi)$	coordinate chart (also a scalar potential)
Φ	angle
φ	angular coordinate
ρ	radial coordinate, (also electric charge (density), three-form (density function))
σ	conductivity (also a permutation)
ς	coordinate chart
θ	angular coordinate
ϑ	differential form
ζ	differential form
Δ_{ij}^{α}	Laplace-like second order scalar differential operator w.r.t. coordinates i, j and material operator α
$\sim$	equivalence relation
$\flat$	flat operator
$(\cdot)_{\parallel}$	horizontal component of a form
$\hat{\star}$	horizontal Hodge operator
$\star$	Hodge operator
$(\cdot)^{-1}$	inverse operator
$\langle \cdot, \cdot \rangle$	vector space inner product
$\|\cdot\|$	vector space norm
$\oplus$	direct sum of vector spaces
$\sharp$	sharp operator
$\tilde{(\cdot)}$	horizontal operators on radial planes
$(\cdot)_{\perp}$	transversal component of a form
$\wedge$	exterior product

1. INTRODUCTION

Electrical machines have been studied and manufactured since the beginning of the 19th century, leading to the current state in which one finds them virtually everywhere. Various types of machinery have been developed for different purposes; of these, a type called permanent magnet axial flux machines offers a suitable solution to applications which pose restrictions on the axial length of the machine. An example of such an application would be elevator drives, which set the motivation for the present research.

In the modern engineering design of electrical machines, proper *mathematical modelling* and numerical simulations are imperative. A well-founded mathematical model should be accurate enough to describe all the essential properties of the design problem at hand. Numerical simulations should not only be accurate but also efficient. There is a trade-off between accuracy and efficiency which motivates the search for better modelling tools.

Various axial flux machine configurations can be modelled with analytical methods, but due to their simplicity, the use of such methods is generally limited to the initial stages of the design. The standard numerical approach is the finite element analysis (FEA). A complete 3D FEA would be ideal, but long computation times tend to make this approach impractical. This has resulted in the widespread use of a 2D analysis on the average radius of the machine core; however, the obtained solutions do not reflect the inherently 3D characteristics of the machine. To compensate for this flaw, a method called *quasi 3D* has been proposed: this approach combines several 2D models in order to describe the overall electromagnetic behaviour of the machine.

The quasi 3D computation relies, as do all 2D modelling schemes, on the symmetry of the posed electromagnetic boundary value problem (BVP): symmetry allows the *dimensional reduction* of the BVP. A general theory for dimensional reduction in electromagnetic field problems was established in [1] using the language of differential geometry. However, no rigorous attempt has yet been made to base the quasi 3D method on this theory.

The focus of this study is to present a formal treatment of the quasi 3D modelling method. In addition, we present different approaches to setting up the resulting separate 2D problems with a generic FEA software. When the theoretical background

is properly set, we can evaluate the procedure with a computational implementation based on existing machine models.

Since the quasi 3D method is already in industrial use, the ultimate goal of this thesis would be visible improvement of the existing method. We will see that the formal approach makes the modelling procedure more accurate and less sensitive to errors arising from *ad hoc* assumptions. The results of the implementation show that there are tangible issues in the current method, which can be remedied by a proper treatment of the theoretical foundation.

The document is structured as follows: In Chapter 2, we introduce the mathematical background for the electromagnetic field theory; namely, the differential geometric tools for modelling electromagnetic fields. Chapter 3 introduces axial flux machines in detail and recaps the state-of-the-art research on the modelling methods, as well as lays the foundation for the general electromagnetic problem setting of the machines. The mathematical tools needed for the dimensional reduction in the quasi 3D method are presented in Chapter 4, while Chapter 5 encompasses a detailed treatment of the quasi 3D method specifically in the axial flux machine setting. In Chapter 6, we define 2D models suitable for computation. These models are then tested and compared against an already existing model in Chapter 7.

A note on the style of the document

Some remarks on the style of this document may be in order. Mathematical definitions are shadowed with a grey background to distinguish them from the text body. All equations, propositions and definitions are numbered with respect to the section numbering, which should make them easy to find by given references.

Accompanying more complex mathematical structures, there is often a brief intuitive explanation. These paragraphs are formatted under the heading 'intuition' and they end with a diamond sign $\diamond$ as shown here:

Intuition This paragraph emphasizes the intuitive viewpoint to the previously defined mathematical structure. $\diamond$

Within these paragraphs, we aim to explain the mathematical structures on a more intuitive level. The aim is to justify for the abstract tools we are defining—thus, while we need the rigorous formalism in order to work out the right mathematical tools for our purposes, this formal manner of writing may often obscure rather than clarify the picture of what we are actually about to model. Hence the dual approach, and we hope that we have managed to do sufficiently well in both ways.

2. MATHEMATICAL BACKGROUND

In the standard expositions of the electromagnetic field theory, the dominating choice for the mathematical framework is that of the classical vector calculus. While this approach has its benefits, the tools of vector calculus are often unsuitable for treatments involving detailed analysis of the *geometry* of electromagnetic problems. Since the solution methods we intend to study rely thoroughly on the analysis of the problem geometry, we see it preferable to work within a different setting.

The purpose of this chapter is to provide sufficient mathematical tools for geometric representation of the electromagnetic field problems. We aim to define all the necessary mathematical structure needed to formulate Maxwell's equations; this manifests as a crash course on differential geometry. Differentiable manifolds are introduced as a generalized model for the problem domain, and the electromagnetic field entities are modelled with differential forms. Metric properties are defined in detail, and the equivalence of problems posed in differing geometries is discussed. We aim to do this in a *structural manner*, so that the greater framework is built piece-by-piece from smaller objects called mathematical structures.

However, before plunging into mathematical details, let us briefly look for motivation behind such abstractions.

2.1 Motivation for the abstraction

As per Wikipedia [2],

> **abstraction** is the thought process wherein ideas are distanced from objects.

Thus, instead of looking at specific instances, the process of abstraction aims for an idea or a set of ideas that coherently describes all the necessary properties of all the conceivable instances: this leads to the model of the phenomenon under consideration.[1] This is the standard procedure of physics, and all science: to work out logically valid models that can be used to explain and predict phenomena regardless of the instances. Hence the same theory of electromagnetism, for example, can be used in various situations, no matter how much they seem to diverge from each other.

[1] What is deemed *necessary* in each case is left to the modeller to decide.

Mathematics, being a formalized tool of logic, is the primary weapon in the fields of physics and engineering to tackle the problem of suitable modelling language. With mathematical logic, physical models can be made rigorous enough to allow theoretical analysis and powerful computation tools for the ease of engineers and physicists alike. Key concept is that of a structure, which refers to high-level abstractions and their relationships.

In mathematics, structures are defined by a collection of premises called *axioms*. These axioms are the gateway to all the related results of mathematical research: To employ a particular structure, all one needs to do is to make sure that the axioms of the structure are satisfied. Then, all the resulting theory needs no further verification, as it depends solely on the axioms.

More specifically, a structure refers to additional mathematical objects—such as operations—on a set such that the added objects somehow relate to the set or its elements.[2] We define a **set** by the property of *belonging* or *membership*:

An object x belongs to the set X if x satisfies the predicate p.

Thus the set X can be identified with the predicate p that defines if any given object x belongs to the set or not, that is, if the statement $p(x)$ evaluates as *true* or *false*. The predicate is subject to the *axioms of the set theory*, which means that the set itself can be seen as a structure, being perhaps the most primitive one. As a further instance of a *structure on a set*, we take the group structure:

Definition 2.1.1. A **group** (X, f) is a pair consisting of a set X and a binary operation

$$f : X \times X \to X$$

governed by the following axioms:

(1) $f(f(a,b),c) = f(a,f(b,c))$ for all $a,b,c \in X$ (associativity),

(2) there exists an element $e \in X$ such that $f(a,e) = f(e,a) = a$ for all $a \in X$ (identity element),

(3) for all $a \in X$, there exists an element $a' \in X$ such that $f(a,a') = f(a',a) = e$ (inverse element).

As such, the group structure is rather abstract. A **model** is an *interpretation of the axioms* of the structure: interpreting the operation f in the definition of the group structure as an addition of integers, that is,

$$f(a,b) := a + b, \quad a,b \in \mathbb{Z},$$

[2] Or subsets, especially the *power set* (the collection of all subsets, including the set itself).

we have created a model for the addition of integers using the group structure. Hence, the act of **modelling** is the choice of abstract structures (the toolbox) and an interpretation of their meaning by axioms (assignment of each tool to a certain task). Regardless of the interpretation, all the results arising from the mathematical research on the chosen structures can be utilized if the axioms are fulfilled.[3]

There are then two levels of abstraction: the higher level of mathematics, wherein structures are studied as themselves, and the lower level of applications, wherein structures are given meaning through models. It is the lower level abstraction that governs most part of this thesis, and our aim is to work out the necessary modelling structures from scratch to aid us in the initially engineering motivated problem. We do this for the following reasons:

(1) Structures give access to all the relevant results of the mathematics guaranteed to work by the axiomatic foundation.

(2) Structural approach helps to differentiate between the necessary and the unnecessary components of the model, which tend to depend on initial assumptions.

  (2.1) This division may help to spot particular problems related to particular modelling decisions.

  (2.2) The unnecessary parts of the model can naturally be left out to clarify the modelling situation.

(3) High level of abstraction makes it easier to work out tools that generalize easily.

(4) Generalized theory may bring in novel approaches to the modelling process by offering connections to seemingly unrelated fields.

(5) Level of eloquence that comes with the more sophisticated mathematics.

While the last point may be more of a day dream of a poetically inclined mathematician,[3] the posed arguments should offer enough motivation to work for higher abstractions.

In our particular case, it is deemed worthwhile to generalize the notion of geometry further than that of Euclidean spaces, and to detach the electromagnetic field theory from the widely used vector calculus. The classical vector calculus makes a complicated structure in that it is inherently tied to (some) metric and relies on the three-dimensionality of the underlying space. Furthermore, in the standard expositions things are often made even worse by introducing the theory with respect to a chosen coordinate system—as if the structures themselves somehow depended on

[3] cf. [4].

the choice of coordinates. For one working with a generalized geometric approach in mind, the metric and the choice of coordinate system should be easily mutable.

In differential geometry, the structure of metric is posed separately: indeed, it is possible to formulate Maxwell's equations without any reference to the metric, let alone choosing any particular coordinates. These coordinate and metric independent equations read:

$$\begin{aligned} \mathrm{d}E &= -\partial_t B, & \mathrm{d}H &= J + \partial_t D, \\ \mathrm{d}D &= \rho, & \mathrm{d}B &= 0, \end{aligned} \tag{2.1.1}$$

where field entities H and E are *one-forms*, flux entities B, D and J are *two-forms* and the charge entity ρ is a *three-form*. Note the single differential operator d called the *exterior derivative*, sufficient for all field differentiation. Aside the Maxwell model of Equations (2.1.1), we have constitutive equations

$$\begin{aligned} B &= \star_\mu H, & D &= \star_\epsilon E, \\ J &= \star_\sigma E, \end{aligned} \tag{2.1.2}$$

where the *Hodge operator* $\star$ maps one-forms into two-forms.

As a comparison, the corresponding vector calculus exposition of the Maxwell's equations is usually given as

$$\begin{aligned} \operatorname{curl} \vec{E} &= -\partial_t \vec{B}, & \operatorname{curl} \vec{H} &= \vec{J} + \partial_t \vec{D}, \\ \operatorname{div} \vec{D} &= \rho, & \operatorname{div} \vec{B} &= 0. \end{aligned}$$

The vector calculus approach does not differentiate between the field entities as they are all, the charge density ρ notwithstanding, vector fields; and instead of a single differential operator, we have at least two.[4] Moreover, the definitions of these operators depend on the underlying metric, being also inherently three-dimensional.

A major part of this chapter aims to lay a proper basis for the expressions in Equations (2.1.1) and (2.1.2). However, while we give exact mathematical definitions, we do not strive to be overly formal. As a consequence, all proofs are omitted. What we deem to be equally important is the *intuitive* picture of the structures. Mathematical rigour is employed as a tool for building the objective, but informal explanations are given equal or perhaps even greater amount of care.

[4] In fact, *three*, when one considers scalar potential formulations such as $\vec{E} = -\operatorname{grad} \phi$. More on potentials in Chapter 3.

2.2 Basic geometric structure

We begin the construction of the necessary mathematical structures by defining the *ambient space* in which electromagnetic field theory can be posed. More specifically, we generalize the notion of Euclidean spaces to differentiable manifolds. While the manifold structure is more abstract than that of a Euclidean space, it makes easy to generalize the theory to almost arbitrary geometries.

The field entities living on the manifolds are introduced as differential forms. Forms on a manifold yield geometrically defined fields that are completely coordinate- and metric-free. The forms are also equipped with the structure of the exterior algebra, which gives powerful computation tools.

2.2.1 Manifolds

An n-dimensional manifold is a geometric domain which is globally arbitrarily shaped but locally resembles a real coordinate space $\mathbb{R}^n$. The **real coordinate space** $\mathbb{R}^n$ is defined as the set of all n-tuples of real numbers:

$$\mathbb{R}^n = \{(x_1, \ldots, x_n) \mid x_i \in \mathbb{R}\},$$

where n is a positive integer; the space $\mathbb{R}^n$ is an n-dimensional vector, or linear space. The local resemblance of the manifold to this linear space is achieved by defining the manifold as a pair consisting of a set of points and a set of mappings such that each point of the manifold has a neighbourhood isomorphic to an open subset of the real coordinate space.

Formally, we define a differentiable, or smooth, manifold as follows [5, p. 3]:

Definition 2.2.1. A pair $(\mathcal{M}, \mathcal{D})$ is an **n-dimensional differentiable manifold**, if

(1) $\mathcal{M}$ is a second countable Hausdorff space,

(2) $\mathcal{D}$ is a differentiable n-dimensional atlas (a differentiable structure) on $\mathcal{M}$.

The Hausdorff property guarantees unique limits for converging sequences, which is crucial when defining calculus. Second countability axiom ensures that the space can be metrized, that is, we can always define a metric—a distance measuring function—for such a space in a way that it is compatible with the topology of the space. Metric plays an important role in electromagnetic modelling, as we shall see. However, these details can very well be passed over in silence for now; hence, we skip the definitions and refer to [6] and [7] for a proper treatment. For us, it suffices that the set $\mathcal{M}$ is a set of points that constitute a topological space. Let us then focus on the differentiable structure.

An atlas is a combination of charts on the set $\mathcal{M}$ [5, p. 1]:

Definition 2.2.2. Let $\mathcal{M}$ be a topological space. An **n-dimensional chart** on $\mathcal{M}$ is a homeomorphism

$$\psi : U \subset \mathcal{M} \to V \subset \mathbb{R}^n,$$

where U is an open subset of the domain $\mathcal{M}$, and V an open subset of an n-dimensional real coordinate space. The open subset U is called the **chart domain**, denoted by $\mathrm{dom}\,(\psi)$. A chart ψ is then a shorthand notation for a pair

$$\psi := (U, \psi)\,.$$

If there exists an n-dimensional chart for all points in the domain $\mathcal{M}$, the **dimension** of $\mathcal{M}$ is said to be n.

For each point in its domain, a chart yields an n-tuple of real numbers called the **coordinates under the chart**. For this reason, charts are often also called by the name **coordinate chart**.

Defining multiple charts over one space $\mathcal{M}$ raises a question if they could be combined. This is achieved with transition mappings [5, p. 2]:

Definition 2.2.3. Let (U_1, ψ_1) and (U_2, ψ_2) be two n-dimensional charts on a topological space. A **transition mapping**, or a **change-of-charts** from ψ_1 to ψ_2 is a homeomorphism

$$\psi_2 \circ \psi_1^{-1} : \psi_1\,(U_1 \cap U_2) \to \psi_2\,(U_1 \cap U_2)\,.$$

The transition mappings give us a way to 'travel' from one subdomain to another—if we have an overlap of two open subsets of the domain wherein two different charts are defined, we can use the transition mapping between the charts to 'leap' from one subdomain to another. Transition mappings, being homeomorphisms, are themselves obviously continuous. Furthermore, two charts ψ_1 and ψ_2 on a topological space are **C^k-compatible** if their transition mapping is k times differentiable, where k is a positive integer. A collection of C^k-compatible charts over the whole domain gives rise to an atlas [5, pp. 2–3]:

Definition 2.2.4. An **atlas** $\mathcal{A}$ on the topological space $\mathcal{M}$ is the collection of charts $\{(U_i, \psi_i)\}_{i \in \mathcal{I}}$, the set $\mathcal{I}$ being an index set, such that

(1) $\bigcup_{i \in \mathcal{I}} U_i$ covers the space $\mathcal{M}$,

(2) The charts ψ_i and ψ_j are C^k-compatible for all $i, j \in \mathcal{I}$.

An atlas is called **k-differentiable** if $k > 0$ and, in particular, a **differentiable structure** when k is arbitrarily large.

Thus, an n-dimensional differentiable manifold $(\mathcal{M}, \mathcal{D})$, or $\mathcal{M}$ for short, constitutes of two things: firstly, of the space of points of the manifold; secondly, of a collection of mappings that pairs the neighbourhood of any point with an n-tuple of coordinates in a real coordinate space, such that the mappings can be combined in a differentiable manner.

Intuition The manifold structure makes the underlying space **locally linear**. Every point in the domain can be mapped into a real coordinate space, which is to say that we can *represent the domain as a collection of linear spaces*. Thus the names chart and atlas: charts function like maps, giving a simple local representation of one part of the selected area in the world, and with a suitable combination of such local representations for different parts, we can characterize the whole area. The transition mappings guarantee that this act of combining the maps works out smoothly. Differentiable structure then ensures that we can define differentiable functions on the manifold.

Note that real coordinate spaces themselves are manifolds; for them, we can define canonical charts as identity mappings. However, if the space is not globally homeomorphic to a real coordinate space, the manifold structure comes useful: Consider, for instance, the surface of a sphere. Intuitively, every surface is two-dimensional, but there is no single coordinate system with which to represent every point on the spherical surface with just two coordinates—hence, the surface does *not* constitute a two-dimensional real coordinate space. However, it can be defined as a two-dimensional manifold when equipped with *two* overlapping coordinate charts. This is the primary reason why the surface of the Earth cannot be projected into a single map on a plane.

From the global viewpoint, a manifold can be almost anything, as long as it locally resembles a linear space. Therefore the dominant idea: *think global, act local.* ⋄

Manifolds can also have boundaries [5, p. 105]: Then, the charts related to **boundary points** map to real coordinate *half-spaces*. The boundary of a manifold $\mathcal{M}$ is denoted by $\partial\mathcal{M}$.

Tangent spaces

Since the real coordinate space is linear, the displacement between two points in the space can be easily given with a single vector. Manifolds, in general, have no global linear properties. Locally, however, we can define a *virtual displacement* with tangent vectors.

Tangent vectors are defined point-wise via smooth curves through a point in the

manifold. A smooth curve on the manifold $\mathcal{M}$ is a smooth mapping c such that

$$c : (-\varepsilon, \varepsilon) \subset \mathbb{R} \to \mathcal{M},$$

where the smoothness is to be understood in the sense of differentiability in $\mathbb{R}$. The curve c is said to pass through the point p if $c(0) = p$. A tangent vector at the point p is then the equivalence class of the curves which share the same tangent at the point p. Formally [5, p. 28]:

Definition 2.2.5. Let $\mathcal{C}_p$ be the set of smooth curves through the point $p \in \mathcal{M}$. A **tangent space** $T_p\mathcal{M}$ at the point p is the set of equivalence classes

$$T_p\mathcal{M} = \mathcal{C}_p / \sim,$$

when the equivalence $c_i \sim c_j$ of any two curves c_i and c_j is defined as

$$(\psi \circ c_i)'(0) = (\psi \circ c_j)'(0),$$

where ψ is an n-dimensional chart defined in the neighbourhood U_p of the point p, and the derivative $(\cdot)'$ is the usual differentiation in the real coordinate space $\mathbb{R}^n$. The elements of the tangent space at the point p are called the **tangent vectors** at the point p.

Intuition A tangent vector constitutes of three things: of a point in the manifold; of a chart relating the neighbourhood of the point to a real coordinate space; and of an n-tuple of components in the real coordinate space. All elements of a single equivalence class have the same array of components under any fixed chart, and hence the equivalence class constitutes a single tangent vector. $\diamond$

Every tangent space constitutes a linear space of the same dimension as the manifold, and thus defines local linearity. This also implies that every n-dimensional tangent space has a basis of n tangent vectors. Given a coordinate chart ψ such that

$$\psi : U_p \to (x_1, \ldots, x_n) \in \mathbb{R}^n,$$

we can define a **coordinate basis** of the tangent space by [5, pp. 42–45]

$$T_p\mathcal{M} = \operatorname{span}\left(\partial_{x_1}, \ldots, \partial_{x_n}\right).$$

This leads to another possible interpretation of tangent vectors as directional derivatives in the direction of coordinate lines.[5]

[5] Hence the notation ∂_{x_i}, which is usually reserved for the differentiation with respect to the

The disjoint union of all tangent spaces associated with the points p of the manifold is called the **tangent bundle** $T_{\mathcal{M}}$ of the manifold. While they all have the same dimension, the tangent spaces of different points need not to be related in any sense, and hence the tangent bundle cannot be a linear space.

A vector field on a manifold is a mapping that selects a unique tangent vector for each point of the manifold [5, p. 44]:

Definition 2.2.6. A **vector field** $\vec{v}$ is a section of the tangent bundle $T_{\mathcal{M}}$, that is, a mapping

$$\vec{v} : \mathcal{M} \to T_{\mathcal{M}}$$

such that for each $p \in \mathcal{M}$, there exists a unique tangent vector $\vec{v}_p \in T_p\mathcal{M}$ such that

$$\vec{v} : p \mapsto (p, \vec{v}_p)\,.$$

A vector field is **smooth** if its compound mapping with the charts is smooth.

The coordinate basis defined on one tangent space can now be extended to all tangent spaces if the basis vectors ∂_{x_i} are understood as vector fields. This yields a structure similar to the vector space, when the addition and scaling are defined point-wise: each vector field $\vec{v}$ can be decomposed point-wise with respect to the basis by setting

$$\vec{v}_p = f_1(p)\partial_{x_1} + \cdots + f_n(p)\partial_{x_n},$$

where the weights f_i are scalar functions over the manifold $\mathcal{M}$. The resulting **space of vector fields** is denoted by $\mathcal{X}$, or $\mathcal{X}_{\mathcal{M}}$ if the underlying manifold $\mathcal{M}$ needs to be made explicit. We make the notational distinction between the local tangent vectors and global vector fields by marking the vector fields with an arrow $\vec{(\cdot)}$.

Given two manifolds and a differentiable mapping between them, we can relate the tangent vectors of the domain to those of the codomain by pushforward [8, p. 55]:

coordinate x_i.

Definition 2.2.7. Let $\mathcal{M}$ and $\mathcal{N}$ be manifolds, and let f be a differentiable mapping

$$f : \mathcal{M} \to \mathcal{N}.$$

Then, the **pushforward** f_* of the mapping f is a mapping

$$f_* : T_p\mathcal{M} \to T_{f(p)}\mathcal{N}$$

such that at each point $p \in \mathcal{M}$

$$f_* (p, [c]) = (f(p), [f \circ c]) ,$$

where $[c]$ is the equivalence class of the curves that defines a unique tangent vector at the point p.

The pushforward is also often called the **differential** of the mapping f and denoted by df. Note that the pushforward as such is defined only locally. The mapping f must be a *diffeomorphism* in order to extend the relation to vector fields [8, p. 56].

Orientation

A concept of 'right-' or 'left-handedness' of a real coordinate space is a specific instance of a vector space orientation. The property can be generalized to manifolds, and is necessary for the definitions of integration and Hodge operator. We focus on the so-called *inner orientation*; there is a similar, and complementary concept of *outer orientation*, but for which we have no immediate use.

The oriented manifold is defined via orientation of its tangent spaces. The general vector space orientation is defined as follows [5, p. 67]:

Definition 2.2.8. Let V be an n-dimensional vector space. The two bases (u_i) and (v_i) share the same orientation if there exists a linear mapping (a matrix)

$$f : V \to V \ \mid \ \sum_j f_{i,j} u_j = v_i$$

such that its determinant $\det f$ is positive. The resulting two classes of orientation are called the **positive and negative orientations**, and the choice of either one of the orientations is the act of **orienting** the vector space V.

For convenience, the orientations of a zero-dimensional space is defined as ± 1. This means that also points can be 'oriented'.

A mapping between two positively oriented vector spaces V and W is said to be **orientation-preserving**, if a positively oriented basis for V is mapped to a positively oriented basis of W. On an n-dimensional manifold $\mathcal{M}$, the family of

orientations $\{\mathcal{O}_p\}$ for the tangent spaces $T_p\mathcal{M}$ is **locally coherent**, if there is an atlas such that for every neighbourhood U_p there exists an orientation-preserving change-of-charts, that is, the Jacobian determinant of each change-of-charts is positive. This defines an orientation on a manifold [9, p. 51]:

Definition 2.2.9. An **orientation** $\mathcal{O}$ of the manifold $\mathcal{M}$ is a locally coherent family of orientations $\{\mathcal{O}_p\}$ for the tangent spaces. An **oriented manifold** is a pair $(\mathcal{M}, \mathcal{O})$.

Not all manifolds can be oriented, but we assume orientability through the treatment. Hence from here onwards, the term **manifold** refers to an oriented, differentiable manifold.

Intuition Following the definition of the vector space orientation, the 'right-' or 'left-handedness' is simply a choice of order of the vectors in the standard basis of a real coordinate space. Similar approach can also be used for the tangent spaces.

It is clear that many familiar geometric objects can be oriented: For instance, a curve drawn on a paper can be oriented by giving a direction by which to travel along the curve. The paper itself, if thought to be a two-dimensional surface, can be oriented by defining a direction by which to travel along its edges. On the other hand, a practical example of a non-orientable manifold is the Möbius strip: the local orientation of the tangent spaces is not preserved when travelling along the surface. ⋄

Submanifolds and foliations

The subsets of a manifold can be manifolds themselves; when the manifold structure of the original manifold is inherited by a subset, we call it a submanifold [5, p. 8]:

Definition 2.2.10. Let $\mathcal{M}$ be an n-dimensional manifold. A **k-dimensional submanifold** $\mathcal{N}$ is a k-dimensional subset $\mathcal{N} \subset \mathcal{M}$ such that at each point p in $\mathcal{N}$, there is a chart (U, ψ) of the manifold $\mathcal{M}$ such that

$$\psi(U \cap \mathcal{N}) = \mathbb{R}^k \cap \psi(U).$$

Such charts are called **submanifold charts**.

The submanifold inherits the differentiable structure through the submanifold charts. Often, we say that the submanifold is **embedded** into the manifold. The **embedding** can defined as a homeomorphic inclusion function $f : \mathcal{N} \to \mathcal{M}$.

Similarly, a manifold can be decomposed into submanifolds via foliations [1, p. 35]:

Definition 2.2.11. A k**-dimensional foliation** of the manifold $\mathcal{M}$ is a decomposition of the manifold into a union of disjoint connected subsets $\{\mathcal{L}_i\}_{i\in\mathcal{I}}$ such that, for each point p of the manifold and all i, there is a chart (U, ψ) such that the $n-k$ coordinates of the intersection $U \cap \mathcal{L}_i$ under the chart are constant, that is

$$x_{k+1} = constant, \ldots, x_n = constant.$$

The subsets $\{\mathcal{L}_i\}_{i\in\mathcal{I}}$ are called the **leaves of the foliation**.

The leaves of the foliation are embedded submanifolds. We will use this property later in Chapter 4 when defining dimensional reduction on a manifold.

2.2.2 Differential forms and exterior algebra

We have now modelled the 'ambient space' for the electromagnetic field problems with a manifold. The field entities themselves are realized through objects called differential forms. Differential forms make a good choice for mainly two reasons: first, they are intrinsically geometric by relating fields to geometric objects such as curves and surfaces; and second, we can define derivation and integration of the forms without any reference to metric or a particular choice of coordinate system.

Covector space

Let V be an n-dimensional vector space. It has a **dual space** ${}^*V$ defined such that its elements $\omega \in {}^*V$ are mappings

$$\omega : V \to \mathbb{R}.$$

An element of the dual space is called a covector, and it can be defined on arbitrary degrees k [5, pp. 49–50]:

Definition 2.2.12. Let V be a vector space. A k**-covector** ω is a multilinear, alternating mapping

$$\omega : \underbrace{V \times \cdots \times V}_{k} \to \mathbb{R},$$

where **alternating** means that for a permutation σ of the argument vectors v_i,

$$\omega(v_1, \ldots, v_k) = \operatorname{sgn}(\sigma)\, \omega(v_{\sigma(1)}, \ldots, v_{\sigma(k)}).$$

The alternating property means that swapping any two of the argument vectors changes the sign of the outcome, which is a real number.

Covectors constitute a vector space, and we denote the **space of** k**-covectors** by ${}^*V^k$. Covectors associated with the tangent spaces of a manifold are called cotangent vectors [1, p. 37]:

Definition 2.2.13. Let $\mathcal{M}$ be an n-dimensional manifold. A **k-cotangent vector** is a multilinear, alternating mapping

$$\omega_p : \underbrace{T_p\mathcal{M} \times \cdots \times T_p\mathcal{M}}_{k} \to \mathbb{R}.$$

The space of all k-cotangent vectors at the point p is called the **k-cotangent space** at the point p, and denoted by ${}^*T_p^k\mathcal{M}$.

The disjoint union of all k-cotangent spaces associated with each point of a manifold is called the **k-cotangent bundle** ${}^*T_{\mathcal{M}}^k$ of the manifold $\mathcal{M}$.

As with the tangent spaces, the cotangent spaces constitute a linear space. Similarly, this implies that every n-dimensional cotangent space has a basis of n cotangent vectors. Given a coordinate basis of the tangent space,

$$T_p\mathcal{M} = \operatorname{span}\left(\partial_{x_1}, \ldots, \partial_{x_n}\right),$$

we can define a **dual coordinate basis** by setting [5, p. 58]

$${}^*T_p\mathcal{M} = \operatorname{span}\left(\mathrm{d}x_1, \ldots, \mathrm{d}x_n\right).$$

The bases relate to each other such that

$$\mathrm{d}x_i(\partial_{x_j}) = \delta_{ij} \quad \forall\, i, j \in \{1, \ldots, n\}.$$

The symbol d refers to exterior derivative, and will be defined later on.

Forms on a manifold

For each point of a manifold, a differential form assigns a covector. Compare this to vector fields: for each point, a vector field assigns a vector. Thus, differential forms could also be called covector fields. Formally [5, p. 55]:

Definition 2.2.14. A **differential k-form** or a **k-form** on the manifold $\mathcal{M}$ is a section of the k-cotangent bundle, that is, a mapping

$$\omega : \mathcal{M} \to {}^*T_{\mathcal{M}}^k$$

such that for each $p \in \mathcal{M}$, there exists a unique cotangent vector $\omega_p \in {}^*T_p^k\mathcal{M}$ such that

$$\omega : p \mapsto (p, \omega_p).$$

A k-form is **smooth** if its compound mapping with the charts is smooth.

Note that the zero-forms are scalar functions defined at each point of the manifold, even if their argument contains no tangent vectors.

Similarly to tangent vectors, the coordinate basis defined on one cotangent space can now be extended to all cotangent spaces if the basis covectors $\mathrm{d}x_i$ are understood as forms. Differential forms have then a structure similar to the vector space, when the addition and scaling are defined point-wise: each one-form ω can be decomposed point-wise with respect to the dual basis by setting

$$\omega_p = f_1(p)\mathrm{d}x_1 + \cdots + f_n(p)\mathrm{d}x_n,$$

where the weights f_i are scalar functions over the manifold $\mathcal{M}$. This can be generalized to arbitrary degrees, and we denote the resulting **space of k-forms** by $\mathcal{F}^k$, or $\mathcal{F}^k_{\mathcal{M}}$ if the underlying manifold $\mathcal{M}$ needs to be made explicit. Similarly, the union of all form spaces is denoted by $\mathcal{F}$, or $\mathcal{F}_{\mathcal{M}}$.

It may seem confusing that we denote both the cotangent vector and the form in the same manner. However, there should not rise any problems with this notational identification. The space of k-cotangent vectors is defined at each point of a manifold, and a k-form is a choice of a single k-cotangent vector at each point. In practice, when we speak of forms, we mean the point-wise defined real-valued mappings that take tangent vectors as their argument.

Intuition In an arbitrary modelling domain, the geometric objects can be characterized locally with tangent vectors. Thus, a curve is modelled with a selection of one tangent vector for each point it passes through; a surface can be modelled with a selection of two tangent vectors; and a volume takes three tangent vectors for each of its points.

Curves, surfaces and volumes are an integral part of the electromagnetic field theory: for instance, the magnetic field is always related to a curve, and hence the natural way of representing the field is a one-form H. Similarly, the magnetic flux is always related to surfaces, and hence the natural way of representing the flux is a two-form B. The outcome of both forms, when given tangent vector arguments, is a real number; that is, the value of the *virtual* current or flux at the selected point in the domain. $\diamond$

Given two manifolds and a differentiable mapping between them, we can relate the forms of the codomain with those of the domain by pullback [8, p. 57]:

Definition 2.2.15. Let $\mathcal{M}$ and $\mathcal{N}$ be manifolds, and let f be a differentiable mapping

$$f : \mathcal{M} \to \mathcal{N}.$$

Then, the **pullback** f^* of the mapping f is a mapping

$$f^* : \mathcal{F}^k_{\mathcal{N}} \to \mathcal{F}^k_{\mathcal{M}}$$

such that for every $\omega \in \mathcal{F}^k_{\mathcal{N}}$, at each point $p \in \mathcal{M}$

$$(f^*\omega)_p(v_1, \ldots, v_k) = \omega_{f(p)}(f_* v_1, \ldots, f_* v_k).$$

The pullback is the generalization of the change of variables. Together, the pushforward and the pullback give powerful tools for moving from a manifold to another.

Exterior algebra

The space of differential forms can be endowed with the structure of **exterior algebra** by defining a wedge, or exterior product [5, pp. 133–134]:

Definition 2.2.16. The **exterior product** $\wedge$ is a bilinear mapping

$$\wedge : \mathcal{F}^k \times \mathcal{F}^l \to \mathcal{F}^{k+l}$$

such that

(1) $(\omega \wedge \vartheta) \wedge \zeta = \omega \wedge (\vartheta \wedge \zeta)$ (associativity),

(2) $\omega \wedge \vartheta = (-1)^{kl} \vartheta \wedge \omega$ (anticommutativity),

(3) $1 \wedge \omega = \omega$.

The exterior product of two forms can be given point-wise as

$$(\omega \wedge \vartheta)(v_1, \ldots, v_{k+l}) = \sum_\sigma \operatorname{sgn}(\sigma)\, (\omega_p)(v_{\sigma(1)}, \ldots, v_{\sigma(k)})(\vartheta_p)(v_{\sigma(k+1)}, \ldots, v_{\sigma(k+l)}),$$

when the permutations σ over the indices $\{1, \ldots, k+l\}$ are defined such that $\sigma(1) < \cdots < \sigma(k)$ and $\sigma(k+1) < \cdots < \sigma(k+l)$. Hence, the computation of a $k+l$-form $\omega \wedge \vartheta$ at a point can be done using only the values of the forms ω and ϑ at the point.

With the exterior product, forms of higher degree can be built from those of lower degree in a consistent manner. Suppose that we have a basis of one-forms, that is,

$$\mathcal{F}^1 = \{f_1 \mathrm{d}x_1 + \cdots + f_n \mathrm{d}x_n\},$$

where the weights f_i are scalar functions over the underlying manifold. We already saw that any one-form can be given as a point-wise linear combination of the basis

one-forms $\mathrm{d}x_i$, that is, the set $\{\mathrm{d}x_i\}$ spans the local cotangent spaces. Furthermore, the basis one-forms can also be used to define a *basis for two-forms* via the exterior product, for

$$\mathrm{d}x_i \wedge \mathrm{d}x_j$$

is a *non-zero* two-form for all $i \neq j$, and the basis obtained via such products spans all two-forms point-wise [5, pp. 135–137]. Similarly, we obtain a basis for any degree k.

The exterior product can be used to define a mapping called extension [1, p. 34]:

Definition 2.2.17. Let ω be a k-form. The **extension** is a mapping

$$j : \mathcal{F}^k \to \mathcal{F}^{k+1}$$

such that for each $p \in \mathcal{M}$, $\vartheta \in \mathcal{F}^1$,

$$j_\vartheta \omega_p(v_1, \ldots, v_{k+1}) = \vartheta_p \wedge \omega_p(v_1, \ldots, v_{k+1}).$$

The extension has a dual mapping called contraction, or interior product [1, p. 34]:

Definition 2.2.18. Let ω be a k-form. The **contraction** is a mapping

$$\iota : \mathcal{F}^k \to \mathcal{F}^{k-1}$$

such that for each $p \in \mathcal{M}$, $\vec{u} \in \mathcal{X}$,

$$\iota_{\vec{u}}\, \omega_p(v_1, \ldots, v_{k-1}) = \omega_p(\vec{u}, v_1, \ldots, v_{k-1}).$$

If ω is a one-form, the following identity holds [10]:

$$\iota_{\vec{u}}\, j_\omega + j_\omega \iota_{\vec{u}} = \iota_{\vec{u}}\, \omega. \tag{2.2.3}$$

The extension and contraction mappings are useful when defining mathematical structures related to dimensional reduction, as we will see in Chapter 4.

2.3 Calculus on manifolds

In the preceding section, field entities were modelled as differential forms on a manifold. The next question is the calculus of these field entities, since the notions of derivation and integration are crucial for electromagnetic field theory. In this section, we will see two differential operators: exterior derivative, which replaces the gradient, divergence and rotor of the vector calculus; and Lie derivative, which is the generalization of the directional derivative. We then briefly comment on integration by introducing the notation and a few important results.

2.3.1 Exterior derivative

The exterior derivative is a generalization of the differential of scalar functions, defined for differentiable forms of any degree [5, pp. 138–139]:

Definition 2.3.1. The **exterior derivative** d is a linear mapping

$$\mathrm{d} : \mathcal{F}^k \to \mathcal{F}^{k+1},$$

such that

(1) $\mathrm{d}f = df$ for smooth zero-forms f,

(2) $\mathrm{d}(\mathrm{d}\omega) = 0$ for all forms ω,

(3) $\mathrm{d}(\omega \wedge \vartheta) = \mathrm{d}\omega \wedge \vartheta + (-1)^k(\omega \wedge \mathrm{d}\vartheta)$ for k-forms ω.

Given a coordinate basis (∂_{x_i}) and a cobasis $(\mathrm{d}x_i)$, an explicit formula for calculating the exterior derivative can be given: In particular,

$$df = \sum_i \partial_{x_i} f \mathrm{d}x_i$$

defines the differential for a zero-form f.[6] Let π be a mapping

$$\pi : \{1, \ldots, k\} \to \{1, \ldots, n\}$$

such that $\pi(1) < \ldots \pi(k)$, and let ω be a k-form, explicitly written with respect to the basis as

$$\omega = \sum_{\pi(1)<\cdots<\pi(k)} \omega(\partial_{x_{\pi(1)}}, \ldots, \partial_{x_{\pi(k)}}) \mathrm{d}x_{\pi(1)} \wedge \cdots \wedge \mathrm{d}x_{\pi(k)},$$

where $\omega(\partial_{x_{\pi(1)}}, \ldots, \partial_{x_{\pi(k)}})$ are the component functions of ω with respect to the coordinates $\{x_i\}$; they are zero-forms, since all the vector arguments are fixed. Then the exterior derivative of ω is [5, pp. 138–142]

$$\mathrm{d}\omega = \sum_{\pi(1)<\cdots<\pi(k)} \mathrm{d}\omega(\partial_{x_{\pi(1)}}, \ldots, \partial_{x_{\pi(k)}}) \wedge \mathrm{d}x_{\pi(1)} \wedge \cdots \wedge \mathrm{d}x_{\pi(k)}.$$

2.3.2 Lie derivative

As a generalization of the directional derivative, we present Lie derivative. The Lie derivative yields the rate of change of a given form under a flow on a manifold [8,

[6] Note that the term ∂_{x_i} acts now as a differential operator—compare the notation for tangent vectors.

pp. 65–66]:

Definition 2.3.2. A **flow** γ on a manifold $\mathcal{M}$ is a mapping

$$\gamma : \mathcal{M} \times \mathbb{R} \to \mathcal{M}$$

such that

(1) $\gamma(p, 0) = p$,

(2) $\gamma(\gamma(p, t), s) = \gamma(p, t + s)$.

For notational simplicity, the flow at a point p for parameter t is denoted by $\gamma(p, t) = \gamma_t(p)$.

The flow induces a vector field $\vec{v}$, for at each point we can define

$$\vec{v}_p = [c(t)] = [\gamma_t(p)].$$

Then, we define the Lie derivative of a form with respect to the flow [8, p. 71]:

Definition 2.3.3. Let γ_t be a flow defined on the manifold $\mathcal{M}$, and $\vec{v}$ the related vector field. The **Lie derivative** $\mathcal{L}$ with respect to the vector field $\vec{v}$ is a mapping

$$\mathcal{L} : \mathcal{F}^k \to \mathcal{F}^k$$

such that for a k-form ω, at a point $p \in \mathcal{M}$

$$(\mathcal{L}_{\vec{v}}\, \omega)_p = \lim_{t \to 0} \frac{(\gamma_t^* \omega)_p - \omega_p}{t}.$$

For differential forms, the Lie derivative could also be defined by **Cartan's magic formula**:

$$\mathcal{L}_{\vec{v}} = \mathrm{d}\iota_{\vec{v}} + \iota_{\vec{v}}\, \mathrm{d}.$$

In particular, if f is a zero-form and $\vec{v} = \partial_t$ is a vector field tangent to the coordinate t, the Lie derivative becomes a simple differentiation:

$$\mathcal{L}_{\vec{v}} f = \mathrm{d}f(\vec{v}) = \vec{v}(f) = \partial_t f.$$

2.3.3 Integration

A proper treatment of the integration of differential forms would have us working with the structures of chains and simplexes. However, since there is no need for these concepts in the present study, we settle for a brief and largely informal introduction. For details, we refer to [5].

The integral of a real-valued function

$$f : \mathbb{R}^k \to \mathbb{R}$$

over a k-dimensional subdomain $S \subset \mathbb{R}^k$ is

$$\int_S f(x_1, \ldots, x_k) \mathrm{d}x_1 \cdots \mathrm{d}x_k \in \mathbb{R},$$

as is known from elementary calculus. We aim at a similar definition for differential forms, with ω being a k-form and $\mathcal{S} \subset \mathcal{M}$ an orientable k-dimensional compact submanifold:

$$\int_{\mathcal{S}} \omega = \int_{\mathcal{S}} f^* \omega \in \mathbb{R},$$

where f is the inclusion mapping of the submanifold.

The submanifold $\mathcal{S}$ is a manifold of its own right. Assuming that it is covered by a single chart ς, we can write

$$\int_{\mathcal{S}} \omega = \int_{\varsigma(\mathcal{S})} (\varsigma^{-1})^* \omega,$$

that is, the form ω is mapped to a real coordinate space by pullback, where it becomes a real-valued function of multiple real variables and which we can integrate with the tools provided by elementary calculus.

We come back to the integration of scalar functions with respect to a given coordinate frame once we have defined a metric, as the *measure* under the chosen coordinates is metric-dependent. However, as an important result, we can already state **Stokes' theorem**: Let $\mathcal{M}$ be an n-dimensional manifold. Then,

$$\int_{\mathcal{M}} \mathrm{d}\omega = \int_{\partial \mathcal{M}} \omega,$$

for all $\omega \in \mathcal{F}_{\mathcal{M}}^{n-1}$. The Stokes' theorem generalizes the Kelvin-Stokes and Ostrogradsky-Gauss theorems of the vector calculus.

2.4 Metric

As the name suggest, metric structure is something that relates to measuring distances. Metric, in fact, is the mathematical structure that gives us the concepts of length and angle: it is our ruler-and-compass tool.

We first define metric as a general distance function, and show how it relates to the concepts of norm and inner product. Then, we define metric on a manifold. We will see that this manifold metric then yields a Hodge operator, which can be used to map k-forms to $(n-k)$-forms; a necessary relation for writing down the

constitutive equations of electromagnetic fields.

2.4.1 Metric as a function

Let us take an arbitrary set X. Then [7, p. 21],

Definition 2.4.1. A **metric D** in the set X is a mapping

$$\mathrm{D} : X \times X \to \mathbb{R}$$

such that for all $x, y, z \in X$

(1) $\mathrm{D}(x, z) \leq \mathrm{D}(x, y) + \mathrm{D}(y, z)$,

(2) $\mathrm{D}(x, y) = \mathrm{D}(y, x)$,

(3) $\mathrm{D}(x, y) = 0 \quad \Leftrightarrow \quad x = y$.

A set equipped with a metric is called a **metric space**. The metric is also called a **distance** in the set X. It is easy to see that the familiar Euclidean distance satisfies these axioms. Note, however, that we do not require anything special from the set X. It does not need to be a vector space, nor a subset of such a space.

However, if we have a vector space, the metric can be defined indirectly with an inner product [7, p. 15]:

Definition 2.4.2. The **inner product** $\langle \cdot, \cdot \rangle$ in a vector space V is a mapping

$$\langle \cdot, \cdot \rangle : V \times V \to \mathbb{R}$$

such that for all $x, y, z \in V$, $\alpha, \beta \in \mathbb{R}$

(1) $\langle x, y \rangle = \langle y, x \rangle$,

(2) $\langle \alpha x + \beta y, z \rangle = \alpha \langle x, z \rangle + \beta \langle y, z \rangle$,

(3) $\langle x, x \rangle \geq 0$,

(4) $\langle x, x \rangle = 0 \quad \Leftrightarrow \quad x = 0$.

A vector space equipped with an inner product is called an **inner product space**. In an inner product space, we can induce a norm [7, p. 17]:

Definition 2.4.3. The **norm** $\|\cdot\|$ in the vector space V is a mapping

$$\|\cdot\| : V \times V \to \mathbb{R}_+ \cup \{0\}$$

such that for all $x, y \in V$, $\alpha \in \mathbb{R}$

(1) $\|x + y\| \leq \|x\| + \|y\|$,

(2) $\|\alpha x\| = |\alpha|\|x\|$,

(3) $\|x\| = 0 \quad \Rightarrow \quad x = 0$.

It is easily seen that the norm of an inner product space can be induced by defining

$$\|x\| = \sqrt{\langle x, x \rangle}.$$

Furthermore, a norm is induced from a metric by defining

$$\mathrm{D}(x, y) = \|x - y\|.$$

Thus, any given inner product space can be metrized. It is clear then that the standard vector calculus indeed bears more structure than initially needed: the inner product structure used to define the calculus also invokes a metric.

An isomorphism between two metric spaces preserving the metric is called an isometry, defined as follows [7, p. 68]:

Definition 2.4.4. Let V and W be metric spaces with metrics D_V and D_W, respectively. A bijective function $f : V \to W$ is **isometric** if $\mathrm{D}_W\left(f(x), f(y)\right) = \mathrm{D}_V(x, y)$ for all $x, y \in V$.

The importance of the isometries comes apparent when we are defining equivalent electromagnetic field problems on two different manifolds; an instance of this can be seen in Chapter 6.

2.4.2 Metric on a manifold

In a Euclidean space, the distance between any two points is easily defined by measuring the norm of the displacement vector between the points. This generalizes to manifolds via tangent vectors, since they were defined as virtual displacements. However, the distance measure becomes now more complicated, since there is no canonical way to relate the tangent spaces at different points to each other, and we also need to define a suitable inner product for each tangent space. This generalized inner product is called metric tensor [5, pp. 215–216]:

Definition 2.4.5. Let $\mathcal{M}$ be an n-dimensional manifold. A **metric tensor g_p at a point** p is a bilinear mapping

$$g_p : T_p\mathcal{M} \times T_p\mathcal{M} \to \mathbb{R}$$

such that

(1) $g_p(u, v) = g_p(v, u)$ (symmetry),

(2) if $g_p(u, v) = 0$ for all v, then $u = 0$ (non-degenerateness),

(3) $g_p(u, u) \geq 0$ and $g_p(u, u) = 0$ if and only if $u = 0$ (positive-definiteness).

From the definition it follows that the metric tensor is an inner product on the tangent spaces. We then define the **metric tensor** as a form g such that for all points p in the manifold $\mathcal{M}$, $g(p) = g_p$.

Intuitively, the distance between any two points a and b on a manifold is the length of the shortest path we can take from one point to another. Since curves give rise to tangent spaces, we can define the measure of the length ℓ of a differentiable curve

$$\gamma : [0, 1] \to \mathcal{M}$$

by setting

$$\ell(\gamma) = \int_0^1 \sqrt{g(\gamma'(t), \gamma'(t))}\, \mathrm{d}t,$$

where the differentiation γ' yields the tangent vectors defined by the curve γ. If we set $\gamma(0) = a$ and $\gamma(1) = b$, and take the greatest lower bound of the path lengths, we have an explicit expression for the **Riemannian metric** on the manifold $\mathcal{M}$:

$$\mathrm{D}(a, b) = \inf_\gamma \int_0^1 \sqrt{g(\gamma'(t), \gamma'(t))}\, \mathrm{d}t.$$

A manifold endowed with a metric tensor that induces the Riemannian metric is called a **Riemannian manifold**. The structure of Riemannian manifolds is the specific geometric framework on which the present study builds, and hence from here onwards, the term **manifold** refers to a Riemannian manifold.

Component representation

If we have a coordinate basis (∂_{x_i}) for the tangent spaces, the metric tensor g can be given explicitly as a matrix G such that its entries are given by

$$g(\partial_{x_i}, \partial_{x_j}) = G_{ij}.$$

We will abbreviate the matrix by $g_{x_1 \cdots x_n}$. This is called the **component representation** of the metric tensor.

Care must be taken to differentiate between the concepts of the metric, metric tensor, and its component representations with respect to coordinate charts: A metric is a function between the points in the manifold, giving the measure of their distance. A metric tensor is the inner product of the tangent spaces, which can be used to induce a metric on the manifold. Its component representation is always given under some coordinate chart, and hence the same metric tensor can have several different representations.

2.4.3 Hodge operator

The metric tensor on a manifold yields two important mappings: a canonical way to identify tangent vectors with cotangent vectors, and a canonical mapping between k and $(n-k)$-forms. The first property gives us a way of representing differential forms through vector fields, and the second property is crucial in defining the constitutive equations for electromagnetic fields.

The metric tensor induces an isomorphism between the tangent and cotangent vectors [5, p. 219]:

Definition 2.4.6. Let $\mathcal{M}$ be an n-dimensional manifold, and u a tangent vector of the tangent space $T_p\mathcal{M}$. The mappings

$$\flat : \mathcal{X}_\mathcal{M} \to \mathcal{F}^1_\mathcal{M}$$

such that

$$\flat \vec{v}_p(u) = g_p(\vec{v}_p, u)$$

and

$$\sharp : \mathcal{F}^1_\mathcal{M} \to \mathcal{X}_\mathcal{M}$$

such that

$$\omega_p(u) = g_p(\sharp \omega_p, u)$$

are called the **musical isomorphisms** under the metric tensor g.

The vector fields $\sharp\cdot$ related to one-forms are often called the **proxy vectors** of the forms.

For the mapping between k and $(n-k)$-forms, we define a Hodge operator [11, p. 160]:

Definition 2.4.7. The **Hodge (operator)** is a mapping

$$\star : \mathcal{F}^k \to \mathcal{F}^{n-k}$$

such that

(1) $\star\, 1 = vol$

(2) $\star\,(\omega \wedge \alpha) = \iota_{\sharp\alpha} \star \omega$, for $\omega \in \mathcal{F}^{k-1}$ and $\alpha \in \mathcal{F}^1$.

The symbol vol is a volume form, defined as follows [5, p. 221]:

Definition 2.4.8. A **volume form** on the manifold $\mathcal{M}$ is a mapping

$$vol : \underbrace{\mathcal{X} \times \cdots \times \mathcal{X}}_{n} \to \mathbb{R}$$

such that, given orthonormal vector fields $(\vec{v}^i)$ that define a positively oriented basis,

$$vol(\vec{v}_p^1, \ldots, \vec{v}_p^n) = 1.$$

The decomposition in the definition of the Hodge operator can be furthered by giving the form ω as a wedge product of a one-form and a $(k-2)$-form; continuing in this manner, we arrive to a point where we can calculate the Hodge for a zero-form, following from the definition.

If we have a positively oriented orthonormal coordinate basis (∂_{x_i}) for the tangent spaces, the image of the Hodge can be given explicitly [1, p. 56]:

$$(\star\omega)(\partial_{x_{k+1}}, \ldots, \partial_{x_n}) = \omega(\partial_{x_1}, \ldots, \partial_{x_k}),$$

for all k-forms ω.

Intuition The Hodge mapping between forms can be thought as a decomposition of an n-dimensional field entity into k- and $(n-k)$-dimensional components: For instance, the magnetic field as a three-dimensional entity is not a single field but a *pair* (B, H) consisting of line-related field H and surface-related flux B, which are coupled via the Hodge mapping. Thus the inherently three-dimensional *phenomenon* of the magnetic interaction is modelled with geometric objects which by themselves relate to one- and two-dimensional entities, and together yield a complete three-dimensional model.

Furthermore, the Hodge mappings give meaning to material relations, since then the electromagnetic properties of the matter can be related to the underlying metric. This manifests as constitutive equations, which we will define later on. ⋄

2.4.4 Integration under coordinates

We now return to define integration of scalar functions under a given coordinate chart. If $\{\partial_{x_i}\}$ is a positively oriented basis for the tangent spaces, and $\{\mathrm{d}x_i\}$ is the dual basis, the volume form can be defined as [5, p. 222]

$$vol = \sqrt{\det g_{x_1 \dots x_n}}\mathrm{d}x_1 \wedge \cdots \wedge \mathrm{d}x_n.$$

This is called the **Riemannian volume form**. Then, the integration of a zero-form f under these coordinates becomes

$$\int_{\mathcal{M}} f\, vol = \int_{\mathcal{M}} f\sqrt{\det g_{x_1 \dots x_n}}\mathrm{d}x_1 \wedge \cdots \wedge \mathrm{d}x_n.$$

2.5 Maxwell's equations in the language of differential geometry

We have now all the tools to define the Maxwell model given in Equation (2.1.1), and the constitutive equations given in (2.1.2). What we need to formalize are the following four statements, as given in [12, pp. 151–156]:

(Maxwell-)Faraday
: The sum of the time variation of a magnetic flux on any surface and the electric circulation on a path around the surface equals zero.

(Maxwell-)Ampère
: An electric current through any surface is equal to the sum of the time variation of the electric flux through the surface and the magnetic circulation on a path around the surface.

Gauss, electric
: An electric charge in any volume is equal to the electric flux throughout the surface bounding the volume.

Gauss, magnetic
: The magnetic flux on a surface bounding any volume element equals zero.

From the definitions of the differential forms, it follows that the suitable models for the **magnetic (circulation) field** and the **electric (circulation) field** are one-forms H and E, respectively. The model for anything living on surfaces is a two-form: hence the **magnetic flux** and the **electric flux** are two-forms B and H, respectively. Likewise, the **(electric) current** is a two-form J. The **(electric) charge** is modelled with a three-form ρ. Then, denoting surfaces with S and volumes with V, we can pose the statements formally as:

(Maxwell-)Faraday

$$\partial_t \int_S B + \int_{\partial S} E = 0 \quad \forall\, S$$

(Maxwell-)Ampère

$$\int_{\partial S} H = \partial_t \int_S D + \int_S J \quad \forall\, S$$

Gauss, electric

$$\int_V \rho = \int_{\partial V} D \quad \forall\, V$$

Gauss, magnetic

$$\int_{\partial V} B = 0 \quad \forall\, V$$

Note that the terms 'density' and 'intensity', as they appear in vector field counterparts, are omitted. This follows from the metric independence of the differential forms—in fact, what was modelled with (surface-related) *flux density* in the vector calculus becomes *virtual flux* in differential geometry; likewise for volume-related densities and line-related intensities. Also, while we earlier argued that the magnetic field is in fact a pair of two entities, namely (B, H), we nevertheless follow the text-book convention of calling the one-form H the magnetic field. Similarly for the electric field: the pair (D, E) and the one-form E are both called by the same name. No confusion should arise in the following treatment, but we deem that this idea of the decomposition of the fields as pairs is important for intuitive picture of the electromagnetic field theory and hence worth mentioning. For more discussion on the naming of the field entities, see [13, pp. 23–24].

Applying Stokes' theorem, we can reformulate the integral equations to yield the already seen point-wise **Maxwell model**:

$$\begin{aligned} \mathrm{d}E &= -\partial_t B, & \mathrm{d}H &= J + \partial_t D, \\ \mathrm{d}D &= \rho, & \mathrm{d}B &= 0. \end{aligned}$$

The definition of the constitutive equations requires a brief discussion on the materials and their relation to the metric.

2.5.1 Metric, materials and constitutive equations

As seen, the Maxwell model can be formulated in a coordinate- and metric-free manner. Metric, however, is important when considering boundary value problems

which arise naturally in many electromagnetic applications [1]. Furthermore, to give constitutive relations as a set of explicit equations, we are bound to look for a metric structure.

Let us first define a **material operator** α as a mapping

$$\alpha : \mathcal{F}^k \to \mathcal{F}^k$$

such that it represents the material of the domain. Therefore, the operator α can be by a property non-linear, anisotropic or inhomogeneous, as it reflects the electromagnetic properties of the material. The material operator is metric-dependent.

Material operator in conjunction with the Hodge then yields the constitutive operator [1, p. 89–90]:

Definition 2.5.1. A **constitutive operator** $\star_\alpha$ is a compound mapping

$$\star_\alpha : \mathcal{F}^k \to \mathcal{F}^{n-k},$$

such that

$$\star_\alpha = \alpha \circ \star,$$

where α is the material operator.

While the material and Hodge operators are metric-dependent, the constitutive operator is *not* [1, p. 89]. This implies that the constitutive *relations* can be posed independently of a metric; however, if explicit equations are to be used, then also the metric has to be defined.

In the literature such as [13], [14] or [15], the electromagnetic properties of the material are given with respect to laboratory measurements. These *material parameters* are related to the material operator by introducing a Euclidean metric on the domain manifold with the aid of a *rigid body*—in other words, the observations and measurements are modelled with a special chart called the **standard parametrization** [1, p. 23–24]. Under this standard parametrization, the decomposition of the constitutive operator is fixed to the Euclidean metric E:

$$\star_\alpha = \alpha_E \circ \star_E.$$

Then, the material parameters can be naturally related to the material operator. For our treatment, it is sufficient to consider isotropic materials only: hence, the material operator can be point-wisely represented by a real-valued function which corresponds to the parameters given by the measurements.[7]

[7] In Chapter 6, we present two different models of which one is posed under the standard parametrization while the other is not. The non-standard parametrization becomes then explicit by a necessary modification of the material parameters.

We define the following material operators: Operators μ and ν are the **permeability** and **reluctivity** of the magnetic materials, respectively. Operators ϵ and σ are the **permittivity** of the dielectric materials and the **conductivity** of the conducting materials, respectively. We can then pose the constitutive equations:

$$B = \star_\mu H, \qquad D = \star_\epsilon E,$$
$$J = \star_\sigma E, \qquad H = \star_\nu B.$$

2.6 Equivalent electromagnetic field problems

If two manifolds $\mathcal{M}$ and $\mathcal{N}$ are diffeomorphic, we can deem that they constitute in fact two different viewpoints to the same domain. This means that, once we have set up an electromagnetic field problem in one manifold, we can take it to the other manifold, solve it there and bring the solution back to the original manifold—and the result is exactly the same as it would be if we had solved the problem there in the first place. This is a crucial point for computational simplicity: given a certain domain and a problem, what would be the simplest and the most efficient way to model the geometry, that is, which parametrized instance of the manifold we should use? A detailed treatment of such equivalence classifications is given in [1]; as a basic example, consider the coordinate change from the 2D Cartesian to the polar coordinates—in many an application this change significantly simplifies actual computation.

In the coordinate change scenario above we do nothing more but map the 'labels' of the points to another set of labels—that is, we use different coordinate charts for the manifold. However, we could also change the metric representation in ways that, from a fixed viewpoint, we would seem to be *deforming* the domain. We will use this property later in Chapter 6, where we define different geometries for analysing 2D submanifolds derived from an originally 3D model of an axial flux machine. These transformation involve, seemingly, bending and twisting the domain via changing the metric representation under the coordinate charts. While the resulting geometries seem to be drastically different, they can be shown to be instances of the same manifold, and hence, from the theoretical point of view, equally suitable for computation.

3. AXIAL FLUX MACHINES

An **axial flux machine** (AFM) is characterized by the axial direction of the magnetic flux in the machine air gap [16]. This stands in contrast to **radial flux machines** (RFMs), in which the flux direction is dominantly radial. While not a new invention, AFMs have not enjoyed widespread use until very recently; however, they are suitable for several applications [17, pp. 1–3]. We focus on permanent magnet disc-type machines, since their industrial use is the motivating force behind the study.

We briefly review the background of the AFMs in industry, including a short discussion on the most important design properties of the electric machines. This design process is then set into the context of the electromagnetic modelling; to this end, the general magnetoquasistatic problem gives the basis for the study. However, the most pressing issues of the modelling procedure lie not so much in the initial problem identification, but in finding the suitable method for solving it. In the last section of this chapter, we present a short review of the state of the art solution methods explicitly concerning AFMs. Both analytical and modern numerical methods are present, and we will later in Chapter 7 use a FEA approach in our example implementation.

3.1 Background

While AFMs were among the very first electrical machines constructed, the industry has been dominated by their radial flux counterpart [17, p. 3]. However, after the introduction of high-performance permanent magnet materials in the 1980s, permanent magnet AFMs have gained more attention as suitable alternatives. Specifically, an AFM may offer a better solution for applications restricting the axial length of the machine [17, pp. 17–19][18, p. 17]. The compact size and *high torque density*, induced by the disc-type shape, has made AFMs suitable for such applications as wind power generators, hybrid electric vehicles and elevator motors [17, pp. 1–3][19].

Several different machine configurations, or topologies,[1] are in use; these include differentiating between single- and double-sided, slotted and slotless, surface mounted and buried, to mention a few alternatives [17, pp. 6–10][18, pp. 17–20]. We will not discuss these differences further, however. While the example implementation in

[1] Not to be confused with the mathematical concept of topology.

Chapter 7 specifically concerns a single-sided, slotted machine with surface mounted magnets, the analysis method present is applicable for all machine types that satisfy the basic modelling assumptions.

The design of AFMs differs from that of RFMs, and while for the latter there is quite an extensive toolbox readily available, the modelling methods for the AFMs are still in their early development [18, p. 14]. This motivates us to look at the core principles behind the machine modelling in search for improvement.

3.1.1 Machine design

From the engineering perspective, the most important feature of a machine is arguably its ability to efficiently transfer energy. For electrical machines, this involves a conversion between mechanical power and electricity; specific to AFMs, the mechanical part of this exchange concerns the machine torque related to the rotor motion.

As is the case of all non-idealised machines, not all energy can be transferred. The *power losses* in AFMs can be divided into three categories: ohmic or eddy current loss due to induced currents in conductive material parts, hysteresis loss due to magnetic material properties, and mechanical loss due to friction and windage [17, pp. 44–50]. In this study, hysteresis and mechanical losses are ignored.

Since the mechanical power is directly related to the machine torque, it is perhaps the single most crucial machine design aspect. In contrast to RFMs, the torque production is radius-dependent [17, p. 37], and hence the design aspects of AFMs are inherently 3D [18, p. 35]. Slotted machines are also subject to the so-called cogging torque—a result of magnetic coupling between the stator slots and the permanent magnets in rotor—which may significantly disturb the machine performance and overall torque output, and is inherently characteristic to many AFM configurations [20]. If a slotted configuration is preferred, the cogging torque may be minimized by skewing the stator stacks and/or magnets [21, p. 209]. Aside the cogging torque, significant axial forces between the stator and rotor may also be present, resulting in undesired machine vibration and acoustic noise [21, p. 217][22]. These forces are largely due to asymmetries between the rotor and the stator over the air gap; hence, skewing the geometry yields a trade-off between the axial forces and the cogging torque [21, p. 217].[2]

Different analysis methods for these parameters have been introduced in the literature, and we review a few such proposals in Section 3.3. Our implementation presented in Chapter 7 considers three of the mentioned aspects—torque, axial force and ohmic losses—and we will use numerical tools in their analysis.

[2]Note that in [21], the term 'radial force' is used since the text deals with RFMs. Nevertheless, the mechanism is the same.

3.2 Electromagnetic modelling

As a rule, electromagnetic modelling is approached from the perspective of boundary value problems. The usual setting includes a governing partial differential equation (PDE), or a system of such equations, together with suitable boundary conditions and additional constraints which are invoked to guarantee a unique solution to the governing equation. The equation and the additional conditions should, naturally, satisfy the known electromagnetic theory. The details of this initial setting are largely up to the decisions of the modeller, as they usually involve simplifications both of the domain geometry and of the general Maxwell system.

Following this procedure, we derive a single PDE from Maxwell's equations such that it adequately describes the situation at hand. Boundary and gauge conditions and are then imposed to create a BVP with a unique solution.

3.2.1 Magnetoquasistatic problem

Let us assume that the magnetic flux two-form B is given by a **magnetic potential** one-form A such that

$$\mathrm{d}A = B.$$

We then consider Ampère's law

$$\mathrm{d}H = J_{tot} + \partial_t D,$$

where the current term J_{tot} holds the information of the total current in the domain, including induced eddy currents and magnetization currents related to permanent magnets. This can be rewritten using the constitutive relation $H = \star_\nu B$:

$$\mathrm{d} \star_\nu \mathrm{d}A = J_{tot} + \partial_t D. \tag{3.2.1}$$

In the AFM setting, the time derivative of the electric flux D is usually neglible; this is related to the absence of capacitive effects in the machine. The assumption

$$\partial_t D = 0$$

leads us towards the **magnetoquasistatic model**.

The total current J_{tot} can be decomposed into **circuit currents** J_c, **eddy currents** J_e and **magnetization currents** J_m:

$$J_{tot} = J_c + J_e + J_m,$$

and the totality of the circuit and magnetization currents is defined as the **source**

current J:

$$J = J_c + J_m.$$

The magnetization currents are related to permanent magnets, and can be given with the **remanence flux** two-form M by [14, p. 228]

$$J_m = \mathrm{d} \star_\nu M.$$

The circuit current term J_c refers to the currents related to the source conductors in the circuit driving the machine. For the main part of the treatment, we do not separate the components of the source current, since the validity of the derivations does not depend on this.

For the eddy currents J_e, we can invoke Ohm's law:

$$J_e = \star_\sigma E,$$

Now, Faraday's law

$$\mathrm{d}E = -\partial_t B$$

can be given via the potential A as

$$\mathrm{d}\left(E + \partial_t A\right) = 0.$$

This gives rise to an auxiliary scalar potential ϕ such that

$$E + \partial_t A = -\mathrm{d}\phi,$$

where the cohomology terms [23] can be included in the potential A. We then have

$$E = -\mathrm{d}\phi - \partial_t A,$$

and thus the following expression for the induced currents:

$$\star_\sigma \left(\mathrm{d}\phi + \partial_t A\right) = -J_e.$$

The governing PDE of the **magnetoquasistatic**, or **eddy currents problem** is then

$$\mathrm{d} \star_\nu \mathrm{d}A + \star_\sigma \left(\mathrm{d}\phi + \partial_t A\right) = J, \tag{3.2.2}$$

where the source current J is assumed to be known.

Furthermore, it follows from Equation 3.2.1 with the assumption of vanishing

term $\partial_t D$ that

$$\mathrm{d}\left(J + J_e\right) = 0,$$

which is known as the **current continuity condition**. If the definition domains for the separated currents J_e and J are assumed to be disjoint, we can make the stronger assumption

$$\begin{cases} \mathrm{d}J = 0 \\ \mathrm{d}J_e = 0. \end{cases}$$

We will use this condition later in Chapter 5, when deriving the geometric decomposition of Equation (3.2.2).

Figure 3.1 gathers the governing equation, the continuity condition, and the magnetization term in vector calculus notation.

$$\boxed{\begin{array}{c} \mathrm{curl}\ \nu\,\mathrm{curl}\ \vec{A} + \sigma\left(\mathrm{grad}\ \phi + \partial_t \vec{A}\right) = \vec{J} \\ \vec{J_e} = -\sigma\left(\mathrm{grad}\ \phi + \partial_t \vec{A}\right) \\ \mathrm{div}\ \vec{J_e} = 0 \\ \vec{J} = \vec{J_m} + \vec{J_c} \\ \vec{J_m} = \mathrm{curl}\ \nu\vec{M} \end{array}}$$

Figure 3.1: *The governing PDE, eddy currents and the continuity condition, and the definition of the magnetization current using vector calculus notation.*

Well-posed problem

It is not guaranteed that the problem given by Equation (3.2.2) has a unique solution. The theory of PDEs states that a *well-posed problem* has to admit additional constraints such as gauge, boundary and initial conditions, and these conditions should guarantee the existence and the uniqueness of the solution.

Informally speaking, the **well-posedness** of a problem is defined by the three following conditions, characterizing the relation between the input and the solution: 1) a solution exists for each admissible input, and 2) the solution obtained for a fixed input is unique, and 3) the solution is continuously dependent on the input [24, p. 155]. The requirements to satisfy these conditions depend largely on the nature of the problem. As a rule, problems arising from mathematical physics are constructed such that their well-posedness is achieved through gauging and additional boundary and initial conditions. The magnetoquasistatic problem as presented is already partially well-posed in that it admits solutions; however, the uniqueness of the solution

requires more details.

Gauge conditions

When considering a connected and conducting domain with known eddy currents, a known potential A ensures a unique derivative $\mathrm{d}\phi$. In turn, the uniqueness of the scalar potential ϕ is then achieved by fixing its value on a single point in the domain. Thus it suffices to find a unique expression for the potential A.[25]

By looking at the definition, the potential A is indeed not unique with respect to the magnetic flux B: rewrite

$$A' = A + \alpha,$$

where $\mathrm{d}\alpha = 0$, and one immediately sees that

$$\mathrm{d}A' = \mathrm{d}A = B.$$

This is an equivalence relation. A transformation relating the potentials A and A' is called the **gauge transformation**, and the field B is said to be **gauge invariant** under this transformation. When utilizing primary field entities such as B, H and E, the uniqueness of the solution is guaranteed by a proper treatment of Maxwell's equations and boundary conditions only [25]. In contrast, additional gauge conditions are needed to satisfy the uniqueness of the solution under the potential formulation.

There exists a wide variety of gauge conditions, some of them stronger than others; these include the Coulomb gauge

$$\mathrm{d} \star A = 0,$$

and the Lorenz gauge[3]

$$\mu \epsilon \partial_t \star \phi + \mathrm{d} \star A = 0,$$

better-suited for wave propagation problems [27]. Later in Chapter 5, we will consider two different gauges: one such that one component of the potential A is assumed to vanish, and another—the so-called Weyl gauge—such that $\phi = 0$ holds. In general, these two conditions cannot be imposed together, and we will see that such a modelling decision is a source of error.

Boundary and initial conditions

The magnetoquasistatic problem is known to be well-posed under a simple domain topology and appropriate boundary and initial conditions; for a general treatment,

[3]Often, erroneously, named as 'Lorentz' gauge as discussed in [26].

we refer to [25]. For us it suffices to restrict ourselves to the particular geometry of an AFM core as depicted in Figure 3.2. Sufficient boundary conditions on the AFM domain can be posed as follows:

1. Periodic boundary surfaces a and b; the periodicity extends the geometry of Figure 3.2 to a full cycle. This reduces the domain into a *symmetry cell* as defined in Chapter 4.

2. Tangential magnetic field surfaces c, d and e; the magnetic flux outside the machine domain is negligible. Alternatively, the boundaries can be 'pushed away' from the machine core and then the potential A can be imposed to vanish on the surfaces. We choose the latter approach in the implementation in Chapter 7.

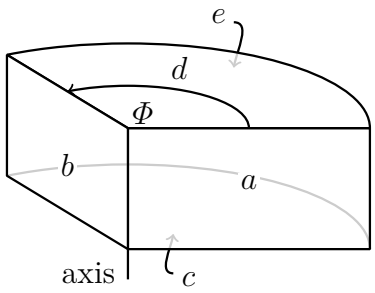

Figure 3.2: *The AFM problem domain: a* $1/3$ *piece of a machine from the axis to the outer core. With appropriate boundary conditions imposed on the surfaces* a–e*, the problem can be made well-posed.*

Since the magnetoquasistatic problem is time-dependent, we also need to impose the potentials everywhere in the domain at the chosen initial time $t = t_0$. The initial values could be set to zero or, as in the implementation in Chapter 7, by using the solution of an equivalent static problem as the initial condition; that is, by dropping out the time-dependent components of the problem, but leaving the static properties untouched. This may reduce the artificial transients during the first time steps if there are non-zero field sources such as permanent magnets present at the initial time.

With these initial, boundary and gauge conditions, Equation (3.2.2) defines the electromagnetic BVP of the AFM setting. This BVP has a solution which, under the posed assumptions, completely describes the electromagnetic behaviour of the machine.

3.3 Solution methods

As noted earlier, the difficulties related to the computational electromagnetism are more pronounced in the actual solving process of the BVP, rather than in building

one. The general theory of PDEs is rich in offering different methods for solving simple problems; however, often the geometry of the problem or the equation itself is too complex for simple analytical approaches. The domain may be simplified, for instance, by posing additional interface and boundary conditions or by neglecting some parts of the domain altogether; the field entities in the governing PDE may be approximated or (partially) neglected. Such simplifications of the problem often lead to standard text book procedures, including separation of variables, eigenfunctions, series expansions in terms of trigonometric and hyperbolic functions, and circuit models [14][28]. To this end, elaborate constructions can be built to minimize the errors due to the simplifications.[4]

However, more detailed solution methods usually involve numerical analysis. From the variety of numerical methods involving the *discretization* of the problem, FEA is commonly employed, and we shall focus on it for the remainder of the study.

3.3.1 Analytical methods

Analytical methods usually involve analysis using a 2D domain, either on the average radius of the machine core or by employing a **quasi 3D** approach, in which several 2D models on different radii are combined in order to account for the asymmetries of the geometry in the radial direction. In the quasi 3D method, the modelling domain is reduced into disjoint 2D surfaces called the **computation slices** (Figure 3.3). The computation slices are then used as domains for separate 2D problems, and the combination of the 2D solutions mimics the full 3D setting. We will focus on the quasi 3D method, due to the inherent 3D characteristics of AFMs, and since analysis on the average radius tends to yield unsatisfactory results [18, p. 35].

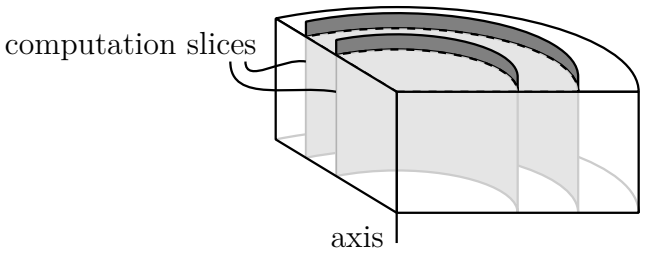

Figure 3.3: *An example of the domain slicing used in the quasi 3D method. The grey surfaces intersect the 3D domain, and define the computation slices for separate 2D problems.*

In [19], a simple model is presented for a two-stators, one-rotor -configuration, using a single computation slice. The model ignores machine curvature, and heavily

[4]These modifications should never compromise the well-posedness of the problem. The question of modelling errors relates to the accuracy of the model in describing the phenomena it is supposed to model, not to its internal consistency.

simplifies the geometry; then, an analytical expression for the magnetic potential is derived as a series expansion involving trigonometric and hyperbolic functions. The results involving magnetic field in the air gap are compared to 2D and 3D FEA solutions and machine measurements, and the method shows adequate accuracy for a basic design. We will use this simple model when validating the FEA implementation in Chapter 7.

A simplified geometry is used to derive similar analytical solutions in [29, 30, 31, 32, 33], the main difference being the employment of the quasi 3D approach. In all these studies, the results of the analytical method are compared to 3D FEA solutions, showing a good agreement in general. However, the radial dependence is admitted to be a source of error, and the end effects are specifically mentioned to be absent. In [29] and [31], the results are improved by introducing a correction function related to the radial field dependence; however, this correction function seems to be defined *ad hoc*, and lacks a proper justification. In [33], reluctance networks are employed in conjunction with geometric simplifications, and this model is later expanded to include a thermal model in [18]; an estimation of the necessary amount of computation slices is also given, although these figures are based on a rather narrow set of data and hence may be lacking generality.

These analytical models are defined under simplifying assumptions which, as a rule, include:

1. Machine curvature is neglected; no genuine radial-dependence is considered.
2. Infinitely permeable stator and rotor cores; given as boundary conditions.
3. Air permeability elsewhere in the domain.
4. No eddy currents.

Of these assumptions, the omission of the true radial-dependence renders these approaches—quasi 3D or not—as inherently two-dimensional. In [32], this radial dependence is discussed most thoroughly. With the exception of [18], none of the cited references consider eddy currents.

In [16], [34] and [35], full 3D geometry is also studied—although [34] can be deemed as semi-analytic, since it involves numerical integration of a Green's function. Not surprisingly, the extension of the dimension from two to three leads to relatively complex models. In [35], a correction factor for the 2D analysis is derived based on the 3D solutions; the justification for this kind of iterative correction is, again, questionable. The study presented in [16] offers perhaps the most thorough discussion available on the effect of the machine curvature. In the initial model, the assumptions include neglecting the core end effects and eddy currents, linear magnetic materials, and several simplifications of the machine geometry, such as the

omission of the stator teeth and slots. The effect of the radial flux on the induced currents is mentioned to be potentially significant, and this is further investigated with a coupled network method. A simple technique is presented to assess whether or not the radial flux component is likely to have a significant effect on the power losses. The study concludes that, in most practical cases, the assumption of a zero radial flux is well-justified.

Analytical methods are best-suited at initial stages of the machine design, due to the ease and efficiency of the implementation—indeed, low computation time seems to be the main motivation for developing such methods, and their flexibility in offering a parametric analysis is also mentioned in several studies. However, since the analytical methods necessarily involve drastic simplifications of the problem, the accuracy of the solution is often compromised. As stated in most of the cited references, while the overall electromagnetic behaviour can be predicted satisfactorily via analytical methods, a more detailed study of, for instance, ripple behaviour and harmonics calls for more complex models. Therefore, we turn to numerical tools and especially to FEA.

3.3.2 Finite element analysis

The method of finite elements is a specific modelling tool from the broader category of numerical discretization procedures. Other approaches such as the method of moments, finite difference methods or finite integration techniques are also widely used [28]; however, based on the literature scan, FEA seems to be the dominating method in the field of AFM modelling [16, p. 8]. Basic treatment of FEA is standard textbook material: for the general theory with functional analysis framework properly included, we refer to [36]; specific for electromagnetic applications, [28] offers a good introduction, while [37] presents a more advanced approach.

While most of the aforementioned studies on AFMs use numerical models as a comparison, the research relying solely on FEA is relatively scarce. In [38] and [39], FEA is discussed from the quasi 3D perspective. Both approaches neglect eddy currents, and mention end effects as a source of error. The results are compared to those of complete 3D models, with satisfying agreement—however, the discussion in both cases is kept rather brief. In [16], scaling of the air gap region in 3D FEA is investigated. This is done in order to the reduce the computational complexity, as the usually thin air gap may lead to unsurmountable meshing problems. However, this scaling procedure could be given a more rigorous treatment by using the tools of differential geometry as presented in Chapter 2.[5]

[5] 'Scaling' of a sub-domain is simply a modification of its metric properties. These modifications are rather easy to derive and implement; a topic suitable for a further study outside this thesis.

In most of the other cited references, the 3D FEA approach is deemed as too time- and power-consuming for practical use: the conclusion seems to be that the computer technology is not yet advanced enough for an accurate 3D FEA of an AFM, when considering widespread industrial use. A complete 3D model in a typical FEA software can run for weeks [18, p. 64], and optimizing these models may require great effort [40]. This gives us a good reason to look for an improved 2D model, and the obvious step towards the improvement is the quasi 3D method.

4. GEOMETRIC DECOMPOSITION AND DIMENSIONAL REDUCTION

The quasi 3D modelling method presented in the preceding chapter relies on the dimensional reduction of the original BVP. In this chapter, we introduce additional structure on the geometric model of electromagnetism presented in Chapter 2. Our aim is to construct a geometric decomposition of an electromagnetic BVP which can then be employed for the dimensional reduction of the problem.

Dimensional reduction is based on the concept of symmetry [1, p. 4]. We begin by a brief, and largely informal, discussion on the symmetry as a mathematical notion. Then, we define an observer structure, and show how it induces a geometric decomposition of fields and operators on a Riemannian manifold. Lastly, we consider dimensional reduction arising from such decompositions.

4.1 Symmetry

Intuitively, something is thought to be symmetric if we can perceive a balance or self-similarity to such an extent that the point of perception could be changed without changing the perception itself. A ball looks like a ball no matter the angle from which we look at it, as long as we are looking towards its center point. Similarly, if we have a cubic sauna room with a heater positioned at the center of one wall, the distribution of the temperature varies symmetrically when walking from one side of the room to another by a line aligned with the heater wall—that is, from judging solely on the temperature measurement, we cannot know if we are on the left or the right side of the heater.

More formally, an object is **symmetric** if it is invariant under a symmetry transformation. A **symmetry transformation** is a mapping between the points of the object. For example, the transformation 'walking from the side of a sauna room to the other' flips the points of perception in the room from left to right; this is reflection symmetry. The changes of the viewing angles of a ball correspond to the rotations of the ball around its center; an instance of spherical symmetry. **Invariance** means that we deem the *a priori* -transformation object to be equivalent to the *a posteriori* -transformation object. The 'equivalence' is, naturally, up to the definition: a ball might be coloured such that the angle matters, if we define an equivalence that considers also colours besides the shape. A more abstract instance

of symmetry is the gauge invariance of the magnetic flux as defined in Section 3.2.1.

The general theory of symmetry leads to such concepts as symmetry groups and group actions—but we leave the discussion as it is, and refer to [1] as a good exposition of the symmetry from the perspective of the electromagnetic modelling. However, an introduction of two of important concepts is in order: We have **continuous symmetry** if the symmetry is present under a continuous transformation. On the other hand, **periodic symmetry** occurs when the symmetry follows periodically from the transformation. The rotation of a ball yields continuous symmetry; the rotation of a cube is an instance of periodic symmetry, since symmetry occurs only periodically at rotations of certain angles. Both symmetries imply redundancy, and hence the problem can be simplified by neglecting the redundant parts. Continuous symmetry implies the possibility of dimensional reduction, whereas periodic symmetry implies that a single subdomain called a **symmetry cell** is sufficient for the analysis of the situation. We will see instances of both continuous and periodic symmetry; already in Chapter 3, we posed boundary conditions to an AFM domain utilizing the concept of periodicity.

4.2 Observer structure

The geometric decomposition of the BVP is attained via the so-called observer structure, with which it is possible to define *splitting* of the manifold and complementary components of the fields. The observer structure stems from the theory of relativity, where it is used to decompose four-dimensional spacetime into one temporal and three spatial dimensions [10]. The structure itself, as presented herein, is however more flexible, and with proper care it can be used to decompose geometries of arbitrary dimensions into complementary sub-geometries [1, p. 60][10].

Formally, the observer structure is defined as a pair consisting of a vector field and a one-form:[1, p. 59]

Definition 4.2.1. Let $\mathcal{M}$ be a differentiable manifold such that $\dim(\mathcal{M}) \geq 2$. An **observer (structure)** for $\mathcal{M}$ is a pair $(\vec{t}, \tau)$ such that

(1) $\vec{t}$ is a smooth nonzero vector field on $\mathcal{M}$,

(2) τ is a smooth one-form on $\mathcal{M}$,

(3) $\tau(\vec{t}_p) = 1$ holds for all $p \in \mathcal{M}$.

Furthermore, an observer is **holonomic** if there exists a zero-form s such that

$$\mathrm{d}s = \tau.$$

Within our treatment, there is no need to consider non-holonomic observers. Thus, from here onwards, the term **observer** refers to a holonomic observer structure.

An observer induces a foliation of the manifold, with sub-manifolds

$$\mathcal{T}_t = \{p \in \mathcal{M} \mid s(p) = t\}$$

as the leaves of this foliation; it is clear that the sets are disjoint, and that their union encompasses all points of the manifold. The leaves, which are the equipotential surfaces of s, are called **horizontal surfaces** induced by the observer. Likewise, for each point p, the vector field $\vec{t}$ defines **transversal direction**. This yields a decomposition of the tangent vectors:

$$T_p\mathcal{M} = \operatorname{span}\left(\vec{t}_p\right) \oplus \ker\left(\mathrm{d}s_p\right),$$

where $\oplus$ is the direct sum of complementary vector spaces. The subspace $\operatorname{span}\left(\vec{t}_p\right)$ is the space of all tangent vectors parallel to the transversal direction, which we then call the **transversal vectors**; the subspace $\ker\left(\mathrm{d}s_p\right)$ is the space of all tangent vectors tangential to the horizontal surface, which we then call the **horizontal vectors**.[1, pp. 59–61]

Intuition The observer structure formalizes the concept of an observer travelling in the domain along a given path; namely, along the trajectories defined by the vector field $\vec{t}$. The horizontal surfaces are the 'scenery' along the path: at each point, the observer 'sees' a subdomain of a dimension one degree lower than the original domain. Point-wise, this creates a *splitting* of the domain into a pair consisting of one-dimensional and $(n-1)$-dimensional subdomains.

For the axial flux machine setting, a cylinder in a three-dimensional domain will be sliced into separate two-dimensional cylindrical surfaces by selecting a radial-directed vector field as the transversal direction. These surfaces are equipotentials in the sense that they are characterized by a constant radius—the radius yields a potential zero-form, which is a constant on every cylindrical surface. ⋄

4.3 Geometric decomposition

Our primary goal is to decompose a partial differential equation, such as the magnetostatic A-formulation

$$\mathrm{d} \star_\nu \mathrm{d}A = J,$$

into components that would allow dimensional reduction to take place. In the case of magnetostatics, this requires not only the decomposition of the fields A and J but also of the operators d and $\star$. The resulting decomposition under an observer

$\left(\vec{t}, \mathrm{d}s\right)$ would be

$$\begin{bmatrix} -\hat{\mathrm{d}} & \mathcal{L}_{\vec{t}} \\ 0 & \hat{\mathrm{d}} \end{bmatrix} \hat{\star}_\nu \begin{bmatrix} \frac{1}{\eta_s} & 0 \\ 0 & \eta_s \end{bmatrix} \begin{bmatrix} \hat{\mathrm{d}} & 0 \\ \mathcal{L}_{\vec{t}} & -\hat{\mathrm{d}} \end{bmatrix} \begin{bmatrix} A_\parallel \\ A_\perp \end{bmatrix} = \begin{bmatrix} J_\perp \\ J_\parallel \end{bmatrix},$$

where $(\cdot)_\parallel$ and $\hat{(\cdot)}$ refer to the objects on the horizontal surfaces, $(\cdot)_\perp$ represent the field components along the transversal direction, and $\eta_s = \|\sharp \mathrm{d}s\|$. The aim of this section is to derive the components of this decomposition, starting from a given observer structure. We do this separately for fields, the exterior derivative, and the Hodge operator. Finally, these operators are brought together in Section 4.3.4, where we discuss the decomposition of the magnetostatic equation in more detail.

For the sake of simplicity, we assume that the domain $\mathcal{M}$ is a 3-dimensional Riemannian manifold; this simplification does not compromise the applicability of what follows, as can be verified from the more general treatment presented in [10].

4.3.1 Fields

Let ω be a k-form on the manifold $\mathcal{M}$. We aim for a decomposition

$$\omega \mapsto \begin{bmatrix} \omega_\parallel \\ \omega_\perp \end{bmatrix},$$

where $\omega_\parallel$ and $\omega_\perp$ are the **horizontal** and **transversal components** of the form ω. This is achieved via **splitting**

$$P : \mathcal{F}^k \to \mathcal{F}^k \times \mathcal{F}^{k-1},$$

defined such that [41]

$$P\omega = \begin{bmatrix} \iota_{\vec{t}} j_{\mathrm{d}s} \\ \iota_{\vec{t}} \end{bmatrix} \omega = \begin{bmatrix} \omega_\parallel \\ \omega_\perp \end{bmatrix}. \tag{4.3.1}$$

Following the identity (2.2.3) and the definition that $\mathrm{d}s(\vec{t}_p) = 1$, the inverse of the splitting can be given as

$$P^{-1} = \begin{bmatrix} 1 & j_{\mathrm{d}s} \end{bmatrix}.$$

For the tangent spaces, it holds that

$$T_p\mathcal{M} = \mathrm{span}\left(\vec{t}_p, u_1, \ldots, u_{n-1}\right),$$

where u_i are linearly independent horizontal vectors at point p. The horizontal

component $\omega_\parallel$ is 'horizontal' in the sense that it vanishes for arguments containing a transversal vector, since

$$\begin{aligned}\omega_\parallel(u_1,\ldots,u_{i-1},\alpha\vec{t}_p,u_{i+1},\ldots,u_k) &= \alpha(\mathrm{d}s\wedge\omega)(\vec{t}_p,u_1,\ldots,u_{i-1},\vec{t}_p,u_{i+1},\ldots,u_k)\\ &= 0,\end{aligned}$$

by the alternating property of differential forms. On the other hand, if the argument contains only horizontal vectors, we have

$$\begin{aligned}\omega_\parallel(u_1,\ldots,u_k) &= (\mathrm{d}s\wedge\omega)(\vec{t}_p,u_1,\ldots,u_k)\\ &= \sum_{i=0}^{k}(-1)^i\mathrm{d}s(u_i)\omega(u_0,\ldots,u_{i-1},u_{i+1},\ldots,u_k) \qquad (\text{Notation: } u_0=\vec{t}_p)\\ &= \mathrm{d}s(\vec{t}_p)\omega(u_1,\ldots,u_k) \qquad (\mathrm{d}s(\vec{t}_p)=1)\\ &= \omega(u_1,\ldots,u_k),\end{aligned}$$

since $\mathrm{d}s(u_i)$ vanishes for all horizontal vectors u_i. Therefore, the horizontal component of a form reacts only to the horizontal components of the tangent vectors. In other words, if $\hat{\omega}$ is the *restriction* of a form to the horizontal surface $\mathcal{T}_t$, we have

$$\hat{\omega}(v_1,\ldots,v_k) = (f^*\omega)(v_1,\ldots,v_k) = \omega\left(f_*(v_1,\ldots,v_k)\right),$$

where v_i are horizontal vectors and the mapping f denotes the embedding of the horizontal surface $\mathcal{T}_t$ into the manifold $\mathcal{M}$; the pushforward f_* maps the horizontal vectors to the corresponding tangent vectors in $\mathcal{M}$. Hence, the horizontal component $\omega_\parallel$ represents the pullback of the form ω to the horizontal surfaces identified with $\mathcal{T}_t$.

The transversal component $\omega_\perp$ is fixed to the direction of the vector field $\vec{t}$ by contraction; thus the lower dimension. Indeed, if $k=1$, then we have

$$\omega_\perp = \omega(\vec{t}_p),$$

which is a zero-form. There is some ambiguity regarding the terminology, however, since strictly speaking the transversal component $\omega_\perp$ is also a horizontal form. The actual transversal component is obtained by taking the extension $j_{\mathrm{d}s}\,\omega_\perp$, which

vanishes for horizontal vectors u_i:

$$\begin{aligned}(j_{\mathrm{ds}}\omega_\perp)(u_1,\ldots,u_k) &= (j_{\mathrm{ds}}\iota_{\vec{t}_p}\,\omega)(u_1,\ldots,u_k)\\ &= \left(1-\iota_{\vec{t}_p}\,j_{\mathrm{ds}}\right)\omega(u_1,\ldots,u_k)\\ &= \omega(u_1,\ldots,u_k)-\omega_\parallel(u_1,\ldots,u_k)\\ &= 0.\end{aligned}$$

Then, every differential form ω can be written as a sum of its geometric components [1, p. 63], that is,

$$\begin{aligned}\omega &= (\iota_{\vec{t}}\,j_{\mathrm{ds}}+j_{\mathrm{ds}}\iota_{\vec{t}})\omega\\ &= \omega_\parallel + j_{\mathrm{ds}}\omega_\perp.\end{aligned}$$

4.3.2 Exterior derivative

The exterior derivative is defined for differential forms $\mathcal{F}^k$ on the manifold $\mathcal{M}$. In order to differentiate horizontal forms, we need to have a splitting for the exterior derivative as well. Let us then consider the expression $\mathrm{d}\omega$: The decomposition can be written as

$$P\,(\mathrm{d}\omega) = P\mathrm{d}P^{-1}P\omega.$$

The term $P\omega$ is known, hence we consider the remainder

$$P\mathrm{d}P^{-1} = \begin{bmatrix}\iota_{\vec{t}}\,j_{\mathrm{ds}}\\ \iota_{\vec{t}}\end{bmatrix}\mathrm{d}\begin{bmatrix}1 & j_{\mathrm{ds}}\end{bmatrix} = \begin{bmatrix}\iota_{\vec{t}}\,j_{\mathrm{ds}}\mathrm{d} & \iota_{\vec{t}}\,j_{\mathrm{ds}}\mathrm{d}j_{\mathrm{ds}}\\ \iota_{\vec{t}}\mathrm{d} & \iota_{\vec{t}}\mathrm{d}j_{\mathrm{ds}}\end{bmatrix}. \tag{4.3.2}$$

Let us define the **horizontal exterior derivative** $\hat{\mathrm{d}}$ as

$$\hat{\mathrm{d}} = \iota_{\vec{t}}\,j_{\mathrm{ds}}\mathrm{d}. \tag{4.3.3}$$

Then, we have

$$\begin{aligned}\iota_{\vec{t}}\,j_{\mathrm{ds}}\mathrm{d} &= \hat{\mathrm{d}}, && \text{(Definition 4.3.3)}\\ \iota_{\vec{t}}\,j_{\mathrm{ds}}\mathrm{d}j_{\mathrm{ds}} &= 0, && \text{(Skew commutativity)}\\ \iota_{\vec{t}}\mathrm{d} &= \mathcal{L}_{\vec{t}}-\mathrm{d}\iota_{\vec{t}}, && \text{(Cartan's magic formula)}\\ \iota_{\vec{t}}\mathrm{d}j_{\mathrm{ds}} &= -\iota_{\vec{t}}\,j_{\mathrm{ds}}\mathrm{d}.\end{aligned}$$

The last identity follows from the properties of the exterior derivative:

$$\begin{aligned} \mathrm{d}(j_{\mathrm{d}s}\omega) &= \mathrm{d}(\mathrm{d}s \wedge \omega) \\ &= \mathrm{d}\mathrm{d}s \wedge \omega - \mathrm{d}s \wedge \mathrm{d}\omega \\ &= -j_{\mathrm{d}s}\mathrm{d}\omega. \end{aligned}$$

Therefore, the decomposition of Equation (4.3.2) is given by

$$P\mathrm{d}P^{-1} = \begin{bmatrix} \hat{\mathrm{d}} & 0 \\ \mathcal{L}_{\vec{t}} - \mathrm{d}\iota_{\vec{t}} & -\hat{\mathrm{d}} \end{bmatrix}.$$

Let ω be a k-form. Then

$$\begin{aligned} P\left(\mathrm{d}\omega\right) &= \begin{bmatrix} \hat{\mathrm{d}} & 0 \\ \mathcal{L}_{\vec{t}} - \mathrm{d}\iota_{\vec{t}} & -\hat{\mathrm{d}} \end{bmatrix} \begin{bmatrix} \omega_{\parallel} \\ \omega_{\perp} \end{bmatrix} \\ &= \begin{bmatrix} \hat{\mathrm{d}}\omega_{\parallel} & 0 \\ (\mathcal{L}_{\vec{t}} - \mathrm{d}\iota_{\vec{t}})\iota_{\vec{t}} j_{\mathrm{d}s}\omega & -\hat{\mathrm{d}}\omega_{\perp} \end{bmatrix} \\ &= \begin{bmatrix} \hat{\mathrm{d}}\omega_{\parallel} & 0 \\ \mathcal{L}_{\vec{t}}\omega_{\parallel} & -\hat{\mathrm{d}}\omega_{\perp} \end{bmatrix}, \end{aligned}$$

since clearly

$$\iota_{\vec{t}}\iota_{\vec{t}} = 0.$$

Thus, the splitting acts on the exterior derivative as follows:

$$P\mathrm{d} = \begin{bmatrix} \hat{\mathrm{d}} & 0 \\ \mathcal{L}_{\vec{t}} & -\hat{\mathrm{d}} \end{bmatrix} P. \tag{4.3.4}$$

4.3.3 Hodge operator

For the decomposition of the Hodge operator, we proceed as with the exterior derivative. Let us consider the equation

$$P(\star\omega) = P \star P^{-1} P\omega,$$

and specifically the term

$$P \star P^{-1} = \begin{bmatrix} \iota_{\vec{t}} j_{\mathrm{d}s} \\ \iota_{\vec{t}} \end{bmatrix} \star \begin{bmatrix} 1 & j_{\mathrm{d}s} \end{bmatrix} = \begin{bmatrix} \iota_{\vec{t}} j_{\mathrm{d}s} \star & \iota_{\vec{t}} j_{\mathrm{d}s} \star j_{\mathrm{d}s} \\ \iota_{\vec{t}} \star & \iota_{\vec{t}} \star j_{\mathrm{d}s} \end{bmatrix}. \tag{4.3.5}$$

Let us denote $\eta_s = \|\sharp \mathrm{d}s\|$. We define the **horizontal Hodge operator** $\hat{\star}$ as [10]

$$\hat{\star} = \frac{1}{\eta_s}\, \iota_{\vec{t}}\, j_{\mathrm{d}s} \star j_{\mathrm{d}s}.$$

It can be shown that the horizontal Hodge fulfills

$$\hat{\star}\omega(u_{k+1}, \ldots, u_{n-1}) = \omega(u_1, \ldots, u_k)$$

for an orthonormal basis (u_i) of any given horizontal surface $\mathcal{T}_t$ and horizontal k-form ω; for details, see Appendix A.

In the decomposition, we make use of the following identities, defined for a k-form ω [10]:

$$\star\, j_{\mathrm{d}s}\, \omega = \iota_{\sharp \mathrm{d}s} \star (-1)^k\, \omega, \tag{4.3.6}$$

and

$$\star\, \iota_{\sharp \mathrm{d}s}\, \omega = j_{\mathrm{d}s} \star (-1)^{k+1}\, \omega. \tag{4.3.7}$$

Now, the terms in the matrix of Equation (4.3.5) can be rewritten:

$$\begin{aligned}
\iota_{\vec{t}}\, j_{\mathrm{d}s} \star &= \frac{1}{\eta_s}\, \iota_{\vec{t}}\, j_{\mathrm{d}s} \star \frac{1}{\eta_s}\, (j_{\mathrm{d}s} \iota_{\sharp \mathrm{d}s} + \iota_{\sharp \mathrm{d}s}\, j_{\mathrm{d}s}) && \text{(Identity (2.2.3))} \\
&= \hat{\star}\, \frac{1}{\eta_s}\, \iota_{\sharp \mathrm{d}s} + \frac{1}{\eta_s^2}\, \iota_{\vec{t}} \star \iota_{\sharp \mathrm{d}s}\, \iota_{\sharp \mathrm{d}s}\, j_{\mathrm{d}s} (-1)^{k+1} && \text{(Identity (4.3.7))} \\
&= \hat{\star}\, \frac{1}{\eta_s}\, \iota_{\sharp \mathrm{d}s} && (\iota_{\sharp \mathrm{d}s}\, \iota_{\sharp \mathrm{d}s} = 0)
\end{aligned}$$

yields the first entry of the first row;

$$\iota_{\vec{t}}\, j_{\mathrm{d}s} \star j_{\mathrm{d}s} = \hat{\star}\, \eta_s$$

yields the second entry of the first row;

$$\begin{aligned}
\iota_{\vec{t}} \star &= \iota_{\vec{t}}\, j_{\mathrm{d}s} \iota_{\vec{t}} \star && (\mathrm{d}s(\vec{t}_p) = 1) \\
&= \frac{1}{\eta_s}\, \iota_{\vec{t}}\, j_{\mathrm{d}s} \star j_{\flat \vec{t}}\, \eta_s\, (-1)^k && \text{(Identity (4.3.6))} \\
&= \frac{1}{\eta_s}\, \iota_{\vec{t}}\, j_{\mathrm{d}s} \star (j_{\mathrm{d}s} \iota_{\sharp \mathrm{d}s} + \iota_{\sharp \mathrm{d}s}\, j_{\mathrm{d}s})\, j_{\flat \vec{t}}\, \frac{1}{\eta_s}\, (-1)^k && \text{(Identity (2.2.3))} \\
&= \frac{1}{\eta_s}\, \iota_{\vec{t}}\, j_{\mathrm{d}s} \star j_{\mathrm{d}s}\, \iota_{\sharp \mathrm{d}s}\, j_{\flat \vec{t}}\, \frac{1}{\eta_s}\, (-1)^k && (j_{\mathrm{d}s} \star \iota_{\sharp \mathrm{d}s} = 0) \\
&= \hat{\star}\, \frac{1}{\eta_s}\, \iota_{\sharp \mathrm{d}s}\, j_{\flat \vec{t}} (-1)^k
\end{aligned}$$

yields the first entry of the second row; and

$$\begin{aligned}
\iota_{\vec{t}} \star j_{\mathrm{d}s} &= \iota_{\vec{t}}\, j_{\mathrm{d}s} \iota_{\vec{t}} \star j_{\mathrm{d}s} && (\mathrm{d}s(\vec{t}_p) = 1) \\
&= \frac{1}{\eta_s}\, \iota_{\vec{t}}\, j_{\mathrm{d}s} \star j_{\flat\vec{t}}\, j_{\mathrm{d}s}\, \eta_s\, (-1)^k && (\text{Identity (4.3.6)}) \\
&= -\frac{1}{\eta_s}\, \iota_{\vec{t}}\, j_{\mathrm{d}s} \star j_{\mathrm{d}s}\, j_{\flat\vec{t}} \eta_s\, (-1)^k && (j_{\flat\vec{t}}\, j_{\mathrm{d}s} = -j_{\mathrm{d}s}\, j_{\flat\vec{t}}) \\
&= -\hat{\star}\, \eta_s\, j_{\flat\vec{t}} (-1)^k
\end{aligned}$$

yields the second entry of the second row. Then, the decomposition of Equation (4.3.5) becomes

$$\begin{bmatrix} \iota_{\vec{t}}\, j_{\mathrm{d}s} \star & \iota_{\vec{t}}\, j_{\mathrm{d}s} \star j_{\mathrm{d}s} \\ \iota_{\vec{t}} \star & \iota_{\vec{t}} \star j_{\mathrm{d}s} \end{bmatrix} = \hat{\star} \begin{bmatrix} \dfrac{1}{\eta_s}\, \iota_{\sharp \mathrm{d}s} & \eta_s \\ \dfrac{1}{\eta_s}\, \iota_{\sharp \mathrm{d}s}\, j_{\flat\vec{t}} (-1)^k & -\eta_s\, j_{\flat\vec{t}} (-1)^k \end{bmatrix}.$$

The decomposition can be further simplified by introducing a vector field $\vec{v}$ such that

$$\vec{v}_p = \vec{t}_p - g_{\mathcal{M}} \left(\frac{\sharp \mathrm{d}s_p}{\eta_s}, \vec{t}_p \right) \frac{\sharp \mathrm{d}s_p}{\eta_s} = \vec{t}_p - \frac{1}{\eta_s^2}\, \sharp \mathrm{d}s_p. \tag{4.3.8}$$

The tangent vectors $\vec{v}_p$ are horizontal, since

$$\mathrm{d}s(\vec{v}_p) = 1 - \frac{1}{\eta_s^2}\, \mathrm{d}s\, (\sharp \mathrm{d}s_p) = 1 - \frac{\eta_s^2}{\eta_s^2} = 0.$$

Now, if $\vec{v} = 0$, we say that the observer is **metric compatible**. The metric compatibility implies that the transversal vectors given by $\vec{t}$ are parallel to the vector field $\sharp \mathrm{d}s$. Then, every transversal vector measures the length of zero under the horizontal metric, which is the pullback of the global metric to the horizontal surfaces [10]. In other words, the transversal vector field is *perpendicular* to the horizontal surfaces:

$$\flat \vec{t} \wedge \mathrm{d}s = 0.$$

From the definition given in Equation (4.3.8), it follows that for a horizontal form ω,

$$\iota_{\sharp \mathrm{d}s}\, \omega = -\eta_s^2\, \iota_{\vec{v}}\, \omega + \eta_s^2 \iota_{\vec{t}} \omega = -\eta_s^2\, \iota_{\vec{v}}\, \omega. \tag{4.3.9}$$

Let us denote $\nu = \flat\vec{v}$,[1] and it follows that

$$\hat{\star}\, j_{\flat\vec{t}} = \hat{\star}\, j_\nu + \frac{1}{\eta_s^2}\,\hat{\star}\, j_{\mathrm{d}s} = \hat{\star}\, j_\nu. \tag{4.3.10}$$

Then, the terms of the decomposition matrix can be further modified:

$$\frac{1}{\eta_s}\,\iota_{\sharp\mathrm{d}s} = -\eta_s\,\iota_{\vec{v}} \qquad \text{(Identity (4.3.9))}$$

yields the first entry of the first row;

$$\begin{aligned}\frac{1}{\eta_s}\,\iota_{\sharp\mathrm{d}s}\, j_{\flat\vec{t}}(-1)^k &= \frac{1}{\eta_s}\left(1 - j_{\flat\vec{t}}\,\iota_{\sharp\mathrm{d}s}\right)(-1)^k && \text{(Identity (2.2.3))}\\ &= \frac{1}{\eta_s}\left(1 + \eta_s^2\, j_\nu\,\iota_{\vec{v}}\right)(-1)^k && \text{(Identities (4.3.9) and (4.3.10))}\end{aligned}$$

yields the first entry of the second row; and

$$-\eta_s\, j_{\flat\vec{t}}(-1)^k = -\eta_s\, j_\nu\,(-1)^k \qquad \text{(Identity (4.3.10))}$$

yields the second entry of the second row. Thus, we have the decomposition matrix of the Hodge operator simplified into

$$\begin{bmatrix} \dfrac{1}{\eta_s}\,\iota_{\sharp\mathrm{d}s} & \eta_s \\ \dfrac{1}{\eta_s}\,\iota_{\sharp\mathrm{d}s}\, j_{\flat\vec{t}}(-1)^k & -\eta_s\, j_{\flat\vec{t}}(-1)^k \end{bmatrix} = \begin{bmatrix} -\eta_s\,\iota_{\vec{v}} & \eta_s \\ \dfrac{1}{\eta_s}\,(1+\eta_s^2\, j_\nu\,\iota_{\vec{v}})\,(-1)^k & -\eta_s\, j_\nu\,(-1)^k \end{bmatrix}.$$

If the observer is metric compatible, the terms $\iota_{\vec{v}}$ and j_ν vanish. Then, the splitting acts on the Hodge operator as follows:

$$P\star = \hat{\star}\begin{bmatrix} 0 & \eta_s \\ \dfrac{1}{\eta_s}(-1)^k & 0 \end{bmatrix} P. \tag{4.3.11}$$

Under a metric compatible observer, the horizontal Hodge operator itself can be redefined as

$$\hat{\star} = (-1)^k \eta_s\,\iota_{\vec{t}}\star\,,$$

[1]Note that we have used the same symbol ν for reluctivity; however, the symbol ν as a reference to a metric compatibility appears only in the few following equations, and hence no confusion should arise from the double usage.

since

$$\begin{aligned}\frac{1}{\eta_s}\,\iota_{\vec{t}}\,j_{\mathrm{d}s}\star\, j_{\mathrm{d}s} &= (-1)^k\frac{1}{\eta_s}\,\iota_{\vec{t}}\,j_{\mathrm{d}s}\iota_{\sharp\mathrm{d}s}\star && \text{(Identity (4.3.6))}\\ &= (-1)^k\frac{1}{\eta_s}\,\iota_{\vec{t}}\left(\eta_s^2-\iota_{\sharp\mathrm{d}s}\,j_{\mathrm{d}s}\right)\star && \text{(Identity (2.2.3))}\\ &= (-1)^k\eta_s\,\iota_{\vec{t}}\star\,. && (\iota_{\vec{t}}\iota_{\sharp\mathrm{d}s}=0)\end{aligned}$$

From here onwards, we consider only metric compatible observers.

4.3.4 Putting it together: magnetostatic example

Having now defined the splittings for the fields and the operators, let us reconsider the magnetostatic equation:

$$\mathrm{d}\star_\nu \mathrm{d}A = J,$$

where ν now refers to the reluctivity of the magnetic materials. Applying the splitting, we have

$$P\left(\mathrm{d}\star_\nu \mathrm{d}A\right) = PJ,$$

which then yields by Equations (4.3.1), (4.3.4) and (4.3.11)

$$\begin{bmatrix}\hat{\mathrm{d}} & 0\\ \mathcal{L}_{\vec{t}} & -\hat{\mathrm{d}}\end{bmatrix}\hat{\star}_\nu\begin{bmatrix}0 & \eta_s\\ \frac{1}{\eta_s}(-1)^k & 0\end{bmatrix}\begin{bmatrix}\hat{\mathrm{d}} & 0\\ \mathcal{L}_{\vec{t}} & -\hat{\mathrm{d}}\end{bmatrix}\begin{bmatrix}A_\parallel\\ A_\perp\end{bmatrix} = \begin{bmatrix}J_\parallel\\ J_\perp\end{bmatrix}.$$

Now, we can set $k=2$, since the term $1/\eta_s(-1)^k$ acts on $\hat{\mathrm{d}}A_\parallel$, which is a two-form. Switching the rows of the right hand side by multiplying with a permutation matrix

$$\begin{bmatrix}0 & 1\\ 1 & 0\end{bmatrix},$$

we arrive at the decomposition presented in the beginning of the chapter:

$$\begin{bmatrix}-\hat{\mathrm{d}} & \mathcal{L}_{\vec{t}}\\ 0 & \hat{\mathrm{d}}\end{bmatrix}\hat{\star}_\nu\begin{bmatrix}\frac{1}{\eta_s} & 0\\ 0 & \eta_s\end{bmatrix}\begin{bmatrix}\hat{\mathrm{d}} & 0\\ \mathcal{L}_{\vec{t}} & -\hat{\mathrm{d}}\end{bmatrix}\begin{bmatrix}A_\parallel\\ A_\perp\end{bmatrix} = \begin{bmatrix}J_\perp\\ J_\parallel\end{bmatrix}. \tag{4.3.12}$$

This decomposition can be then used as a basis for dimensional reduction.

4.4 Dimensional reduction

Intuitively, a solution to a BVP is symmetric, if the fields, sources, boundary conditions, constitutive relations and the problem defining equations themselves are

symmetric. This symmetry then implies that, for solving the problem, it is sufficient to consider only a fraction of the domain, even to such an extent that the dimension of the domain is reduced.

The idea of the observer induced geometric decomposition of the problem is that the symmetry would reveal itself through a suitably chosen observer. Should such a revelation occur, the system of equations of the decomposed problem becomes decoupled. This implies the possibility of dimensional reduction, since then either of the equations can be considered separately.

The system of equations of the decomposed magnetostatic problem in Equation (4.3.12) is coupled, and hence the problem is inherently in three dimensions. However, if the geometry of the problem can be built such that there is symmetry along the transversal direction given by the vector field $\vec{t}$, the terms containing the Lie derivative $\mathcal{L}_{\vec{t}}$ vanish. If also the material properties 'hidden' in the horizontal constitutive operator exhibit similar symmetry [1, p. 103–104], the system of equations is decoupled.

Under $\vec{t}$-directed symmetry, the decomposition of the magnetostatic problem given by Equation (4.3.12) becomes

$$\begin{bmatrix} -\hat{\mathrm{d}} & 0 \\ 0 & \hat{\mathrm{d}} \end{bmatrix} \hat{\star}_\nu \begin{bmatrix} \dfrac{1}{\eta_s} & 0 \\ 0 & \eta_s \end{bmatrix} \begin{bmatrix} \hat{\mathrm{d}} & 0 \\ 0 & -\hat{\mathrm{d}} \end{bmatrix} \begin{bmatrix} A_\parallel \\ A_\perp \end{bmatrix} = \begin{bmatrix} J_\perp \\ J_\parallel \end{bmatrix}.$$

The decomposition then yields two decoupled equations posed on the horizontal surfaces:

$$-\hat{\mathrm{d}}\,\hat{\star}_\nu\,\eta_s\,\hat{\mathrm{d}}\,A_\perp = J_\parallel,$$

relating to a problem in which the source current $J_\parallel$, being a two-form, is transversal to the surface; and

$$-\hat{\mathrm{d}}\,\hat{\star}_\nu\,\frac{1}{\eta_s}\,\hat{\mathrm{d}}\,A_\parallel = J_\perp,$$

which relates to a problem in which the source current $J_\perp$, being a one-form, is contained in the surface. Therefore, if we have continuous symmetry transversal to the horizontal surfaces, the dimension of the problem can be reduced such that solving a pair of decoupled 2D problems is sufficient. This yields the justification for the dimensional reduction under continuous symmetry.

However, we will see in the next chapter that such continuous symmetry does not occur with axial flux machines. For the quasi 3D method, we introduce two complementary observers. Then, with further assumptions, the governing equations related to these observers can be made decoupled, and we have separate 2D problems—unfortunately, in this case an *infinite number of surfaces* will be needed in contrast to the single computation slice arising from continuous symmetry.

5. QUASI 3D MODELLING

The quasi 3D method arises from the need to improve 2D models involving a single computation slice, as was discussed in Chapter 3. The full 3D geometry is avoided by splitting the domain into a number of disjoint surfaces called the computation slices. Then, a 2D BVP can be posed separately on each slice, and the combination of the solutions mimics the 3D situation.

In this chapter, we decompose the magnetoquasistatic problem given by Equation (3.2.2) using the observer structure introduced in Chapter 4. We will point out the assumptions required to reduce the dimension of the original BVP; in addition, the dimensional reduction gives rise to residuals, which can be used to investigate the modelling errors. Lastly, we briefly comment on the discretization procedure and on the efficiency of the quasi 3D compared to the true 3D setting.

5.1 Decomposition and dimensional reduction

An AFM is cylindrical by construction, and hence it is natural to set the problem using the standard cylindrical coordinate chart. This is made possible when we assume that the 3D model can be further divided into symmetry cells by imposing periodic symmetry; since the cylindrical chart has a periodic angular coordinate, only a part of the machine can be considered under a single coordinate chart (see Figure 5.1). Hence, we model a $1/n$ -part of the machine, where n refers to the number of periods, and then extend this model into complete geometry by periodic boundary conditions.

Let us define the chart χ_{cyl} over the machine domain:

Definition 5.1.1. Let χ_{cyl} be a coordinate chart over a 3-dimensional manifold $\mathcal{M}$ such that

$$\chi_{cyl} : \mathcal{M} \to \mathbb{R}^3 : p \mapsto (r, \varphi, z) \in (0, R] \times [0, \Phi) \times \mathbb{R},$$

where R is a positive real number that can be fixed to the outer radial boundary of the machine, and $\Phi = 2\pi/n$, $n \in \mathbb{N}$, is the angle of the periodic symmetry. The chart χ_{cyl} is called the **cylindrical chart**, and it admits the standard metric representation

$$g_{r\varphi z} = \operatorname{diag}\left(1, r^2, 1\right).$$

For the Hodge operator under the cylindrical chart, we have the relations:

$$\star : \begin{cases} 1 & \mapsto & r\,\mathrm{d}r \wedge \mathrm{d}\varphi \wedge \mathrm{d}z & \mapsto & 1 \\ \mathrm{d}r & \mapsto & r\,\mathrm{d}\varphi \wedge \mathrm{d}z & \mapsto & \mathrm{d}r \\ \mathrm{d}\varphi & \mapsto & \frac{1}{r}\,\mathrm{d}z \wedge \mathrm{d}r & \mapsto & \mathrm{d}\varphi \\ \mathrm{d}z & \mapsto & r\,\mathrm{d}r \wedge \mathrm{d}\varphi & \mapsto & \mathrm{d}z \end{cases}.$$

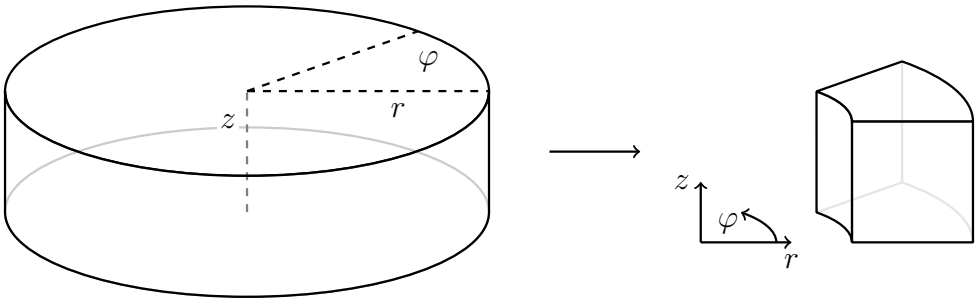

Figure 5.1: *Cylindrical chart over a part of the machine domain: complete machine geometry on the left, restriction to the subdomain on the right.*

We begin the decomposition by introducing an observer called the **radial observer** $\mathcal{O}_r = (\partial_r, \mathrm{d}r)$. This observer introduces a splitting natural to a cylindrical machine: every **cylindrical surface** with radius r as a positive constant can be employed as a computation slice. The vector field ∂_r characterizes the radial direction outward from the machine axis, and is related to the normalized basis vector $\vec{e}_r$ by the equation

$$\vec{e}_r = \frac{1}{\|\partial_r\|}\partial_r = \partial_r.$$

Armed with the radial observer, we first decompose the magnetostatic equation into horizontal and transversal parts, and then add the separately decomposed terms arising from the induced eddy currents. This decomposition can be further used to reduce the dimension of the problem by applying additional assumptions, and the arising 2D problem can then be posed on the horizontal surfaces defined by the observer.

5.1.1 Geometric decomposition

We can expand the relevant field entities A and J using the cylindrical coordinates:

$$A = A_r\mathrm{d}r + A_\varphi\mathrm{d}\varphi + A_z\mathrm{d}z$$
$$J = J_r\mathrm{d}\varphi \wedge \mathrm{d}z + J_\varphi\mathrm{d}z \wedge \mathrm{d}r + J_z\mathrm{d}r \wedge \mathrm{d}\varphi.$$

For further simplification, we can assume as a gauge condition that $\iota_{\partial_z} A = 0$ holds,[1] and then,

$$A = A_r \mathrm{d}r + A_\varphi \mathrm{d}\varphi.$$

With these expansions, the fields are split into the horizontal components

$$\begin{aligned} A_\parallel &= \iota_{\partial_r} j_{\mathrm{d}r} A = A_\varphi \mathrm{d}\varphi \\ J_\parallel &= \iota_{\partial_r} j_{\mathrm{d}r} J = J_r \mathrm{d}\varphi \wedge \mathrm{d}z, \end{aligned}$$

and into the transversal components

$$\begin{aligned} A_\perp &= \iota_{\partial_r} A = A_r \\ J_\perp &= \iota_{\partial_r} J = J_z \mathrm{d}\varphi - J_\varphi \mathrm{d}z. \end{aligned}$$

We can now write the geometric decomposition of the magnetostatic equation.

Magnetostatics

The governing equation for the magnetostatic problem reads as

$$\mathrm{d} \star_\nu \mathrm{d}A = J.$$

Using the general form of the decomposition given in Equation (4.3.12), the radial observer yields the system of equations

$$\begin{bmatrix} -\hat{\mathrm{d}} & \mathcal{L}_{\partial_r} \\ 0 & \hat{\mathrm{d}} \end{bmatrix} \hat{\star}_\nu \begin{bmatrix} \dfrac{1}{\eta_r} & 0 \\ 0 & \eta_r \end{bmatrix} \begin{bmatrix} \hat{\mathrm{d}} & 0 \\ \mathcal{L}_{\partial_r} & -\hat{\mathrm{d}} \end{bmatrix} \begin{bmatrix} A_\parallel \\ A_\perp \end{bmatrix} = \begin{bmatrix} J_\perp \\ J_\parallel \end{bmatrix},$$

where the Lie derivative $\mathcal{L}_{\partial_r}$ simplifies into differentiation ∂_r, the horizontal operators on the cylindrical surfaces are denoted by $\hat{(\cdot)}$, and

$$\eta_r = \|\sharp \mathrm{d}r\| = 1$$

holds. Expressed in coordinates, we have gathered two equations:

$$\begin{aligned} -\hat{\mathrm{d}} \, \hat{\star}_\nu \, \hat{\mathrm{d}} A_\varphi \mathrm{d}\varphi + \partial_r \, \hat{\star}_\nu \, \partial_r A_\varphi \mathrm{d}\varphi - \partial_r \, \hat{\star}_\nu \, \hat{\mathrm{d}} A_r &= J_z \mathrm{d}\varphi - J_\varphi \mathrm{d}z \\ \hat{\mathrm{d}} \, \hat{\star}_\nu \, \partial_r A_\varphi \mathrm{d}\varphi - \hat{\mathrm{d}} \, \hat{\star}_\nu \, \hat{\mathrm{d}} A_r &= J_r \mathrm{d}\varphi \wedge \mathrm{d}z. \end{aligned}$$

[1] Computing $B = \mathrm{d}A$ shows that this gauging does not pose any restrictions on the B field, which is of primary interest.

The horizontal Hodge operator was defined by $\hat{\star} = (-1)^k \eta_r \iota_{\partial_r} \star$, that is,

$$\hat{\star} : \begin{cases} 1 & \mapsto & r\,\mathrm{d}\varphi \wedge \mathrm{d}z & \mapsto & 1 \\ \mathrm{d}\varphi & \mapsto & \frac{1}{r}\,\mathrm{d}z & \mapsto & -\mathrm{d}\varphi \\ \mathrm{d}z & \mapsto & -r\,\mathrm{d}\varphi & \mapsto & -\mathrm{d}z \end{cases}.$$

Together with the material operators $\mu, \nu : \mathcal{F}^1 \to \mathcal{F}^1$, the constitutive operators are given explicitly as

$$B = \hat{\star}_\mu H = \mu \circ \hat{\star} H$$
$$H = \hat{\star}_\nu B = \nu \circ \hat{\star} B.$$

The operators μ and ν can be nonlinear or inhomogeneous, but they are demanded to be isotropic; anisotropic operators would require separate decomposition, which we have not presented. Hence, the material operators are point-wise scalar functions which locally scale the given one-form according to the material properties.

For notational clarity, let us introduce the second order differential operators

$$\Delta^\nu_{\varphi z} = \partial_\varphi \nu \frac{1}{r} \partial_\varphi + \partial_z \nu r \partial_z$$
$$\Delta^\nu_{rz} = \partial_r \nu \frac{1}{r} \partial_r + \partial_z \nu \frac{1}{r} \partial_z,$$

where now ν is a scalar function corresponding to the point-wise material operator on forms. Then, we have the decomposed system

$$\begin{bmatrix} \Delta^\nu_{\varphi z} & -\partial_\varphi \nu \frac{1}{r} \partial_r \\ -\partial_r \nu \frac{1}{r} \partial_\varphi & \Delta^\nu_{rz} \\ -\partial_r \nu r \partial_z & -\partial_\varphi \nu \frac{1}{r} \partial_z \end{bmatrix} \begin{bmatrix} A_r \\ A_\varphi \end{bmatrix} = - \begin{bmatrix} J_r \\ J_\varphi \\ J_z \end{bmatrix}.$$

It is easily seen that these equations satisfy the current continuity condition $\mathrm{d}J = 0$. Let us assume conversely that the current continuity holds, that is,

$$\partial_r J_r + \partial_\varphi J_\varphi + \partial_z J_z = 0.$$

Then, the reduced system

$$\begin{bmatrix} \Delta^\nu_{\varphi z} & -\partial_\varphi \nu \frac{1}{r} \partial_r \\ -\partial_r \nu \frac{1}{r} \partial_\varphi & \Delta^\nu_{rz} \end{bmatrix} \begin{bmatrix} A_r \\ A_\varphi \end{bmatrix} = - \begin{bmatrix} J_r \\ J_\varphi \end{bmatrix} \tag{5.1.1}$$

implies that

$$\partial_z \left(\partial_r \nu r \partial_z A_r + \partial_\varphi \nu \frac{1}{r} \partial_z A_\varphi - J_z \right) = 0, \tag{5.1.2}$$

which yields the missing equation in the system (5.1.1). Now, since

$$\nu r \partial_z A_r = H_\varphi$$
$$\nu \frac{1}{r} \partial_z A_\varphi = -H_r,$$

the implication (5.1.2) can be rewritten such that

$$\partial_z \iota_{\vec{e}_z} j_{\mathrm{d}z} (\mathrm{d}H - J) = 0,$$

which is the projection of Ampère's law onto planes with constant height z. This can then be given as a boundary condition, as fixing the projection Ampère's law for some constant z ensures the fulfillment of the missing third equation of the system in (5.1.1). Hence, Equation (5.1.1) equipped with boundary and initial conditions and the current continuity gives us the **decomposed 3D magnetostatic BVP**. The first entry of the system matrix in Equation (5.1.1),

$$\Delta^\nu_{\varphi z} A_r = -J_r, \tag{5.1.3}$$

gives the governing magnetostatic equation on a fixed cylindrical surface.

The apparent symmetry of the decomposition is explained by introducing another observer called the **angular observer** $\mathcal{O}_\varphi = (\partial_\varphi, \mathrm{d}\varphi)$. This observer introduces slicing into **radial planes** characterized by surfaces with constant angle φ. The transversal direction given by the vector field ∂_φ corresponds to the angular displacement around the machine axis, and is related to the normalized vector field $\vec{e}_\varphi$ by the equation

$$\vec{e}_\varphi = \frac{1}{\|\partial_\varphi\|} \partial_\varphi = \frac{1}{r} \partial_\varphi.$$

Then, it can be seen that the second diagonal entry of the system matrix in Equation (5.1.1) gives the governing magnetostatic equation on a fixed radial plane. Let us show this in detail.

Angular observer and radial planes

Let us denote the horizontal operators related to the radial planes by $\tilde{(\cdot)}$. For the metric compatible angular observer $\mathcal{O}_\varphi$, it holds that

$$\flat \partial_\varphi \wedge \mathrm{d}\varphi = 0 \quad \text{and} \quad \eta_\varphi = \|\sharp \mathrm{d}\varphi\| = \frac{1}{r}.$$

Then, on the radial planes, the horizontal Hodge operator becomes

$$\tilde{\star} : \begin{cases} 1 & \mapsto & -\mathrm{d}r \wedge \mathrm{d}z & \mapsto & 1 \\ \mathrm{d}r & \mapsto & -\mathrm{d}z & \mapsto & -\mathrm{d}r \\ \mathrm{d}z & \mapsto & \mathrm{d}r & \mapsto & -\mathrm{d}z \end{cases} .$$

In the decomposition earlier, we had the equation on a fixed cylindrical surface

$$-\hat{\mathrm{d}}\,\eta_r\,\hat{\star}_\nu\,\hat{\mathrm{d}}\,A_\perp + \hat{\mathrm{d}}\,\eta_r\,\hat{\star}_\nu\,\mathcal{L}_{\partial_r}\,A_\parallel = J_\parallel. \tag{5.1.4}$$

This can be related to the angular observer by setting

$$\tilde{A}_\perp = \iota_{\partial_\varphi} A = A_\varphi = \iota_{\partial_\varphi}\,A_\parallel,$$

and, conversely,

$$A_\parallel = j_{\mathrm{d}\varphi}\tilde{A}_\perp.$$

Applying this to Equation (5.1.4), we have

$$\begin{aligned} \hat{\mathrm{d}}\,\eta_r\,\hat{\star}_\nu\,\mathcal{L}_{\partial_r}\,A_\parallel &= \hat{\mathrm{d}}\,\eta_r\,\hat{\star}_\nu\,\mathcal{L}_{\partial_r}\,j_{\mathrm{d}\varphi}\,\tilde{A}_\perp = \hat{\mathrm{d}}\,\iota_{\partial_\varphi}\,\eta_r\,\eta_\varphi^2\,\hat{\star}_\nu\,\mathcal{L}_{\partial_r}\,\tilde{A}_\perp \\ &= \mathcal{L}_{\partial_\varphi}\,\eta_r\,\eta_\varphi^2\,\hat{\star}_\nu\,\mathcal{L}_{\partial_r}\,\tilde{A}_\perp. \end{aligned}$$

By interchanging the two horizontal terms, we gather the system of equations

$$\begin{bmatrix} -\hat{\mathrm{d}}\,\eta_r\,\hat{\star}_\nu\,\hat{\mathrm{d}} & \mathcal{L}_{\partial_\varphi}\,\eta_r\eta_\varphi^2\,\hat{\star}_\nu\,\mathcal{L}_{\partial_r} \\ \mathcal{L}_{\partial_r}\,\eta_\varphi\eta_r^2\,\tilde{\star}_\nu\,\mathcal{L}_{\partial_\varphi} & -\tilde{\mathrm{d}}\,\eta_\varphi\,\tilde{\star}_\nu\,\tilde{\mathrm{d}} \end{bmatrix} \begin{bmatrix} A_\perp \\ \tilde{A}_\perp \end{bmatrix} = \begin{bmatrix} J_\parallel \\ \tilde{J}_\parallel \end{bmatrix}, \tag{5.1.5}$$

where

$$\tilde{J}_\parallel = \iota_{\partial_\varphi} j_{\mathrm{d}\varphi} J = J_\varphi\,\mathrm{d}z \wedge \mathrm{d}r.$$

By coordinate expansion, Equation (5.1.5) corresponds to the magnetostatic system given by Equation (5.1.1). The diagonal entries of the system matrix are the governing equations for the 2D problems on the cylindrical slices and radial planes, respectively. The off-diagonal entries imply that *these 2D problems are coupled*; additional assumptions are needed for decoupling and, hence, dimensional reduction. The decomposition is illustrated in Figure 5.2.

Next, let us briefly comment on the decomposition of the terms arising from permanent magnets before expanding the magnetostatic problem to include eddy currents.

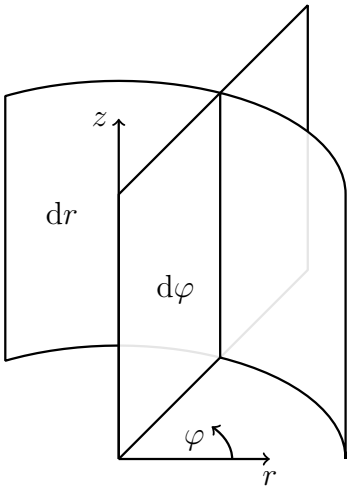

Figure 5.2: *The two observers $\mathcal{O}_r$ and $\mathcal{O}_\varphi$ split the domain into the surfaces characterized by one-forms* $\mathrm{d}r$ *and* $\mathrm{d}\varphi$*, wherein coupled 2D problems can be posed.*

Magnetization currents

The source current J was defined to contain the magnetization current J_m related to the permanent magnets, that is

$$J = J_c + J_m.$$

While the magnetization can be well handled this way, we derive the decomposition for the magnetization currents given by equation

$$J_m = \mathrm{d} \star_\nu M,$$

where M is the remanence flux . This is motivated by the implementation in Chapter 7, where we model permanent magnets with known remanence flux.

The coordinate expansion of the remanence flux yields

$$M = M_r \mathrm{d}\varphi \wedge \mathrm{d}z + M_\varphi \mathrm{d}z \wedge \mathrm{d}r + M_z \mathrm{d}r \wedge \mathrm{d}\varphi,$$

which gives the two equations of the decomposition:

$$\begin{aligned} \hat{\mathrm{d}}\, \hat{\star}_\nu \, (M_z \mathrm{d}\varphi - M_\varphi \mathrm{d}z) &= J_{m,r} \mathrm{d}\varphi \wedge \mathrm{d}z \\ \partial_r \hat{\star}_\nu \, (M_z \mathrm{d}\varphi - M_\varphi \mathrm{d}z) - \hat{\mathrm{d}}\, \hat{\star}_\nu \, M_r \mathrm{d}\varphi \wedge \mathrm{d}z &= J_{m,z} \mathrm{d}\varphi - J_{m,\varphi} \mathrm{d}z. \end{aligned}$$

This yields the decomposed system:

$$\begin{bmatrix} 0 & -\partial_z \nu r & \partial_\varphi \nu \frac{1}{r} \\ \partial_z \nu \frac{1}{r} & 0 & -\partial_r \nu \frac{1}{r} \\ -\partial_\varphi \nu \frac{1}{r} & \partial_r \nu r & 0 \end{bmatrix} \begin{bmatrix} M_r \\ M_\varphi \\ M_z \end{bmatrix} = \begin{bmatrix} J_{m,r} \\ J_{m,\varphi} \\ J_{m,z} \end{bmatrix}.$$

Let us consider the special case, in which the magnetization is constant and solely in the axial direction of the machine, that is

$$M = M_z \mathrm{d}r \wedge \mathrm{d}\varphi,$$

and $\partial_r M_z = 0$. The effect of the magnetization is then seen only in the terms

$$\partial_\varphi \nu \frac{1}{r} M_z = J_{m,r} \tag{5.1.6}$$

and

$$-\partial_r \nu \frac{1}{r} M_z = J_{m,\varphi},$$

of which Equation (5.1.6) corresponds to the cylindrical slices. We will use this simplified model later in the implementation.

Induced currents

The induced current J_e is expressed with the term

$$- \star_\sigma \left(\partial_t A + \mathrm{d}\phi \right) = J_e,$$

with the material operator σ referring to conductivity. Decomposition yields two equations

$$\begin{aligned} \hat{\star}_\sigma \, \partial_t A_\varphi \mathrm{d}\varphi + \hat{\star}_\sigma \, \hat{\mathrm{d}} \, \phi &= J_{e,z} \mathrm{d}\varphi - J_{e,\varphi} \mathrm{d}z \\ - \left(\hat{\star}_\sigma \, \partial_t A_r + \hat{\star}_\sigma \, \partial_r \phi \right) &= J_{e,r} \mathrm{d}\varphi \wedge \mathrm{d}z, \end{aligned}$$

from which we gather the system of equations

$$\begin{bmatrix} \sigma r \partial_t & 0 & \sigma r \partial_r \\ 0 & \sigma \frac{1}{r} \partial_t & \sigma \frac{1}{r} \partial_\varphi \\ 0 & 0 & \sigma r \partial_z \end{bmatrix} \begin{bmatrix} A_r \\ A_\varphi \\ \phi \end{bmatrix} = \begin{bmatrix} J_{e,r} \\ J_{e,\varphi} \\ J_{e,z} \end{bmatrix}.$$

Then, we expand Equation (5.1.1) to contain the scalar potential ϕ by Equation

(3.2.2):

$$\begin{bmatrix} \Delta^{\nu}_{\varphi z} - \sigma r \partial_t & -\partial_\varphi \nu \frac{1}{r} \partial_r & -\sigma r \partial_r \\ -\partial_r \nu \frac{1}{r} \partial_\varphi & \Delta^{\nu}_{rz} - \sigma \frac{1}{r} \partial_t & -\sigma \frac{1}{r} \partial_\varphi \end{bmatrix} \begin{bmatrix} A_r \\ A_\varphi \\ \phi \end{bmatrix} = - \begin{bmatrix} J_r \\ J_\varphi \end{bmatrix}. \tag{5.1.7}$$

Since the system given by Equation (5.1.7) is underdetermined, we need to apply additional conditions. We pose that the current continuity holds also for the induced currents alone, that is,

$$-\mathrm{d} \star_\sigma (\partial_t A + \mathrm{d}\phi) = \mathrm{d} J_e = 0.$$

Decomposition yields the equations

$$\text{(a)} \qquad \hat{\mathrm{d}}\, \hat{\star}_\sigma\, \partial_t A_\varphi \mathrm{d}\varphi + \hat{\mathrm{d}}\, \hat{\star}_\sigma\, \hat{\mathrm{d}}\phi + \partial_r\, \hat{\star}_\sigma\, \partial_t A_r + \partial_r\, \hat{\star}_\sigma\, \partial_r \phi = 0$$

$$\text{(b)} \qquad -\hat{\mathrm{d}}\, (\hat{\star}_\sigma\, \partial_t A_r + \hat{\star}_\sigma\, \partial_r \phi) = 0.$$

Equation (b) is trivially satisfied, since the term $\hat{\star}_\sigma \partial_t A_r + \hat{\star}_\sigma \partial_r \phi$ is a two-form, and hence its horizontal exterior derivative vanishes. Equation (a) implies

$$\left(\Delta^{\sigma}_{\varphi z} + \partial_r \sigma r \partial_r\right) \phi + \partial_\varphi \sigma \frac{1}{r} \partial_t A_\varphi + \partial_r \sigma r \partial_t A_r = 0.$$

Let us modify the terms related to the scalar potential by setting[2]

$$\phi = \partial_t \psi,$$

and assuming that $\partial_t \sigma = 0$.[3] Then, we have the complete system of equations

$$\begin{bmatrix} \Delta^{\nu}_{\varphi z} - \sigma r \partial_t & -\partial_\varphi \nu \frac{1}{r} \partial_r & -\partial_t \sigma r \partial_r \\ -\partial_r \nu \frac{1}{r} \partial_\varphi & \Delta^{\nu}_{rz} - \sigma \frac{1}{r} \partial_t & -\partial_t \sigma \frac{1}{r} \partial_\varphi \\ \partial_r \sigma r \partial_t & \partial_\varphi \sigma \frac{1}{r} \partial_t & \Delta^{\sigma}_{\varphi z} + \partial_r \sigma r \partial_r \end{bmatrix} \begin{bmatrix} A_r \\ A_\varphi \\ \psi \end{bmatrix} = - \begin{bmatrix} J_r \\ J_\varphi \\ 0 \end{bmatrix}. \tag{5.1.8}$$

Equation (5.1.8) represents a complete 3D system decomposed with respect to the cylindrical slices. Equipped with boundary and initial conditions, along with the current continuity condition, it gives us the **decomposed 3D magnetoquasistatic BVP**—no other assumptions are made, and the system of equations fully describes the general 3D eddy current problem. To reduce the dimensions from three to two, and to be able to pose a collection of 2D BVPs on the cylindrical slices, we need to impose further assumptions.

[2] This step is not necessary, but we do it for the sake of symmetry in the system matrix.

[3] A condition well-justified in usual modelling problems concerning AFMs.

5.1.2 Dimensional reduction: required assumptions

Our goal is to reduce the four degrees of the freedom in the potential (A, ψ) to one; that is, we want to be able to formulate a BVP in the cylindrical surface in terms of the radial potential

$$A = A_r \mathrm{d}r.$$

Thus, we must investigate the sufficient assumptions for terms A_φ, A_z and ψ to vanish.

We already saw that the initial gauge $A_z = 0$ is justified. We can further show that posing the additional condition $A_\varphi = 0$ is equivalent to assuming that *there is no radial flux* in the machine domain. The vanishing scalar potential, however, does not seem to have an equally meaningful physical interpretation.

Zero radial flux

Let us prove that the condition $A = A_r \mathrm{d}r$ equals to the assumption that there is no radial flux in the domain.

Proposition 5.1.1. Let the domain $\mathcal{M}$ be a symmetry cell of a cylindrical volume as given in Definition (5.1.1), and let us assume the gauge condition $\iota_{\partial_z} A = 0$ and the geometric decompositions as defined in Section 5.1.1. Then, $A_\parallel = 0$ if and only if $B_\parallel = 0$.

Proof. Trivially, $A_\parallel = 0$ implies $B_\parallel = \hat{\mathrm{d}} A_\parallel = 0$.

For the converse, let us consider the equivalence[4]

$$A' \sim A \;\Leftrightarrow\; \mathrm{d}A' = \mathrm{d}A,$$

yielding

$$A' = A + \mathrm{d}\alpha,\ \forall\, \alpha \in \mathcal{F}^0.$$

Now, to achieve

$$\iota_{\partial_z} A' = 0,$$

it must hold that

$$\mathcal{L}_{\partial_z} \alpha = -\iota_{\partial_z} A = 0, \tag{5.1.9}$$

which then gives the refined gauge transformation

$$A' = A + \mathrm{d}\alpha,\ \forall\, \alpha \in \mathcal{F}^0 \text{ such that } \mathcal{L}_{\partial_z} \alpha = 0.$$

[4] See Chapter 3.

Let us decompose the potential with respect to the radial observer:

$$\begin{bmatrix} A_\parallel \\ A_\perp \end{bmatrix} = \begin{bmatrix} A'_\parallel \\ A'_\perp \end{bmatrix} - \begin{bmatrix} \hat{\mathrm{d}} & 0 \\ \mathcal{L}_{\partial_r} & -\hat{\mathrm{d}} \end{bmatrix} \begin{bmatrix} \alpha \\ 0 \end{bmatrix},$$

and we have

$$B_\parallel = \hat{\mathrm{d}} A'_\parallel - \hat{\mathrm{d}}\hat{\mathrm{d}}\alpha.$$

Thus,

$$B_\parallel = 0 \;\Leftrightarrow\; \hat{\mathrm{d}} A'_\parallel = 0.$$

The potential $A'_\parallel$ can be expressed as

$$A'_\parallel = \hat{\mathrm{d}}\beta + c,\; c \in \mathcal{H}^1,$$

where $\mathcal{H}^1$ is the first cohomomology group of the horizontal domain. For the cohomology part c to vanish, it must hold that

$$\int_\Gamma A'_\parallel = 0,$$

where Γ is a generator of the first homology group of the horizontal domain.[5] Since we restricted our considerations to a segment of the complete domain under the assumption of periodicity, the horizontal domain is simply connected, and the additional condition is effectively satisfied. Hence $A'_\parallel = \hat{\mathrm{d}}\beta$.[23, pp. 15–22]

The decomposition of the operator ι_{∂_z} is

$$\begin{bmatrix} \iota_{\partial_z} & 0 \\ 0 & -\iota_{\partial_z} \end{bmatrix},$$

therefore,

$$\iota_{\partial_z} A' = 0 \;\Rightarrow\; \iota_{\partial_z} A'_\parallel = 0 \;\Rightarrow\; \mathcal{L}_{\partial_z}\beta = 0,$$

and, by condition (5.1.9), we can choose $\alpha = \beta$. Thus,

$$A_\parallel = A'_\parallel - \hat{\mathrm{d}}\alpha = \hat{\mathrm{d}}\beta - \hat{\mathrm{d}}\beta = 0.$$

□

As a desired property, an AFM ought to conform to the 'zero radial flux' - assumption.[6] However, this condition is not necessarily satisfied in practice, and the omission of the radial flux is a potential source of error [18, pp. 35–36]. We make

[5] This means that *there cannot be net axial flux* enclosed by the computation surface.
[6] Hence the name 'axial'.

the *modelling decision* not to include it, for the quasi 3D method relies on this. For a more thorough discussion on the radial flux, we refer to [16].

Under the assumption that the component A_φ of the potential vanishes, we have the governing system of equations

$$\begin{bmatrix} \Delta^{\nu}_{\varphi z} - \sigma r \partial_t & -\partial_t \sigma r \partial_r \\ -\partial_r \nu \frac{1}{r} \partial_\varphi & -\partial_t \sigma \frac{1}{r} \partial_\varphi \\ \partial_r \sigma r \partial_t & \Delta^{\sigma}_{\varphi z} + \partial_r \sigma r \partial_r \end{bmatrix} \begin{bmatrix} A_r \\ \psi \end{bmatrix} = - \begin{bmatrix} J_r \\ J_\varphi \\ 0 \end{bmatrix}.$$

Since the system contains three equations and two unknown variables, it is overdetermined and may not have a solution. Omitting the second row of the system matrix, we have the reduced system

$$\begin{bmatrix} \Delta^{\nu}_{\varphi z} - \sigma r \partial_t & -\partial_t \sigma r \partial_r \\ \partial_r \sigma r \partial_t & \Delta^{\sigma}_{\varphi z} + \partial_r \sigma r \partial_r \end{bmatrix} \begin{bmatrix} A_r \\ \psi \end{bmatrix} = - \begin{bmatrix} J_r \\ 0 \end{bmatrix},$$

plus a *residual*

$$\partial_r \nu \frac{1}{r} \partial_\varphi A_r + \partial_t \sigma \frac{1}{r} \partial_\varphi \psi - J_\varphi = \mathcal{R},$$

which, if non-zero, indicates an error in the reduced system due to the assumption of vanishing radial flux.

Yet, even the reduced system does not yield a 2D problem. For dimensional reduction, we also have to eliminate the scalar potential ψ.

Zero scalar potential

Zero scalar potential yields the system of equations

$$\begin{bmatrix} \Delta^{\nu}_{\varphi z} - \sigma r \partial_t \\ -\partial_r \nu \frac{1}{r} \partial_\varphi \\ \partial_r \sigma r \partial_t \end{bmatrix} A_r = - \begin{bmatrix} J_r \\ J_\varphi \\ 0 \end{bmatrix},$$

which, again, is overdetermined, and hence possibly not solvable. If the system is reduced to the first row only,

$$\left(\Delta^{\nu}_{\varphi z} - \sigma r \partial_t \right) A_r = -J_r, \tag{5.1.10}$$

we have an equation which contains no derivatives in the radial direction, and thus gives the governing equation for the desired 2D BVP on each cylindrical slice. Equation (5.1.10) is the characteristic equation of inhomogeneous *diffusion* or *heat problem*, which is known to have a unique solution under appropriate boundary and

initial conditions [42].[7]

However, we also have the **residuals**

$$\partial_r \nu \frac{1}{r} \partial_\varphi A_r - J_\varphi = \mathcal{R}_1 \tag{5.1.11a}$$

$$\partial_r \sigma r \partial_t A_r = \mathcal{R}_2, \tag{5.1.11b}$$

which *cannot be accounted for in the 2D setting*. The omission of these residuals bears consequences on the accuracy of the solution.

5.1.3 Dimensional reduction: residuals

The residual in Equation (5.1.11a) arises from the magnetostatic part of the decomposition. It is related to the assumption of zero radial flux, since it is induced by the vanishing term A_φ.

The second residual given by Equation (5.1.11b) is due to the extension of the magnetostatics to include eddy currents, and it is related to the vanishing scalar potential ψ.

Magnetostatics: Ampère's law

Equation (5.1.11a) can be rewritten as

$$\partial_r H_z + J_\varphi = -\mathcal{R}_1.$$

This relates to Ampère's law on a *radial plane* (Figure 5.3): Let us consider the angular observer and the decompositions of general field entities H' and J':[8]

$$\mathrm{d}H' = \begin{bmatrix} \tilde{\mathrm{d}} & 0 \\ \partial_\varphi & -\tilde{\mathrm{d}} \end{bmatrix} \begin{bmatrix} \tilde{H}'_\parallel \\ \tilde{H}'_\perp \end{bmatrix}$$

and

$$J' = \begin{bmatrix} \tilde{J}'_\parallel \\ \tilde{J}'_\perp \end{bmatrix}.$$

Ampère's law on the radial plane is now expressed by $\tilde{\mathrm{d}}\tilde{H}'_\parallel = \tilde{J}'_\parallel$. In coordinates, we have

$$(-\partial_z H'_r + \partial_r H'_z)\,\mathrm{d}z \wedge \mathrm{d}r = -J'_\varphi\,\mathrm{d}z \wedge \mathrm{d}r.$$

[7] In the implementation presented in Chapter 7, the initial conditions are posed by solving the static problem as given by Equation (5.1.3) at $t = t_0$. We had already assumed periodic conditions on parts of the boundary; the remaining part can be prescribed with a homogeneous Neumann condition or by posing zero potential 'at infinity' (see Chapter 3).

[8] 'General' in the sense they are not necessarily related to Equation (5.1.3) and its solution.

This gives us

$$\partial_r H'_z + J'_\varphi = \partial_z H'_r,$$

which then implies that

$$\mathcal{R}_1 = -\partial_z H'_r.$$

Now, it is clear that if there is no radial flux, the term H'_r must vanish. Therefore, assuming that Ampère's law holds throughout the domain, the first residual vanishes if the 'zero radial flux' -assumption holds.

Let us conversely assume that we have obtained a magnetic field H by solving a set of magnetostatic problems given by Equation (5.1.3), with the source current J and the underlying assumption of zero radial flux. By integration over a radial plane S, Equation (5.1.11a) yields

$$\int_S \partial_r H_z \,\mathrm{d}z \wedge \mathrm{d}r + \int_S J_\varphi \,\mathrm{d}z \wedge \mathrm{d}r = -\int_S \mathcal{R}_1 \,\mathrm{d}z \wedge \mathrm{d}r,$$

which, by Stokes' theorem, takes the form

$$\int_{\partial S} H_z \,\mathrm{d}z - \int_S J_\varphi \,\mathrm{d}z \wedge \mathrm{d}r = \int_S \mathcal{R}_1 \,\mathrm{d}z \wedge \mathrm{d}r.$$

Under the assumption of zero radial flux, we recover Ampère's law with the addition of the first residual:

$$\int_{\partial S} H - \int_S J = \int_S \mathcal{R}_1 \,\mathrm{d}z \wedge \mathrm{d}r.$$

Hence, a *non-zero residual is an indication that the 'zero radial flux' -assumption leads to a failure to comply with Ampère's law.*

$$\int_{\partial S} H - \int_S J = \int_S \mathcal{R}_1 \,\mathrm{d}z \wedge \mathrm{d}r$$

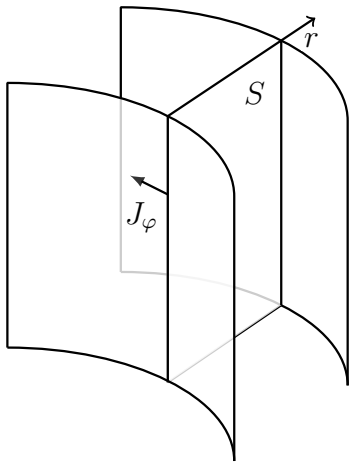

Figure 5.3: *An interpretation of the first residual: integration of the residual over the surface S corresponds to evaluating Ampère's law between two computation slices with the assumption of zero radial flux. The current J on the surface S is given solely by the component J_φ.*

Eddy currents: current continuity

In the following, we assume zero radial flux; that is, $A = A_r \mathrm{d}r$ holds.

Equation (5.1.11b) is related to the continuity condition on a *volume* between the computation slices (Figure 5.4): Consider the continuity equation

$$\mathrm{d}J'_e = 0,$$

posed on general induced current J'_e.[9] We have

$$J'_e = - \star_\sigma \, \partial_t \left(\mathrm{d}\psi' + A' \right).$$

Coordinate expansion yields

$$J'_e = -\sigma r \partial_t A'_r \, \mathrm{d}\varphi \wedge \mathrm{d}z - \sigma \partial_t \left(r \partial_r \psi' \, \mathrm{d}\varphi \wedge \mathrm{d}z + \partial_\varphi \frac{1}{r} \psi' \, \mathrm{d}z \wedge \mathrm{d}r + \partial_z r \psi' \, \mathrm{d}r \wedge \mathrm{d}\varphi \right),$$

and, by taking the exterior derivative, we obtain[10]

$$\begin{aligned} \partial_r \sigma r \partial_t A'_r &= -\partial_t \left(\partial_r \sigma r \partial_r + \partial_\varphi \sigma \frac{1}{r} \partial_\varphi + \partial_z \sigma r \partial_z \right) \psi' \\ &= -\partial_t \left(\partial_r \sigma r \partial_r + \Delta^\sigma_{\varphi z} \right) \psi', \end{aligned}$$

which then implies that

$$\mathcal{R}_2 = -\partial_t \left(\partial_r \sigma r \partial_r + \Delta^\sigma_{\varphi z} \right) \psi'.$$

Therefore, assuming that the current continuity condition holds throughout the domain, the second residual vanishes if the 'zero scalar potential' -assumption holds.

Let us conversely assume that we have obtained a magnetic potential A and an induced current J_e by solving a set of eddy current problems given by Equation (5.1.10), with the source current J and the underlying assumptions of zero radial flux and zero scalar potential. By integration over a volume V, Equation (5.1.11b) yields

$$\int_V \partial_r \sigma r \partial_t A_r \, \mathrm{d}r \wedge \mathrm{d}\varphi \wedge \mathrm{d}z = \int_V \mathcal{R}_2 \, \mathrm{d}r \wedge \mathrm{d}\varphi \wedge \mathrm{d}z.$$

Under the assumption of zero scalar potential, we recover the current continuity

[9] 'General' in the sense that it is not necessarily related to Equation (5.1.10) and its solution.
[10] Compare to the last row of the system matrix in Equation (5.1.8).

condition for the induced currents with the addition of the second residual:

$$\begin{aligned}\int_V \mathcal{R}_2 \,\mathrm{d}r \wedge \mathrm{d}\varphi \wedge \mathrm{d}z &= \int_V \partial_r \sigma r \partial_t A_r \,\mathrm{d}r \wedge \mathrm{d}\varphi \wedge \mathrm{d}z \\ &= -\int_V \partial_r J_{e,r} \,\mathrm{d}r \wedge \mathrm{d}\varphi \wedge \mathrm{d}z \\ &= -\int_{\partial V} J_{e,r} \,\mathrm{d}\varphi \wedge \mathrm{d}z \\ &= -\int_{\partial V} J_e.\end{aligned}$$

Hence, a *non-zero residual is an indication that the 'zero scalar potential' -assumption leads to a failure of the induced currents to comply with the continuity condition*, since then a net current 'leaks' out of the volume.

$$-\int_{\partial V} J_e = \int_V \mathcal{R}_2 \,\mathrm{d}r \wedge \mathrm{d}\varphi \wedge \mathrm{d}z$$

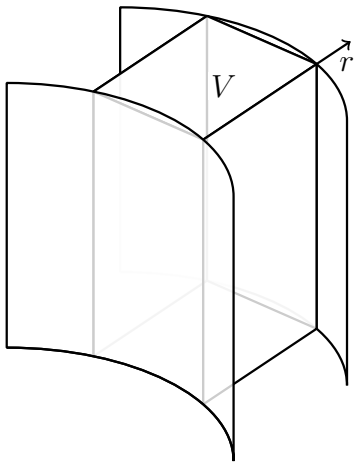

Figure 5.4: *An interpretation of the second residual: integration of the residual over the volume V corresponds to the evaluation of the current continuity condition applied to the induced currents on two computation slices. The underlying assumptions are zero radial flux and zero scalar potential.*

The residuals can be evaluated once we know the solution of the separate 2D BVPs for several cylindrical slices. However, while the residuals can be intuitively explained, there are no guidelines as to how to interpret their possible non-zero values. This would require a comparison to a complete 3D solution—then we would have a measure with which to evaluate the assumption induced errors. Even if the 3D computation was deemed infeasible, it might be possible to derive error bounds related to the residuals by mathematical means. These considerations remain open for further study.

Open question 1. How to interpret the values of the residuals? Are there definite error bounds that could be related to the residuals?

5.1.4 2D boundary value problem

Let us gather the results of the decomposition and the dimensional reduction. We assume that the computation domain has been split into cylindrical computational slices as described earlier. Then, on each slice we can pose a 2D BVP governed by the equation

$$\left(\Delta^{\nu}_{\varphi z} - \sigma r \partial_t\right) A_r = -J_r, \tag{5.1.12}$$

where we have defined the differential operator $\Delta^{\nu}_{\varphi z}$ by

$$\Delta^{\nu}_{\varphi z} = \partial_\varphi \nu \frac{1}{r} \partial_\varphi + \partial_z \nu r \partial_z,$$

and the scalar functions A_r and J_r follow from the coordinate expansion of the field entities under the cylindrical chart.

Equation (5.1.12) is accompanied by the residuals

$$\text{(a)} \qquad \partial_r \nu \frac{1}{r} \partial_\varphi A - J_\varphi = \mathcal{R}_1$$

$$\text{(b)} \qquad \partial_r \sigma r \partial_t A = \mathcal{R}_2,$$

which relate to the following assumptions:

(a) Zero radial flux. The presence of radial flux leads to a non-zero value of the residual, and implies a failure of the solution to fulfill Ampère's law on radial planes.

(b) Zero scalar potential. The presence of scalar potential leads to a non-zero value of the residual, and implies a failure of the induced currents to fulfill the current continuity condition.

Since the residuals are related to the domain between the computation slices, they can be evaluated only after solutions for several slices are known.

5.1.5 Equivalent formulations in vector calculus

Using the standard vector calculus notation, the relevant field entities are expressed in the cylindrical coordinates as

$$\vec{A} = A^r \vec{e}_r + A^\varphi \vec{e}_\varphi + A^z \vec{e}_z$$
$$\vec{J} = J^r \vec{e}_r + J^\varphi \vec{e}_\varphi + J^z \vec{e}_z,$$

where the normalized vector fields $\vec{e}_i$ relate to the basis ∂_i by

$$\vec{e}_r = \partial_r, \quad \vec{e}_\varphi = \frac{1}{r}\partial_\varphi, \quad \text{and} \quad \vec{e}_z = \partial_z.$$

The components A^i and J^i are obtained from the differential form counterparts by

$$\begin{aligned}\vec{A} = \sharp A &= \sharp\left(A_r \mathrm{d}r + A_\varphi \mathrm{d}\varphi + A_z \mathrm{d}z\right) \\ &= A_r\partial_r + A_\varphi \frac{1}{r^2}\partial_\varphi + A_z\partial_z \\ &= A_r\vec{e}_r + \frac{1}{r}A_\varphi\vec{e}_\varphi + A_z\vec{e}_z,\end{aligned}$$

and

$$\begin{aligned}\vec{J} = \sharp(\star J) &= \sharp\left(\star\left(J_r \mathrm{d}\varphi\wedge\mathrm{d}z + J_\varphi \mathrm{d}z\wedge\mathrm{d}r + J_z\mathrm{d}r\wedge\mathrm{d}\varphi\right)\right) \\ &= \sharp\left(J_r\frac{1}{r}\mathrm{d}r + J_\varphi r\mathrm{d}\varphi + J_z\frac{1}{r}\mathrm{d}z\right) = J_r\frac{1}{r}\partial_r + J_\varphi\frac{1}{r}\partial_\varphi + J_z\frac{1}{r}\partial_z \\ &= \frac{1}{r}J_r\vec{e}_r + J_\varphi\vec{e}_\varphi + \frac{1}{r}J_z\vec{e}_z.\end{aligned}$$

Hence, we gather

$$\begin{aligned}(A^r, A^\varphi, A^z) &= \left(A_r, \frac{1}{r}A_\varphi, A_z\right) \\ (J^r, J^\varphi, J^z) &= \left(\frac{1}{r}J_r, J_\varphi, \frac{1}{r}J_z\right).\end{aligned}$$

Gauging $A^z = 0$ yields the decomposed 3D magnetoquasistatic system of equations equivalent to (5.1.8)

$$\begin{bmatrix} \Delta_\nu^{\varphi z} - \sigma\partial_t & -\partial_\varphi\nu\frac{1}{r^2}\partial_r r & -\partial_t\sigma\partial_r \\ -\partial_r\nu\frac{1}{r}\partial_\varphi & \Delta_\nu^{rz} - \sigma\partial_t & -\partial_t\sigma\frac{1}{r}\partial_\varphi \\ \frac{1}{r}\partial_r\sigma r\partial_t & \partial_\varphi\sigma\frac{1}{r}\partial_t & \Delta_\sigma^{\varphi z}\partial_t + \frac{1}{r}\partial_r\sigma r\partial_r\partial_t \end{bmatrix} \begin{bmatrix} A^r \\ A^\varphi \\ \psi \end{bmatrix} = - \begin{bmatrix} J^r \\ J^\varphi \\ 0 \end{bmatrix},$$

where we have the differential operators

$$\begin{aligned}\Delta_\nu^{\varphi z} &= \partial_\varphi\nu\frac{1}{r^2}\partial_\varphi + \partial_z\nu\partial_z \\ \Delta_\nu^{rz} &= \partial_r\nu\frac{1}{r}\partial_r r + \partial_z\nu\partial_z \\ \Delta_\sigma^{\varphi z} &= \partial_\varphi\sigma\frac{1}{r^2}\partial_\varphi + \partial_z\sigma\partial_z.\end{aligned}$$

The governing equation on the horizontal surfaces is then

$$\left(\Delta_\nu^{\varphi z} - \sigma\partial_t\right)A^r = -J^r.$$

The governing equation is accompanied by the residuals

$$\partial_r \nu \frac{1}{r} \partial_\varphi A^r - J^\varphi = \mathcal{R}^1 = \mathcal{R}_1$$
$$\frac{1}{r} \partial_r \sigma r \partial_t A^r = \mathcal{R}^2 = \frac{1}{r} \mathcal{R}_2,$$

which, under the zero radial flux and zero scalar potential assumptions, can be rewritten:

$$\int_S \mathcal{R}^1 dS = \int_{\partial S} \vec{H} \cdot \vec{dl} - \int_S \vec{J} \cdot \vec{dS}$$

for the first residual, with S denoting radial planes (see Figure 5.3); and

$$\mathcal{R}^2 = -\text{div } \vec{J_e}$$

for the second residual (see Figure 5.4), with the induced current density $\vec{J_e}$ given as

$$\vec{J_e} = -\sigma \partial_t A^r \vec{e_r}.$$

5.2 Reconstruction of the 3D model

By definition, the **quasi 3D method** refers to the combination of separate 2D problems, in which several computation slices mimic the original 3D geometry. The usual approach is to divide the domain into equidistant slices and simply compute the average of the independent results with the depth of the machine core as a weighing parameter; we shall follow this practice in the implementation presented in Chapter 7.

On the other hand, the quasi 3D method can be viewed as the *discretization* of the domain. This interpretation would naturally encompass the residuals in the quasi 3D computation. To achieve the discretization as a low-level procedure within a FEA software, one would need to construct element meshes such that they are compatible in the radial direction—that is, the element nodes of the separate slices should lie on the same radial planes. No such a construction has yet been established, and it remains as the subject of a further study to investigate its feasibility.

In practice, the number of slices and their placement are decided according to engineering intuition. It is known that a differing amount of slices is needed to account for variable design parameters such as no-load phase voltage or cogging torque [33]; furthermore, the equidistant positioning of slices may not be the optimal method of discretization. Since the act of combining the slices is effectively integration in the radial direction, one possible course to improve this step would be to employ an *adaptive integration procedure*. This would ideally result in an automated mechanism which limits the number of the slices and adaptively decides their radial position.

A wide variety of such tools are available, such as Romberg's method, Gaussian quadrature or Clenshaw–Curtis quadrature (for general perspective and examples, see [43] and [44]). With an adaptive method, the number of the computation slices could be varied with user-given error bounds or by imposing an accepted maximum. Compared to the equidistant positioning, the possible improvement would be either equally accurate results with fewer slices or more accurate results with the equal number of slices. However, this remains to be tested, and is outside the scope of our work.

Open question 2. Would it be feasible to evaluate the residuals in the quasi 3D method by a proper alignment of the element meshes on the separate slices?

Open question 3. Could the currently equidistant slice positioning be improved with adaptive methods?

5.3 Efficiency and accuracy

Although analytical methods exist, their use is usually restricted to initial machine design states only. For more accurate analysis, a proper FEA is better-suited approach. The two key parameters when comparing such methods are the *efficiency* of the computation and the *accuracy* of its solution. Let us compare the full 3D and quasi 3D approaches in this respect.

By computation time comparison as reported in [33] for one time step, 3D FEA takes 23 min whereas one 2D FEA for one slice takes 6 s. For these models, 2D would become more time-consuming if the number of the computation slices was 200—which is a very impractical figure, since the usual number of slices is under 30. With several hundred time steps, the full 3D computation might take weeks, while the quasi 3D method with 10–30 slices would yield results well within a work day.

Naturally, the computation times are highly dependent on the model used: in our implementation presented in Chapter 7, one time step of a 2D model computes for 30 s, as an average. We employ 900 time steps, which then yields the overall computation time of about 7.5 hours. There are no estimates available for the computation times when using a full 3D with similar setting; based on the figures presented in [33], an educated guess would make the time needed close to two months. Thus, the quasi 2D method is clearly more efficient.

The accuracy, however, remains open for a further study. Clearly, the assumptions that allow the dimensional reduction may have significant effects on the overall results, but detailed comparisons are scarce in the literature; likewise, measuring the actual machine behaviour has proven to be difficult [40]. As for the model used in our implementation, there is no optimized 3D benchmark model to use as a

comparison.

Open question 4. What is the accuracy of the quasi 3D method compared to the full 3D approach?

6. 2D MODELS

Having now decomposed the 3D cylindrical machine model into 2D computation slices, we further present these slices with 2D coordinate charts which can be implemented in a generic FEA software. We classify these charts by the type of the apparent rotor motion; namely, to translational and rotational motion.[1] These charts together with their respective metric properties are then referred to as the translational and rotational models.

The geometry of the chosen model has implications concerning the posed BVP on the domain. We shall see that using different models may involve modifications in the initial problem setting as well as in the post-processing computations, when practical software aspects are taken into account. This sets our way to the example problem presented in Chapter 7.

6.1 Classification of coordinate charts

Let us consider a 2D chart with coordinates (a, b) involving unidirectional motion; **unidirectional** meaning that the motion is defined by the mapping

$$\Psi : p = (a, b) \mapsto p' = (a', b),$$

that is, the motion involves only one of the chosen coordinates. We choose this direction to be the apparent direction of the rotor motion, and build the coordinate charts in such a manner that unidirectional motion is achieved.

To begin with, we assume the 2D cylindrical chart involving coordinates (φ, z) as the *restriction* of the 3D chart introduced in Chapter 5 to a slice domain denoted by $\mathcal{M}_r$. We identify the chart χ_{cyl} as the 2D restriction; since we are now completely in 2D, there should not rise any confusion from the double notation. The r-coordinate is now fixed as a parameter, and we consider only one slice $\mathcal{M}_r$ at a time. In these coordinates, the rotor motion is φ-directed.

[1] The terms 'translational' and 'rotational' should be intuitively understood from the perspective of the standard Cartesian coordinate chart; their generalized abstractions called the transformation groups are outside the scope of this thesis.

6.2 Translational model

Informally, translational motion involves objects moving in such a way that their distance to any fixed point varies. Let us choose one fixed point as origin, denoted by 0 in a given coordinate system (a, b). We define **translational model** such that the motion of the objects is the mapping $\Psi : p \mapsto p'$, where $\mathrm{D}(p, 0) \neq \mathrm{D}(p', 0)$ whenever $p \neq p'$. Typical situation in the orthonormal coordinate system (x, y) can be seen in Figure 6.1.

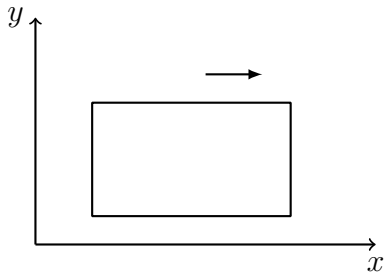

Figure 6.1: *Typical 2D translational coordinate system. The object is moving in the direction of the x-coordinate only.*

6.2.1 Constructing the translational chart

Intuitively, the translational chart is obtained by 'unrolling' a cylindrical slice. This transformation is rather straightforward to construct and yields a standard metric representation of the Cartesian coordinates.

Given the cylindrical coordinate chart, we introduce the translational chart and the orthonormal coordinate system (x, y) with the change-of-charts mapping.

Definition 6.2.1. Let χ_{tr} be a coordinate chart over $\mathcal{M}_r$ such that

$$\chi_{tr} : \mathcal{M}_r \to (x, y) \in \mathbb{R}^2,$$

and let $f = \chi_{tr} \circ \chi_{cyl}^{-1}$ be the change-of-charts mapping. The chart χ_{tr} is called the **translational chart**, if

$$f : (\varphi, z) \mapsto (x, y) \quad \text{such that} \quad x = r\varphi,\ y = z,$$

where r is a positive real number referring to the radius of the chosen slice $\mathcal{M}_r$.

The translational chart now defines a translational coordinate frame

$$\partial_x = \frac{1}{r}\partial_\varphi \quad \text{and} \quad \partial_y = \partial_z,$$

and the dual frame

$$\mathrm{d}x = r\mathrm{d}\varphi \quad \text{and} \quad \mathrm{d}y = \mathrm{d}z.$$

As the translational chart is akin to the familiar Cartesian geometry, we would also like to employ the standard representation for the metric. Then, the metric tensor should be

$$g_{xy} = \mathrm{diag}\,(1, 1)\,.$$

This implies *isometry*. For f as defined above, we have

$$g_{\varphi z} = f^* g_{xy},$$

which is straightforward to see: if $u, v \in T_p\mathcal{M}_r$, then a direct computation shows that

$$g_{xy}\,(df(u), df(v)) = g_{\varphi z}(u, v).$$

Therefore, the use of the standard metric representation is well-justified.

The properties of the translational chart with respect to the cylindrical chart, along with the explicit representation of the metric tensor, are gathered in Figure 6.2.

$$\begin{array}{rcl} \partial_x & = & 1/r\,\partial_\varphi \\ \partial_y & = & \partial_z \\ \mathrm{d}x & = & r\,\mathrm{d}\varphi \\ \mathrm{d}y & = & \mathrm{d}z \\ g_{xy} & = & \mathrm{diag}\,(1, 1) \end{array}$$

Figure 6.2: *Translational chart with respect to the cylindrical chart.*

6.3 Rotational model

Another suitable model for the motion is the rotational model, where all motion is confined around a fixed axis point. In contrast to the translational model, the distance of the moving objects to the fixed axis point is invariant. Assuming the fixed axis to be the origin, the **rotational model** is defined such that the motion is the mapping $\Psi : p \mapsto p'$, where $\mathrm{D}(p, 0) = \mathrm{D}(p', 0)$. Typically, one would choose the orthogonal coordinate system (ρ, θ) as in Figure 6.3.

We consider the change-of-charts between the 2D cylindrical and the rotational models. Further, we take a closer look at one such sub-class of mappings, namely *conformal mappings*. Our aim is to show that these type of mappings have certain desirable properties, thus motivating their use in the present modelling problem.

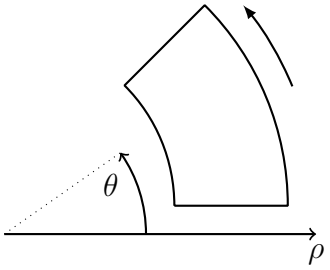

Figure 6.3: *Typical 2D rotational coordinate system. The object is moving in the direction of the θ-coordinate only.*

6.3.1 Constructing the rotational chart

Intuitively, the rotational chart is obtained by further 'twisting' an unrolled cylindrical slice. The transformation is, however, more involved than with the translational chart, and yields a metric representation that does not admit a standard form.

Given the cylindrical coordinate chart, we introduce the rotational chart and the orthogonal coordinate system (ρ, θ) with the change-of-charts mapping.

Definition 6.3.1. Let χ_{rot} be a coordinate chart over $\mathcal{M}_r$ such that

$$\chi_{rot} : \mathcal{M}_r \to (\rho, \theta) \in \mathbb{R}^2,$$

and let $f = \chi_{rot} \circ \chi_{cyl}^{-1}$ be the change-of-charts mapping. The chart χ_{rot} is now called the **rotational chart**, if

$$f : (\varphi, z) \mapsto (\rho, \theta) \quad \text{such that} \quad \theta = \varphi,\ \rho = h(z) \quad \text{with} \quad h_z = \partial_z h(z) \neq 0\ \forall z \in \mathbb{R}.$$

The rotational chart then defines a rotational coordinate frame

$$\partial_\theta = \partial_\varphi \quad \text{and} \quad \partial_\rho = \frac{1}{h_z}\partial_z,$$

and the dual frame

$$\mathrm{d}\theta = \mathrm{d}\varphi \quad \text{and} \quad \mathrm{d}\rho = h_z \mathrm{d}z.$$

Imposing isometry, we have the metric tensor

$$g_{\rho\theta} = \mathrm{diag}\left(\frac{1}{h_z^2}, r^2\right).$$

How to define the mapping h? Choosing simply $h(z) = z$ would give the metric tensor

$$g_{\rho\theta} = \mathrm{diag}\left(1, r^2\right).$$

While there is nothing peculiar in this metric tensor from the theoretical point of

view, *implementability* with a generic FEA software is another question. Generally, it is not possible for an end-user to freely modify the metric used in the software; one is usually restricted to use the standard metric, which, in the case of the rotational model, would be related to the polar coordinate system and of the form $g_{\rho\theta} = \operatorname{diag}(1, \rho^2)$. Using the metric induced by the mapping $h(z) = z$ would then result in apparently *anisotropic materials for all regions of the domain—air included.* Naturally, we would want to avoid such a situation.

If, on the other hand, we could construct a metric tensor such that

$$g_{\rho\theta} = \alpha \operatorname{diag}\left(1, \rho^2\right), \tag{6.3.1}$$

where α is a smooth and positive mapping

$$\alpha : \mathcal{M}_r \to \mathbb{R}_+,$$

the problem with global anisotropy would be solved. The metric tensor of this kind is said to be **conformal**, and there is a class of mappings that can be used to achieve this. If we construct f in such a way that it preserves the angles, we get the desired representation for the metric tensor. A mapping of this kind is called a **conformal mapping**.[2]

Conformal mappings

Suppose then we choose the function h such that it satisfies the conformal condition. For the metric representation, the assumption yields

$$\operatorname{diag}\left(\frac{1}{h_z^2}, r^2\right) = \alpha \operatorname{diag}\left(1, h^2\right),$$

from which we gather

$$\alpha = \frac{r^2}{h^2} = \frac{1}{h_z^2}.$$

We have an ordinary differential equation

$$\partial_z h(z) = \frac{1}{r}\, h(z),$$

[2]Conformal mappings have their background in complex analysis, and the mappings can be viewed from the perspective of projecting the geometry to a complex plane. The study of conformal mappings leads to the general theory of the so-called Riemann surfaces, which are an instance of *complex manifolds.* The idea of the complex plane may be useful for developing intuition of the subject if one is familiar with such transformations, but it is not necessary for our application.

which has a solution

$$h(z) = c \exp\left(\frac{z}{r}\right), \quad c \in \mathbb{R}_+ \setminus \{0\}.$$

Since $\rho = h(z)$, we have for the coordinate frames

$$\partial_\rho = \frac{r}{\rho}\partial_z \quad \text{and} \quad \mathrm{d}\rho = \frac{\rho}{r}\mathrm{d}z.$$

We denote $\lambda = r/\rho$, and call this term the **conformal factor**. For the metric tensor, we now have the representation

$$g_{\rho\theta} = \mathrm{diag}\left(\lambda^2, r^2\right) = \lambda^2 \mathrm{diag}\left(1, \rho^2\right),$$

which fulfills the desired property of Equation (6.3.1). The mapping f is clearly isometric; looking at Figure 6.3 on page 80, every circumferential curve around origin measures the same length with this metric representation, as should be. However, since this metric representation is not the standard one that would typically be employed in the polar coordinate system, any simulation model has to be carefully constructed to take this into account. These considerations are detailed in Section 6.4.

The parameter c in the mapping h can be chosen freely. One approach is to fix a **neutral line** in the rotational chart: let us set a fixed coordinate $\hat{\rho}$ and corresponding $\hat{z}$ such that $\lambda = 1$ holds on this line. This is achieved if we pose

$$c = r \exp\left(-\frac{\hat{z}}{r}\right).$$

Thus we can define

$$f : (\varphi, z) \mapsto (\rho, \theta) \quad \text{such that} \quad \theta = \varphi,\ \rho = r \exp\left(\frac{z - \hat{z}}{r}\right). \tag{6.3.2}$$

From here on, we reserve the term **rotational model** for the models that utilize conformally transformed geometry as defined in Equation 6.3.2. The properties of the rotational chart with respect to the cylindrical chart, along with the explicit representation of the metric tensor, are gathered in Figure 6.4.

$$
\begin{aligned}
\partial_\theta &= \partial_\varphi \\
\partial_\rho &= \lambda\,\partial_z \\
\mathrm{d}\theta &= \mathrm{d}\varphi \\
\mathrm{d}\rho &= 1/\lambda\,\mathrm{d}z \\
g_{\rho\theta} &= \lambda^2\,\mathrm{diag}\,(1,\rho^2) \\
\lambda &= r/\rho
\end{aligned}
$$

Figure 6.4: *Rotational chart with respect to the cylindrical chart.*

6.4 Problem setting in the 2D models

The governing equation of the 2D BVP in the cylindrical chart was given by Equation (5.1.12) as

$$\left(\Delta^{\nu}_{\varphi z} - \sigma r \partial_t\right) A_r = -J_r.$$

In this section, we investigate the equivalent problem as expressed in the translational and rotational geometries. This involves applying the change-of-charts to the governing equation, as well as to the material parameters induced by the metric-dependent constitutive equations of the fields.

This transformation is rather straightforward when the translational model is concerned, and the equivalent problem can be posed with minimal modifications. However, due to the conformal metric, the transformation to the rotational model becomes more complicated. Furthermore, we investigate the post-processing aspects of the rotational model from the perspective of a standard metric of the polar coordinate chart, since it is acknowledged that one may be restricted to use the standard metric when modelling with a generic FEA software.

6.4.1 Translational model

The transformation of Equation (5.1.12) to the translational chart gives

$$(\Delta^{\nu}_{xy} - \sigma\partial_t)A_r = -\frac{1}{r}J_r,$$

where the differential operator Δ^{ν}_{xy} is akin to the standard scalar Laplacian under Cartesian coordinates:

$$\Delta^{\nu}_{xy} = \partial_x \nu \partial_x + \partial_y \nu \partial_y.$$

The right hand side factor $1/r$ ensures that the total current remains unchanged under the change-of-charts.

Since the translational model employs the standard Cartesian metric, constructing the problem with the translational model is rather straightforward, and the

only needed modification is the scaling of the current J_r by the factor $1/r$. Post-processing functionals such as torque integration can be trivially derived by applying the cylindrical-to-translational transformation.

Vector calculus formulation

Following the vector calculus formulation given in Section 5.1.5, the governing equation in the translational model becomes

$$(\Delta_\nu^{xy} - \sigma\partial_t)A^r = -J^r,$$

where the differential operator is unchanged,

$$\Delta_\nu^{xy} = \partial_x\nu\partial_x + \partial_y\nu\partial_y.$$

The coordinate basis for the vector fields is trivial:

$$\vec{e}_x = \partial_x \quad \text{and} \quad \vec{e}_y = \partial_y.$$

6.4.2 Rotational model

Due to the conformal metric, the transformation to the rotational model is more involved. Under the change-of-charts, the differential operator $\Delta_{\varphi z}^\nu - \sigma r\partial_t$ transforms by

$$\begin{aligned}
\Delta_{\varphi z}^\nu - \sigma r\partial_t &= \partial_\varphi\nu\frac{1}{r}\partial_\varphi + \partial_z\nu r\partial_z - \sigma r\partial_t \\
&= \partial_\theta\nu\frac{1}{r}\partial_\theta + \frac{1}{\lambda}\partial_\rho\nu r\frac{1}{\lambda}\partial_\rho - \sigma r\partial_t \\
&= \frac{\rho}{r}\partial_\theta\nu\frac{1}{\rho}\partial_\theta + \frac{1}{\lambda}\partial_\rho\nu\rho\partial_\rho - \frac{r}{\rho}\sigma\rho\partial_t \\
&= \frac{1}{\lambda}\left(\partial_\theta\nu\frac{1}{\rho}\partial_\theta + \partial_\rho\nu\rho\partial_\rho - \lambda^2\sigma\rho\partial_t\right) \\
&= \frac{1}{\lambda}\left(\Delta_{\theta\rho}^\nu - \lambda^2\sigma\rho\,\partial_t\right).
\end{aligned}$$

Hence, the governing equation in the rotational chart is

$$\left(\Delta_{\theta\rho}^\nu - \lambda^2\sigma\rho\,\partial_t\right)A_r = -\lambda J_r. \tag{6.4.3}$$

However, in contrast to the translational model, the differential operator $\Delta_{\theta\rho}$ is *not* the standard scalar Laplacian under the polar coordinate system. The right hand side factor λ ensures that the total current remains unchanged under the change-of-charts. However, the *conductivity needs to be scaled by the conformal factor squared*.

This leads to inhomogeneity in the direction of the coordinate ρ.

Vector calculus formulation

Following the vector calculus formulation given in Section 5.1.5, the governing equation in the rotational model becomes

$$(\Delta_{\nu}^{\theta\rho} - \lambda^2\sigma\partial_t)A^r = -\lambda^2 J^r, \tag{6.4.4}$$

where the differential operator $\Delta_{\nu}^{\theta\rho}$ is akin to the standard scalar Laplacian under the polar coordinates:

$$\Delta_{\nu}^{\theta\rho} = \frac{1}{\rho^2}\partial_\theta\nu\partial_\theta + \frac{1}{\rho}\left(\partial_\rho\nu\rho\partial_\rho\right).$$

The orthonormal coordinate basis for the vector fields is given by

$$\vec{e}_\rho = \frac{1}{\lambda}\partial_\rho \;\text{ and }\; \vec{e}_\theta = \frac{1}{\lambda\,\rho}\partial_\theta,$$

due to the conformal metric.

The material parameter ν can be, in general, nonlinear. This yields no problems if we can use the conformal metric in computations; however, if we are restricted to the standard metric representations—mainly, due to limitations in the modelling software—the implementation becomes more complicated. The aim of the next subsection is to derive correct formulations under the assumption that we are modelling with a software that employs the standard metric representation for polar coordinates.

6.4.3 Implementing the rotational model

Let us define the **standard polar metric representation** $g_{\rho\theta}^{std}$ as

$$g_{\rho\theta}^{std} = \operatorname{diag}\left(1, \rho^2\right),$$

and assume that we are forced to carry the computations using this metric. It is clear that the representation is not correct for the rotational model; more formally, *the transformation to this model is not isometric*. Hence, we cannot directly rely on the change-of-charts. Furthermore, this implies that the conformal factor in the magnetoquasistatic problem as given in Equation (6.4.4) is presumably a constant $\lambda = 1$ under the standard software implementation. This necessitates modifications for the metric-dependent material operators and integration formulas under the metric-induced measure: from the perspective of the implementation, we need

to build a separate interface for the software to ensure that the computations yield correct results. Note that this complexity is *not an inherent characteristic of the rotational model* itself, but imposed upon by the inflexibility of the standard modelling software.

The following treatment relies on the vector calculus notation, since it is the standard language for modelling software.

Constitutive relations

From Equation (6.4.4) we obtain that the conductivity σ, as given in the original cylindrical chart, has to be scaled by the conformal factor squared. Hence, we define the conductivity σ_{std} under the standard polar metric as

$$\sigma_{std} = \lambda^2 \sigma.$$

Magnetic materials are usually characterized in terms of **magnetization curves**, that is, by giving a relation of pairs $\left(\|\vec{B}\|, \|\vec{H}\|\right)$ defined at each point in the domain—this relation is, for practical use, assumed to be functional.[3] Naturally, these field norms depend on the metric, and hence we see the effect of the conformal metric in the material parameters. In other words, we need to define the operator ν_{std} accordingly.

We know that the magnetic potential A^r, being a scalar function, is invariant under the transformation. We can then pose

$$\vec{B} = \text{curl } \vec{A},$$

where the curl -operator depends on metric, and, by the assumptions posed in the preceding chapter,

$$\vec{A} = A^r \vec{e}_r.$$

Under an orthogonal coordinate system (u_1, u_2, u_3) with the metric representation

$$g_{u_1 u_2 u_3} = \text{diag}\left(g_1^2, g_2^2, g_3^2\right),$$

[3] In general, the assumption may be flawed; consider for instance *hysteresis loops* [14, p. 233].

the explicit coordinate expansion of the curl -operator reads [15]

$$\text{curl } \vec{v} = \begin{bmatrix} \frac{1}{g_2 g_3}\left(\partial_{u_2} v^3 g_3 - \partial_{u_3} v^2 g_2\right) \\ \frac{1}{g_1 g_3}\left(\partial_{u_3} v^1 g_1 - \partial_{u_1} v^3 g_3\right) \\ \frac{1}{g_1 g_2}\left(\partial_{u_1} v^2 g_2 - \partial_{u_2} v^1 g_1\right) \end{bmatrix}, \tag{6.4.5}$$

where

$$\vec{v} = v^1 \vec{e}_{u_1} + v^2 \vec{e}_{u_2} + v^3 \vec{e}_{u_3}.$$

In two dimensions with $\vec{v} = v^3 \vec{e}_{u_3}$, we then have the curl_2 -operator

$$\text{curl}_2 \ \vec{v} = \begin{bmatrix} \frac{1}{g_2}\partial_{u_2} v^3 \\ -\frac{1}{g_1}\partial_{u_1} v^3 \end{bmatrix}.$$

Hence, under the rotational chart $(u_1, u_2) = (\rho, \theta)$, the $\vec{B}$-field has the following components:

$$B^\rho = \frac{1}{\lambda\rho}\partial_\theta A^r \ \text{ and } \ B^\theta = -\frac{1}{\lambda}\partial_\rho A^r,$$

under the orthonormal coordinate basis $(\vec{e}_\rho, \vec{e}_\theta)$. On the other hand, using the standard polar metric yields the components

$$B^\rho_{std} = \frac{1}{\rho}\partial_\theta A^r \ \text{ and } \ B^\theta_{std} = -\partial_\rho A^r,$$

under the orthonormal coordinate basis $(\vec{e}_{\rho,std}, \vec{e}_{\theta,std})$. This gives us the relationship between the field components under the different geometries:

$$\left(\lambda B^\rho, \lambda B^\theta\right) = \left(B^\rho_{std}, B^\theta_{std}\right).$$

Furthermore, by the definition of the vector norm under an orthonormal basis $(\vec{e}_1, \vec{e}_2)$,

$$\|\vec{v}\| = \|v^1\vec{e}_1 + v^2\vec{e}_2\| = \sqrt{(v^1)^2 + (v^2)^2},$$

we have

$$\|\vec{B}\|_{std} = \sqrt{(B^\rho_{std})^2 + (B^\theta_{std})^2} = \sqrt{(\lambda B^\rho)^2 + (\lambda B^\theta)^2} = \lambda \|\vec{B}\|.$$

Similar relationship holds for the $\vec{H}$-field: Consider the equation

$$\text{curl } \vec{H} = \vec{J},$$

which, by Equation (6.4.5), yields that

$$-J^r = \frac{1}{\lambda^2 \rho} \left(\partial_\theta \lambda H^\rho - \partial_\rho \lambda \rho H^\theta \right)$$

and

$$-J^r_{std} = \frac{1}{\rho} \left(\partial_\theta H^\rho_{std} - \partial_\rho \rho H^\theta_{std} \right).$$

Since by Equation (6.4.4) $J^r_{std} = \lambda^2 J^r$, we have

$$\left(\lambda H^\rho, \lambda H^\theta \right) = \left(H^\rho_{std}, H^\theta_{std} \right),$$

and

$$\|\vec{H}\|_{std} = \lambda \|\vec{H}\|.$$

Therefore, for the magnetic material relations under the change to the standard metric, it holds that

$$\left(\|\vec{B}\|, \|\vec{H}\| \right) \mapsto \left(\lambda \|\vec{B}\|, \lambda \|\vec{H}\| \right) = \left(\|\vec{B}\|_{std}, \|\vec{H}\|_{std} \right).$$

For linear magnetic materials, the magnetization curve can be explicitly expressed as a linear function:

$$\lambda \|\vec{H}\| = \nu_{std} \, \lambda \|\vec{B}\|, \quad \text{where} \quad \nu_{std} \in \mathbb{R},$$

and then, the conformal factor can be divided from both sides. Therefore, no change is needed for linear magnetic material curves, and $\nu_{std} = \nu$.

For nonlinear magnetic materials, we have the general form

$$\lambda \|\vec{H}\| = \nu_{std} \left(\lambda \|\vec{B}\| \right),$$

where ν_{std} is now a nonlinear real-valued function, dependent on the magnetic field values. In such cases, both $\|\vec{B}\|$ and $\|\vec{H}\|$ must be scaled with the conformal factor in the magnetization curve. This leads to inhomogeneity in the direction of the coordinate ρ.

The implications are that the nonlinear magnetic and all conductive regions from the cylindrical model become inhomogeneous in the rotational model. Depending on the modelling software, this may make the implementation cumbersome. We see an example in Chapter 7, where additional discretization in such material regions is

introduced to tackle the problem.

Permanent magnets

In Chapter 3, the magnetization current related to the permanent magnets was imposed as a source term:

$$J^r = J^r_c + J^r_m.$$

We define the remanence flux density $\vec{M}$ of the magnets with axial-directed permanent magnetization by

$$\vec{M} = M^z \vec{e}_z := M\vec{e}_z$$

under the cylindrical chart, and it is related to the magnetization current by

$$\text{curl } \nu \vec{M} = \vec{J}_m,$$

in which the material operator ν is assumed to be linear, and hence $\nu_{std} = \nu$.

By Equation (5.1.6),

$$J^r_m = \frac{1}{r} J_{m,r} = \frac{1}{r}\partial_\varphi \nu \frac{1}{r} M_z = \partial_\varphi \nu \frac{1}{r} M^z = \partial_\theta \nu \frac{1}{\lambda\rho} M$$

is the explicit expression for the magnetization current density. Since Equation (6.4.4) gives the source current density J^r_{std} as

$$J^r_{std} = \lambda^2 J^r,$$

we have

$$J^r_{m,std} = \lambda^2 J^r_m = \partial_\theta \nu \frac{\lambda}{\rho} M.$$

On the other hand, by Equation (6.4.5), we obtain the expression under the standard polar metric:

$$J^r_{m,std} = \left(\text{curl } \nu \vec{M}_{std}\right)^r = \partial_\theta \nu \frac{1}{\rho} M_{std}.$$

Therefore, the remanence flux density M must be scaled with the conformal factor:

$$M \mapsto \lambda M = M_{std}.$$

Post-processing: integration

In the example implementation in Chapter 7, we are interested in the values of machine torque, axial force on the stator teeth and ohmic losses in the rotor. All these involve integration of a scalar function under a given coordinate chart, and are consequently metric-related: the explicit integration formulas under the chart then depend on the metric-induced measure. Intuitively, the line lengths and surface areas are not computed in the standard manner, which leads to modifications in the integrands if we are forced to use standard polar representation of the metric.

Following from the definition of the Riemannian volume form in Chapter 2, the integral of a scalar function f under the standard polar metric yields

$$\int_\Omega f \,\mathrm{d}\Omega = \int_P \int_\Theta f \,\sqrt{\det g^{std}_{\rho\theta}}\,\mathrm{d}\rho\,\mathrm{d}\theta = \int_P \int_\Theta f\,\rho\,\mathrm{d}\rho\,\mathrm{d}\theta,$$

for integrals over a surface confined within the bounds

$$\Theta = (\theta_{min}, \theta_{max}) \quad \text{and} \quad P = (\rho_{min}, \rho_{max})\,.$$

Likewise, path integrals over paths Γ_θ and Γ_ρ are given by

$$\int_{\Gamma_\theta} f \,\mathrm{d}\Gamma_\theta = \int_\Theta f\,\rho\,\mathrm{d}\theta,$$

and

$$\int_{\Gamma_\rho} f \,\mathrm{d}\Gamma_\rho = \int_P f\,\mathrm{d}\rho.$$

The integration domains under the polar coordinate system are illustrated in Figure 6.5.

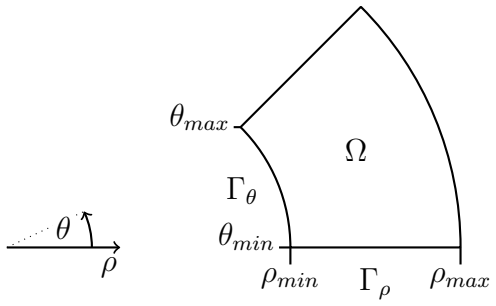

Figure 6.5: *Integration domains under the polar coordinates (ρ, θ). The coordinate-directed paths Γ_ρ and Γ_θ are defined by their respective boundaries (ρ_{min}, ρ_{max}) and $(\theta_{min}, \theta_{max})$.*

Torque Let us assume that we are computing the machine torque by integrating the Maxwell stress tensor over a surface with constant coordinate z in the air gap

between the rotor and stator, using periodicity to restrict the computation domain to a symmetry cell of the complete machine. Then, the torque density T_r per slice with a fixed radius r is given by

$$T_r = \frac{r^2}{\mu_0} \int_{\Phi} B^{\varphi} B^z \, \mathrm{d}\varphi,$$

where the integration is carried over the path confined within the bounds

$$\Phi = (\varphi_{min}, \varphi_{max}) \, .$$

For details of the derivation, see Appendix A. The overall torque T can be then computed by integrating the contribution of the slices:

$$T = \int_R T_r \, \mathrm{d}r,$$

where the integral is computed over the radial-directed path bounded by

$$R = (r_{min}, r_{max}) \, .$$

Under the rotational chart, we have

$$T_r = \frac{r^2}{\mu_0} \int_{\Theta} B^{\theta} B^{\rho} \, \mathrm{d}\theta = \frac{\lambda^2 \rho^2}{\mu_0} \int_{\Theta} B^{\theta} B^{\rho} \, \mathrm{d}\theta,$$

where now ρ is a fixed constant. This yields the integration formula under the standard polar metric:

$$T_r = \frac{\rho}{\mu_0} \int_{\Theta} B^{\theta}_{std} B^{\rho}_{std} \, \rho \, \mathrm{d}\theta = \frac{\rho}{\mu_0} \int_{\Gamma_\theta} B^{\theta}_{std} B^{\rho}_{std} \mathrm{d}\Gamma_\theta.$$

Axial force The axial force on the stator teeth is likewise computed in the air gap between the rotor and stator, by integrating over a surface with constant value of z. The force density F_r per slice with a fixed radius r is given by [22, Eq. (12)]

$$F_r = \frac{r}{2\mu_0} \int_{\Phi} (B^z)^2 \, \mathrm{d}\varphi.$$

The total force F is then obtained by integrating the contributions of the slices:

$$F = \int_R F_r \, \mathrm{d}r.$$

Under the rotational chart, the formula for the force density becomes

$$F_r = \frac{\lambda^2\rho^2}{2r\mu_0}\int_\Theta (B^\rho)^2\,\mathrm{d}\theta,$$

with ρ as a fixed constant. Hence the equation under the standard polar metric:

$$F_r = \frac{\rho}{2r\mu_0}\int_\Theta (B^\rho_{std})^2\,\rho\,\mathrm{d}\theta = \frac{1}{2\lambda\mu_0}\int_{\Gamma_\theta} (B^\rho_{std})^2\,\mathrm{d}\Gamma_\theta.$$

Ohmic losses The ohmic losses are computed over the conductive regions. Considering the density of the dissipated power P_r related to a region Ω defined on a slice with a fixed radius r, the general equation is

$$P_r = r\int_Z\int_\Phi \sigma(E^r)^2\,\mathrm{d}\varphi\,\mathrm{d}z,$$

where the integration is carried over the surface partially within the bounds

$$Z = (z_{min}, z_{max})\,.$$

Under the assumption of vanishing scalar potential from Chapter 5, the electric field E^r is a scalar function such that

$$E^r = -\partial_t A^r.$$

The total dissipated power P can then be computed by integrating the contributions of the separate slices:

$$P = \int_R P_r\,\mathrm{d}r.$$

Under the rotational chart, the power density is computed by

$$P_r = r\int_P\int_\Theta \sigma(E^r)^2\,\lambda\,\mathrm{d}\theta\,\mathrm{d}\rho,$$

and yields the formula under the standard polar metric as

$$P_r = \int_P\int_\Theta \lambda^2\sigma(E^r)^2\,\rho\,\mathrm{d}\theta\,\mathrm{d}\rho = \int_\Omega \lambda^2\sigma(E^r)^2\,\mathrm{d}\Omega.$$

By using the conductivity σ_{std} under the standard polar metric as defined earlier, we gather the expression

$$P_r = \int_\Omega \sigma_{std}(E^r)^2\,\mathrm{d}\Omega.$$

The density integrals and the transformations for the point-wise field values are gathered in Figure 6.6. Scalar functions such as the potential A^r and the electric field E^r remain unchanged. These entities are crucial to acknowledge when considering

the implementation of the rotational model with the standard tools of a generic software.

Torque:	$\frac{\rho}{\mu_0}\int_{\Gamma_\theta} B^\theta_{std} B^\rho_{std} \mathrm{d}\Gamma_\theta$	B^ρ_{std}	$=$	λB^ρ,	B^θ_{std}	$=$ λB^θ
		H^ρ_{std}	$=$	λH^ρ,	H^θ_{std}	$=$ λH^θ
Axial force:	$\frac{1}{2\lambda\mu_0}\int_{\Gamma_\theta} (B^\rho_{std})^2 \,\mathrm{d}\Gamma_\theta$	J^r_{std}	$=$	$\lambda^2 J^r$,	M_{std}	$=$ λM
Dissipated power:	$\int_\Omega \sigma_{std}(E^r)^2 \,\mathrm{d}\Omega$	σ_{std}	$=$	$\lambda^2\sigma$		

Figure 6.6: *Post-processing in the rotational chart with built-in standard polar metric: slice-wise density integrals and point-wise field values. Scalar functions A^r and E^r remain unchanged. The density integrals refer to integration on a slice with a fixed radius r, from which the overall values can be computed by integrating the contributions of the separate slices.*

7. COMPUTATIONAL IMPLEMENTATION

This study was motivated by an already existing quasi 3D modelling scheme used at KONE Corporation, which we refer to as the **simple model**. This model employs a rotational-like chart; however, the geometry is based more on engineering intuition rather than a mathematically exact transformation. While the results obtained with the simple model are satisfactory [40], we aim to show that the formal treatment of the geometry would enhance the outcome—along with the obvious benefit that the modelling scheme rests now on a more solid base as the approach is mathematically better-founded.

Our simulations show the deviations created by the slightly inexact geometry used in the simple model. We also present a comparison of the results from the translational and rotational simulations. In theory, they yield the same solution—however, limitations in the modelling software affect the outcome.

We begin building up the simulations by introducing simple test cases to validate the software implementation. This is done with the rotational model especially in mind, due to its apparent complexity compared to the translational model. For the FEA, we use Flux® modelling software.

7.1 Simplified test models

Before launching the computation of the actual machine models, we present simplified models for testing the software implementation of the computation models. We aim to keep this as brief as possible; the details of the computation models and proper justification for the analytical solutions can be found in Appendix B.

7.1.1 Basic models and solutions for magnetic potential

As a basis for testing the implementation, we use a simplified model for two-stators, one-rotor -configuration as presented in [19]: we call this setting by the name **basic model**. The rotor and stator cores are replaced with infinitely permeable boundaries, and the rotor wiring and the magnetization currents are modelled with a thin current sheet in an air region (Figure 7.1). Under the translational chart, equations (3) and (5) in [19] give the analytical solution for the magnetic potential relative to

the current sheet at $y = y_1$ as

$$A^r(x,y) = \begin{cases} \sum_n \dfrac{\mu_0}{u_n} \dfrac{\cosh(u_n y_1)}{\sinh(u_n y_2)} \cosh(u_n (y_2 - y))\, K_n(x),\ y_1 < y \leq y_2 \\ \sum_n \dfrac{\mu_0}{u_n} \dfrac{\cosh(u_n y)}{\sinh(u_n y_2)} \cosh(u_n (y_2 - y_1))\, K_n(x),\ 0 \leq y \leq y_1 \end{cases}$$

where the imposed source current $K_n(x)$ is harmonically distributed by imposing

$$K_n(x) = \hat{K}_n \sin(u_n x),$$

with $\hat{K}_n$ denoting the amplitude of the current in the sheet. The factor u_n is related to the pole pitch of the machine:

$$u_n = 2\pi n/\ell,$$

with the term ℓ being twice the pole pitch.[1]

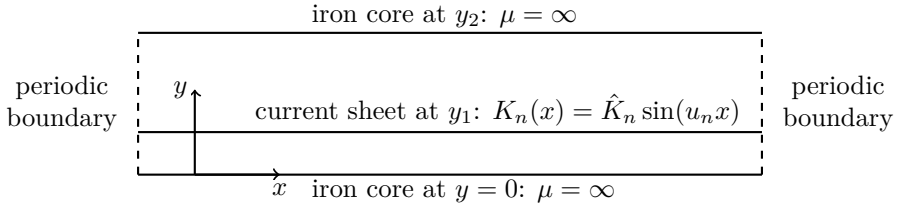

Figure 7.1: *The symmetry cell of the basic model as defined in [19], Fig. 3.*

In the case of a cylindrical slice, the solution becomes dependent on the radius r of the slice. The pole pitch is related to the symmetry cell as defined in Figure 3.2 on page 37 by

$$\ell = r\,\Phi.$$

We then gather the radius-dependent source current for a solenoidal sheet as

$$K_n(r\varphi, r) = \hat{K}_n(r) \sin(u_n r\varphi) = \hat{K}_n(r) \sin\left(2\pi n \frac{\varphi}{\Phi}\right),$$

where the amplitude $\hat{K}_n(r)$ is inversely proportional to the radius r in order to fulfill the current continuity condition in the radial direction. Following the coordinate transformation as presented in Chapter 6, the solution relative to the current sheet

[1] The chosen positive direction of the current is that of normal vector $\vec{e}_r$—in [19], the opposite holds, which yields different signature for the solution.

at $z = z_1$ is

(7.1.1)

$$A^r(r,\varphi,z) = \begin{cases} \sum_n \dfrac{\mu_0}{u_n} \dfrac{\cosh(u_n z_1)}{\sinh(u_n z_2)} \cosh(u_n (z_2 - z))\, K_n(r\varphi, r), & z_1 < z \leq z_2 \\ \sum_n \dfrac{\mu_0}{u_n} \dfrac{\cosh(u_n z)}{\sinh(u_n z_2)} \cosh(u_n (z_2 - z_1))\, K_n(r\varphi, r), & 0 \leq z \leq z_1. \end{cases}$$

This is a proper solution to the 2D problem defined by Equation (5.1.12) under the assumption of zero radial flux—however, it does not fulfill Maxwell's equations in general, since the assumption-related residual (Equation (5.1.11a)) might no vanish. This problem could be circumvented by introducing φ- and z-directed current components, which would, in turn, expand the problem to full 3D geometry: For a given radial source current we obtain the solution for the magnetic potential, from which we gather the magnetic field values in the domain. From these field values we obtain a current distribution which has the same radial component as the prescribed source current but, in general, may also have φ- and z-directed components. It should be emphasized that the decision to neglect these additional current components is a modelling simplification, and a source of error.[2]

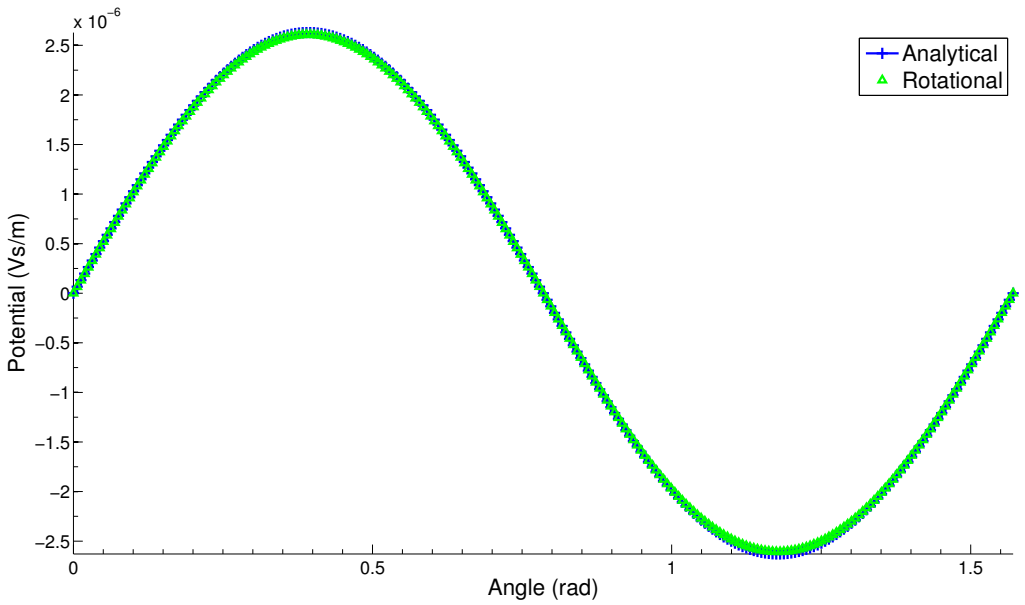

Figure 7.2: *Basic model: magnetic potential comparison between the analytical method and the rotational model on a fixed radius r. Details on the used computation models can be found in Appendix B.*

For further simplification, we consider only the restriction to $n = 1$. Results between the analytical method by Equation (7.1.1) and the Flux® models are consistent; an example of the comparison above the current sheet can be seen in Figure 7.2.

[2] Cf. [29], [30] or [31], in which this fact is not considered at all.

To generalize the situation, the air region surrounding the current sheet is replaced with regions of arbitrary yet linear and finite permeabilities: we pose μ_1 below and μ_2 above the current sheet. This yields the solution

$$A^r(r,\varphi,z) = \begin{cases} \sum_n \dfrac{\mu_2\,(1+\eta)}{u_n} \dfrac{\cosh\left(u_n\,(z_2-z)\right)\cosh\left(u_n z_1\right)}{\sinh\left(u_n z_2\right)+\eta\sinh\left(u_n\,(z_2-2z_1)\right)} K_n(r\varphi,r),\ z_1 < z \leq z_2 \\ \sum_n \dfrac{\mu_2\,(1+\eta)}{u_n} \dfrac{\cosh\left(u_n\,(z_2-z_1)\right)\cosh\left(u_n z\right)}{\sinh\left(u_n z_2\right)+\eta\sinh\left(u_n\,(z_2-2z_1)\right)} K_n(r\varphi,r),\ 0 \leq z \leq z_1, \end{cases}$$

where

$$\eta = \frac{\mu_1-\mu_2}{\mu_1+\mu_2}.$$

An example of the comparison with the results computed with the Flux® models can be seen in Figure 7.3

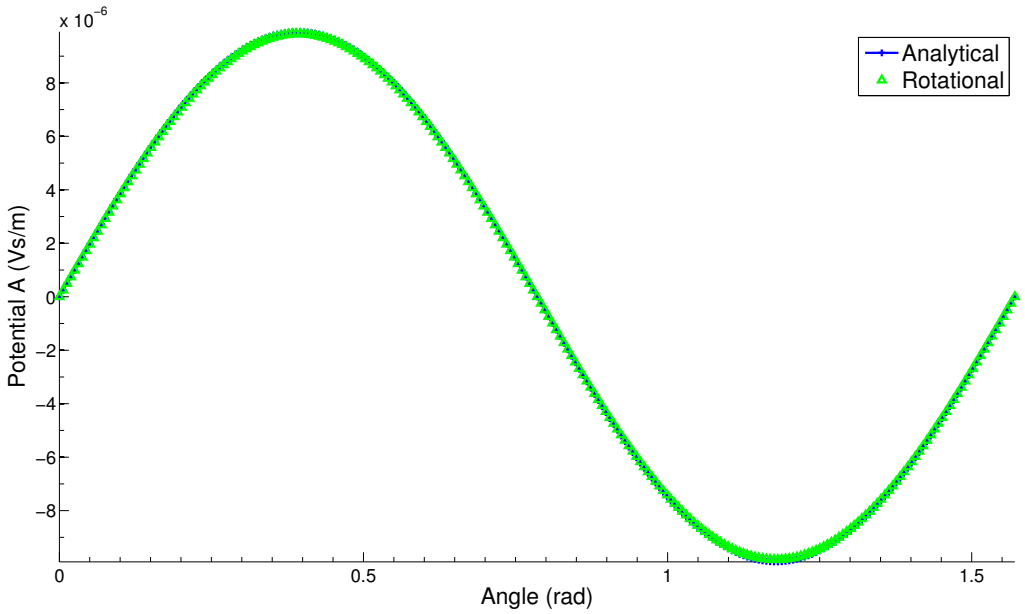

Figure 7.3: *Differing permeabilities: magnetic potential comparison between the analytical method and the rotational model on a fixed radius r. Details on the used computation models can be found in Appendix B.*

In a more realistic machine model, we would want to employ nonlinear magnetic materials. Unfortunately, no analytical method seems to be available for solving the problem when nonlinear materials are involved. Therefore, we revert to comparing the translational and the rotational models with respect to each other. This can be deemed as a valid procedure, since in the translational model there is no need for any modifications of the material parameters, and hence it can serve as a benchmark. In the rotational model, we have to scale nonlinear magnetization curves with the conformal factor, as was demonstrated in Section 6.4.

To validate the implementation of this procedure, we take the basic model and

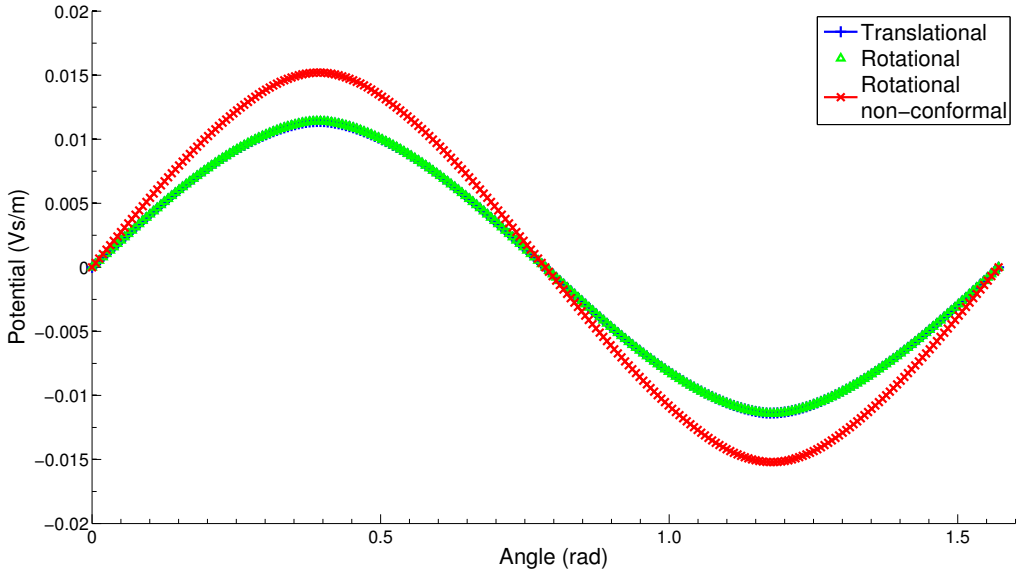

Figure 7.4: *Nonlinear materials: magnetic potential comparison between the analytical method and the rotational model on a fixed radius r. A solution from the rotational model without the conformal correction is also shown for contrast. Details on the used computation models can be found in Appendix B.*

add an extra layer of nonlinear magnetic material above the current sheet. In terms of Flux® implementation, this means further discretization of the nonlinear magnetic regions in the rotational model. These separate regions are then assigned corresponding values of the conformal factor. In the case of our simple test model, we use a division into two regions, each weighed with the average value of the conformal factor in the region. A comparison between the translational and rotational models is shown in Figure 7.4. The importance of the material modification in the rotational model is made clear by showing the ensuing discrepancy when the conformal factor is left out.

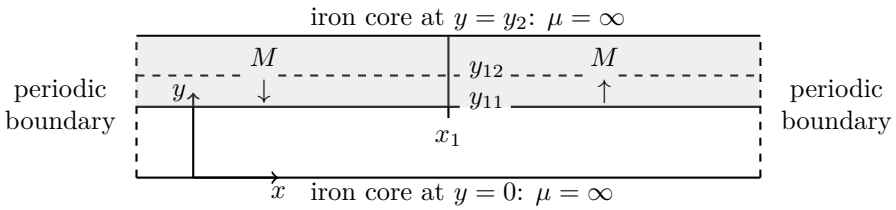

Figure 7.5: *The test model geometry for permanent magnets under the translational chart. Two magnets with opposite directions create a magnetic flux with a non-zero circulation. The dashed line at $y = y_{12}$ marks the point of division for the rotational model.*

The last geometric instance to test is the permanent magnets. The basic model is no longer sufficient, since it hides the magnetization in the source currents. We use a setting of two magnets with opposite magnetization direction, as depicted under

the translational chart in Figure 7.5.

As shown in Section 6.4, the remanence flux M needs to be scaled with the conformal factor in the rotational model, and hence we need an additional discretization. For the test computation, we use a division into two regions, each weighed with the average values of the conformal factor in the region. A comparison between the translational and rotational model is shown in Figure 7.6. The importance of the conformal factor is made visible by showing also the results of the rotational model without the correction.

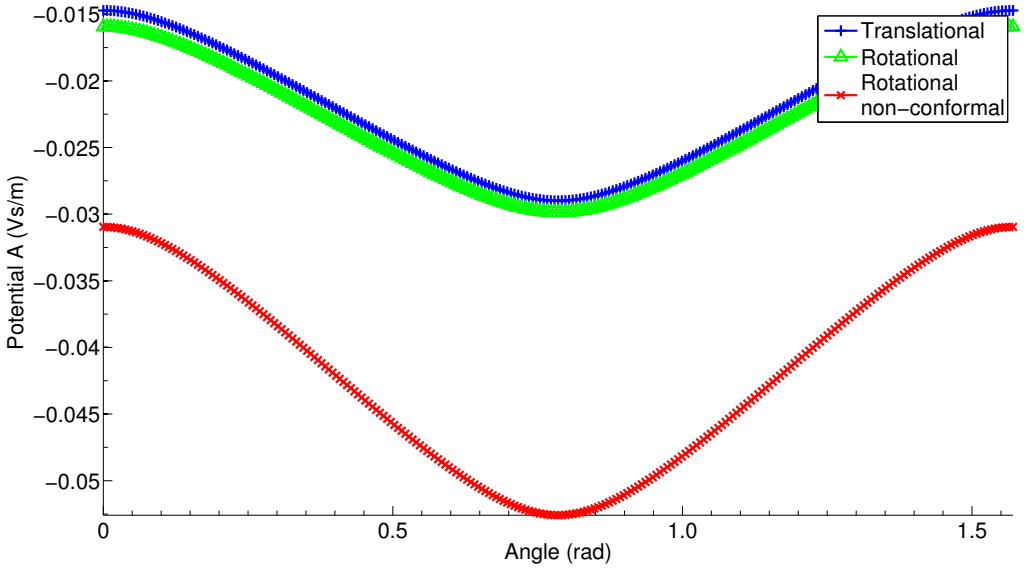

Figure 7.6: *Permanent magnets: magnetic potential comparison between the analytical method and the rotational model on a fixed radius r. A solution from the rotational model without the conformal correction is also shown for contrast. Details on the used computation models can be found in Appendix B.*

7.1.2 Post-process computations

So far, we have compared only the values of the magnetic potential as solutions to the problem defined by Equation (5.1.12). We also need to further investigate the validity of the implementation in terms of post-processing quantities such as torque and ohmic losses arising from induced eddy currents. Both of these quantities are computed by integration, and hence the metric properties of the rotational model become important as detailed in Section 6.4. Furthermore, to account for the eddy current losses, conductive regions must be imposed, and this leads to the modification of material parameters in the similar manner as with nonlinear magnetic materials.

Torque

For torque, an analytical solution can be derived by modifying the basic model as in Figure 7.1. We pose two current sheets surrounded by air such that the currents are

$$K(r\varphi, r) = \hat{K}_n(r) \sin\left(2\pi n \frac{\varphi}{\Phi}\right) \quad \text{and} \quad J(r\varphi, r) = \hat{J}_n(r) \cos\left(2\pi n \frac{\varphi}{\Phi}\right)$$

in the radial direction, and the sheets are contained in the planes $z = z_{j1}$ and $z = z_{j2}$, respectively. The model geometry using the translational coordinate chart is shown in Figure 7.7.

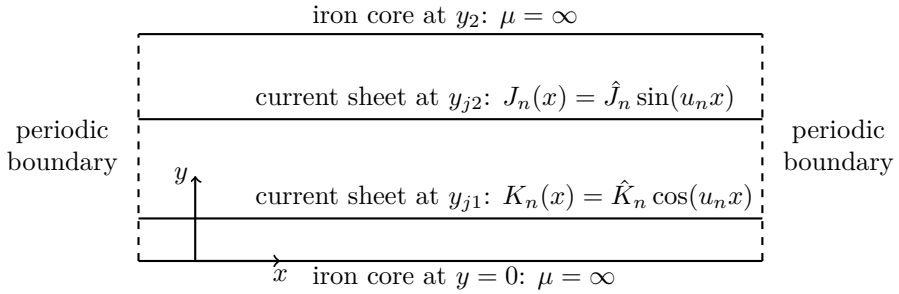

Figure 7.7: *Simplified test model for the torque computation depicted under the translational chart.*

The phase shift of the currents yields to a tangential force acting between the current sheets. It can be then shown that the torque T derived from the Maxwell stress tensor is given by [45]

$$T = \sum_n T_n = -\frac{\mu_0 \Phi}{2} \sum_n \int_{r_0}^{r_1} \hat{K}_n(r) \hat{J}_n(r) \frac{\cosh\left(u_n z_{j1}\right) \cosh\left(u_n \left(z_2 - z_{j2}\right)\right)}{\sinh\left(u_n z_2\right)} r^2 \mathrm{d}r,$$

when the integration is done in the sub-domain constrained within $(r_0, r_1) \times (0, \Phi) \times (0, z_2)$. Again, we restrict the consideration to $n = 1$.

Table 7.1 compares the translational and rotational models with respect to the analytical method at three different values of radius. The Flux®-computed torque density values are within 3% from the analytical solution; the minor deviations in the rotational model are likely due to differences in the discretization of the domain. The slice-wise contributions to the torque density are then averaged to obtain the total torque.

Table 7.1: *Torque comparison between the analytical method and the two different Flux® models. Details on the used computation models can be found in Appendix B.*

	Torque density $[Nm/m]$		
Radius $[m]$	Analytical	Translational	Rotational
0.5	-5.88	-5.87	-5.75
1.0	-12.01	-12.01	-11.92
1.5	-18.10	-18.10	-18.03
	Torque $[Nm]$		
	Analytical	Translational	Rotational
	-12.00	-12.00	-11.90

Ohmic losses

Let us next assume that the model contains conductive regions, and switch from magnetostatics to quasistatics. Then, we can investigate ohmic losses generated by induced eddy currents. A model for this is built on similar principles as we did in the case of the nonlinear magnetic materials—the difference being that now the regions are assumed to be conductive. Again, there is no known simple analytical solution for this setting, and hence we compare the translational and rotational models.

In the rotational model, we need to scale the conductivity parameters by the principle presented in Section 6.4. Similarly to the nonlinear magnetic material case, this results also in additional ρ-directed discretization for the conductive regions. We employ division into four regions, each weighed with the average value of the conformal factor in the region. An example can be seen in Figure 7.8—again, the importance of the conformal correction is highlighted by a comparison to a solution obtained with a rotational model where the conformal factor is not employed.

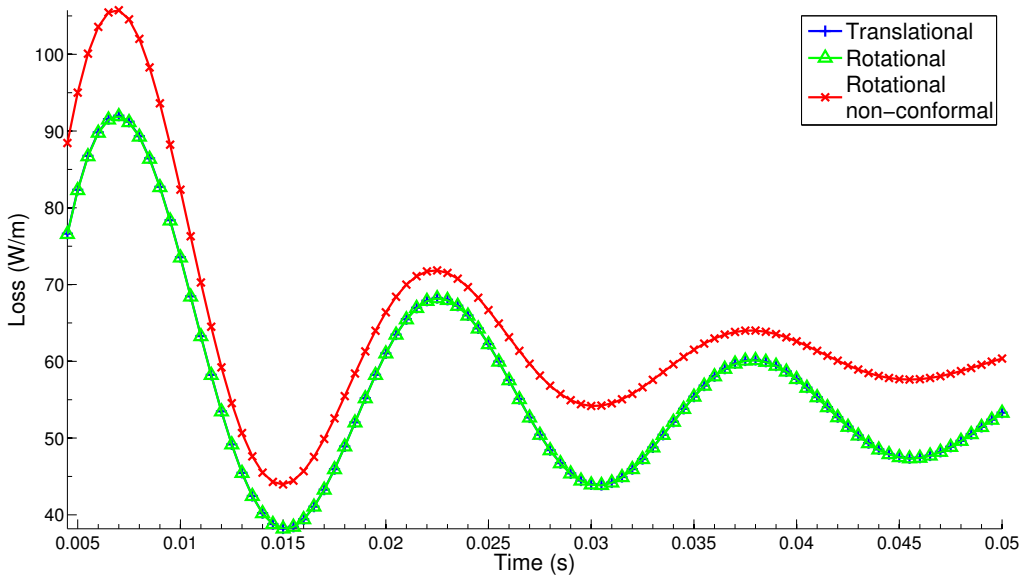

Figure 7.8: *Ohmic losses comparison between the translational and rotational models on a fixed radius r. A solution from the rotational model without conformal correction is also shown for contrast. Details on the used computation models can be found in Appendix B.*

7.2 3D machine model

Having validated the software implementation of the geometries, we now turn back to the actual modelling scheme used at KONE Corporation. The 3D machine model can be divided into symmetry cells describing one fourth of the overall geometry. Figure 7.9 depicts a part of the **machine core** as such a cell in the cylindrical coordinate system.

The model cannot be reduced to a single 2D problem, and we are thus motivated to use the quasi 3D method. In the usual quasi 3D computation, the number of slices can range from 10 to 25 [33]. However, to test our implementation, we employ only three computation slices: one from the average radius of the machine core, and two from the mid-points between the average radius and the outer boundaries of the core (see Figure 7.14 on page 107). This restriction is done to limit computation time, and it is not a recommended approach if accurate machine modelling is needed.

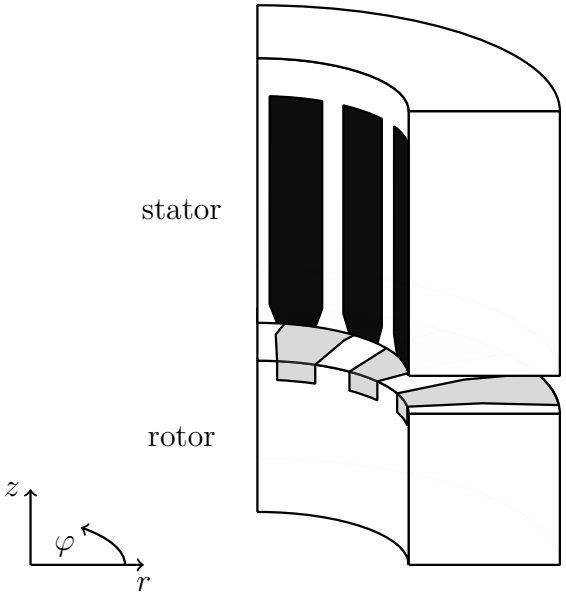

Figure 7.9: *The machine core part of the 3D symmetry cell in the cylindrical coordinate system. Compare Figure 3.2 on page 37.*

7.3 2D machine models

Since we cannot model the separate cylindrical slices with the Flux® software using the natural cylindrical coordinates, the slices are further transformed into three different planar models: the simple model, which is already in industrial use, and the translational and the rotational models, which were constructed for this study. Formal transformations from the 2D cylindrical model into the translational and the rotational models were presented in Chapter 6. The simple model is constructed according to engineering principles, as opposed to an exactly known mathematical transformation.

7.3.1 Simple model

The simple model presents a rotational-like geometry. A simplification of the stator/-rotor symmetry cells is depicted in Figure 7.10.

The model employs the standard metric representation. All dimensions in the radial direction correspond to the actual machine. In the angular direction, the stator baseline preserves its actual length, and the stator slots are constructed such that they retain their actual shape. Otherwise, angular dimensions are skewed—this can be seen especially in the teeth geometry due to the imposed shape of the slots. Thus, it is clear that *the metric of this model does not correspond to that of the original cylindrical model*. This metric distortion is a possible source of error in the computation scheme.

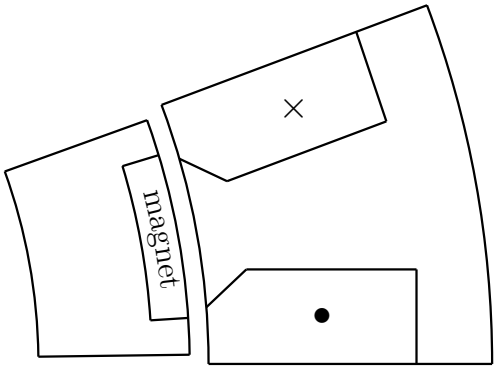

Figure 7.10: *Essential components of the 2D geometry in the simple model. Notice the rectangular shape of the stator slots, which corresponds to the dimensions of the actual machine.*

7.3.2 Translational model

The translational model is constructed by 'unrolling' the cylindrical slice into a plane. In the model, the standard metric representation is employed, and no conformal factors are needed. Therefore, the dimensions correspond to those of the actual machine. A simplified geometry for the stator/rotor symmetry cells is depicted in Figure 7.11.

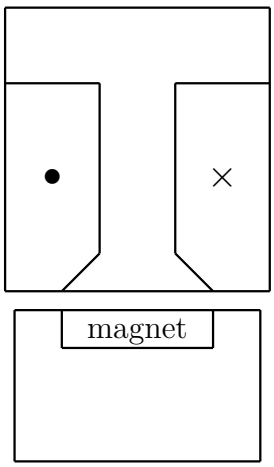

Figure 7.11: *Essential components of the 2D geometry in the translational model.*

Since the transformation to the translational model is rather straightforward and indeed isometric, we assume that the results obtained with this model are less prone to errors, and hence we look to it as a benchmark for the 2D computations. However, due to the assumptions of zero radial flux and vanishing scalar potential made in Chapter 5, any conclusions on complete machine behaviour in 3D should be taken as preliminary.

7.3.3 Rotational model

If the translational model represented an unrolled cylindrical slice, the transformation to the rotational model would mean further 'twisting' of the unrolled slice. This twisting invokes a non-standard metric representation in the chosen chart, which seems to result in the distortion of line lengths in both radial and angular direction. However, a conformally built metric tensor compensates for this apparent distortion, as detailed in Chapter 6. A simplified geometry for the stator/rotor symmetry cells is depicted in Figure 7.12.

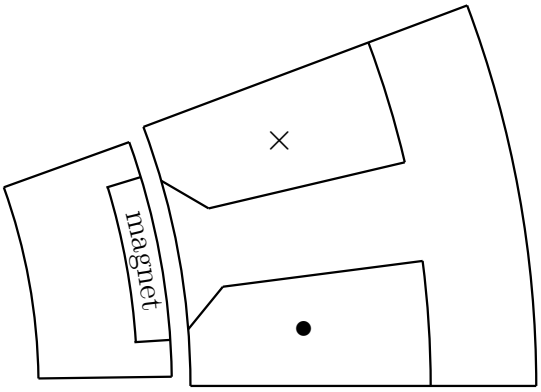

Figure 7.12: *Essential components of the 2D geometry in the rotational model, when the neutral line is set to the stator baseline.*

Theoretically, the rotational model brings in no additional errors compared to the translational model. However, in practice we need to introduce discretization in the material regions where the conformal factor is to be applied (namely, regions with conductivity and nonlinear permeability, as was shown in Section 6.4). *This is due to the limitations in the modelling software and is not an inherent character of the modelling scheme itself.* An example of the discretization can be seen in Figure 7.13.

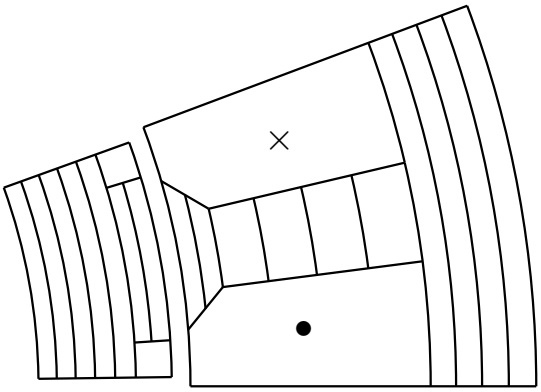

Figure 7.13: *The rotational model after additional discretization for conducting and nonlinear magnetic material regions.*

Open question 5. How to optimize the material discretization in the rotational model, if software limitations require it?

7.4 Results and analysis

The 3D domain is discretized in the radial direction to contain three computation slices, which we refer to as the inner, middle and outer slices; inner meaning the slice closest to the machine axis, middle being defined at the middle point between the core boundaries, and outer closest to the outer boundary of the machine core (Figure 7.14).

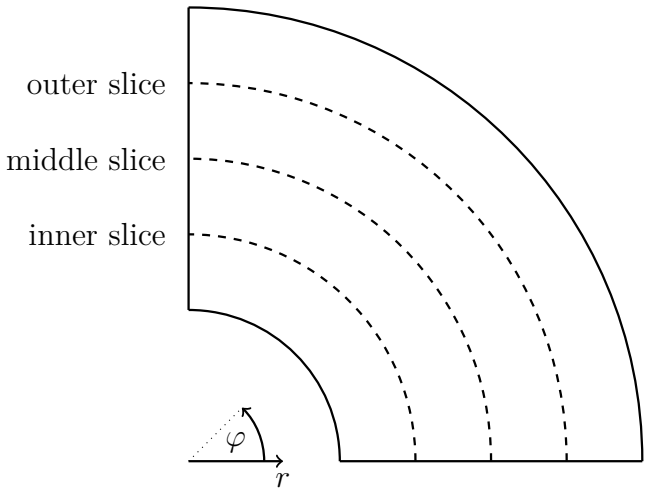

Figure 7.14: *Slicing of the computation domain.*

Relevant computation quantities are torque, axial force on the stator teeth and ohmic losses in the rotor. We compare these quantities on the separate slices, as it is seen that the models exhibit radius-dependent behaviour, and further integrate them over the complete domain to obtain the overall values. Further details on the computations can be found in Appendix B.

7.4.1 Analysis on separate slices

Table 7.2 contains a comparison between the three models on the separate slices in terms of the average values for the torque, axial force and rotor losses. The solutions from the 2D computations are weighed with the core depth in the radial direction, that is, they represent the results as if the slice in question was used to compute the quantities over the complete domain.

We see that the greatest deviations are in the ripple values; otherwise, the models are close to each other if only the average values are considered. For a more detailed analysis, the ripple waveforms and their harmonic content (obtained via discrete Fourier transform) are presented per slice in Figures 7.15–7.23.

Table 7.2: *Comparison of the three models on the separate slices. Average values for the torque, axial force and rotor losses are presented; ripple values represent the difference between the maximum and the minimum value over the computation period.*

	Simple	Translational	Rotational
Inner slice			
Torque $[Nm]$	284	274	273
Torque ripple $[Nm]$	1.43 (0.5%)	5.97 (2.2%)	5.88 (2.2%)
Force $[kN]$	8.43	8.37	8.45
Force ripple $[N]$	26.7 (0.3%)	71.6 (0.9%)	67.6 (0.8%)
Rotor losses $[W]$	108	100	100
Middle slice			
Torque $[Nm]$	352	354	354
Torque ripple $[Nm]$	1.67 (0.5%)	3.60 (1.0%)	3.72 (1.1%)
Force $[kN]$	11.1	11.2	11.3
Force ripple $[N]$	30.3 (0.3%)	67.7 (0.6%)	72.2 (0.6%)
Rotor losses $[W]$	178	188	189
Outer slice			
Torque $[Nm]$	418	422	421
Torque ripple $[Nm]$	2.67 (0.6%)	4.02 (1.0%)	3.98 (0.9%)
Force $[kN]$	13.8	14.0	14.1
Force ripple $[N]$	40.8 (0.3%)	51.0 (0.4%)	59.7 (0.4%)
Rotor losses $[W]$	264	284	286

The translational and rotational models agree consistently: the differences between the two models are less than 1% on all slices. However, the simple model is apparently more dependent on the radius. We see that on the inner slice, the simple model yields higher values than the other two, while on the outer slice the situation is opposite—on the middle slice, the models are closest to each other. This behaviour is true for all the computation quantities, and is presumed to be the effect of the geometric differences between the models.

Torque

The ripple and its harmonic content for the torque on each slice are depicted in Figures 7.15–7.17.

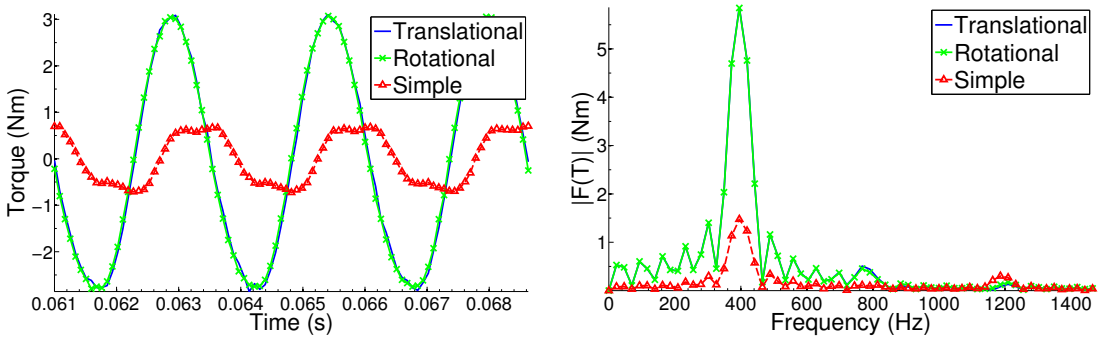

(a) Ripple waveform. (b) Frequency components of the ripple.

Figure 7.15: *Torque ripple on the inner slice.*

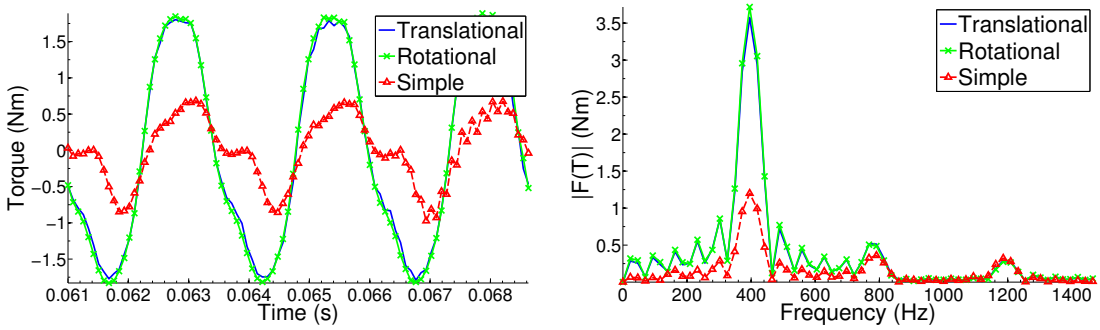

(a) Ripple waveform. (b) Frequency components of the ripple.

Figure 7.16: *Torque ripple on the middle slice.*

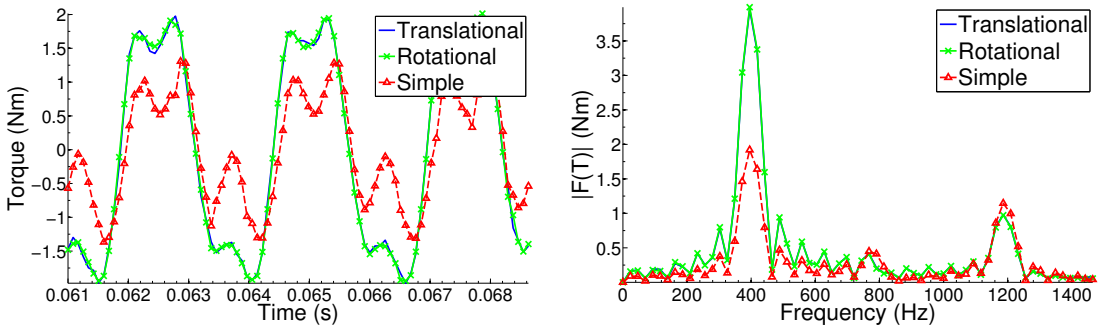

(a) Ripple waveform. (b) Frequency components of the ripple.

Figure 7.17: *Torque ripple on the outer slice.*

Axial force on stator teeth

The ripple and its harmonic content for the axial force on each slice are depicted in Figures 7.18–7.20.

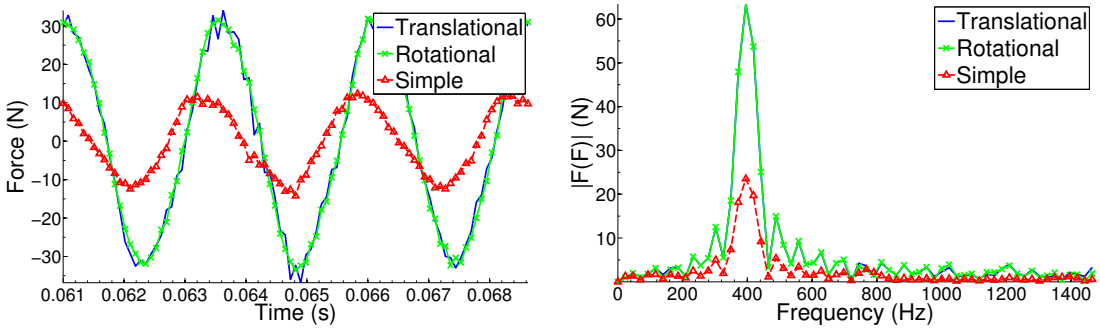

(a) Ripple waveform. (b) Frequency components of the ripple.

Figure 7.18: *The axial force ripple on the inner slice.*

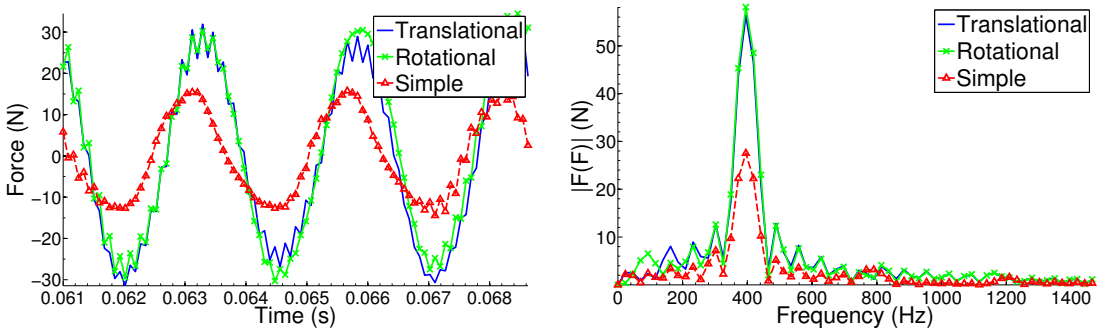

(a) Ripple waveform. (b) Frequency components of the ripple.

Figure 7.19: *The axial force ripple on the middle slice.*

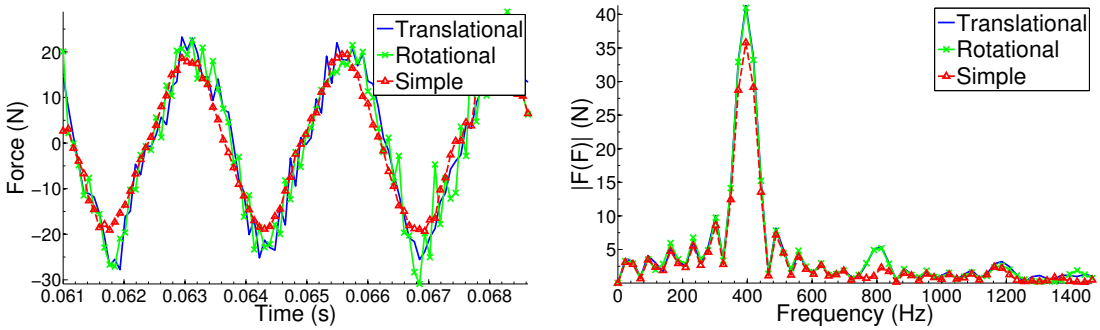

(a) Ripple waveform. (b) Frequency components of the ripple.

Figure 7.20: *The axial force ripple on the outer slice.*

Rotor losses

The ripple and its harmonic content for the ohmic losses in the rotor on each slice are depicted in Figures 7.21–7.23.

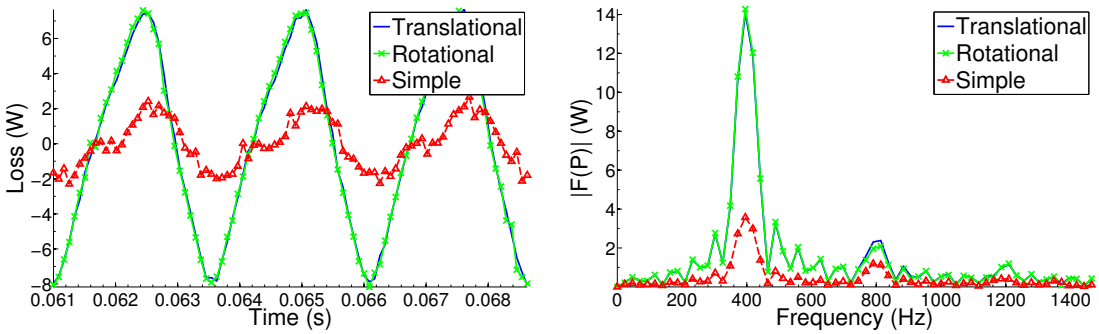

(a) Ripple waveform. (b) Frequency components of the ripple.

Figure 7.21: *Rotor losses ripple on the inner slice.*

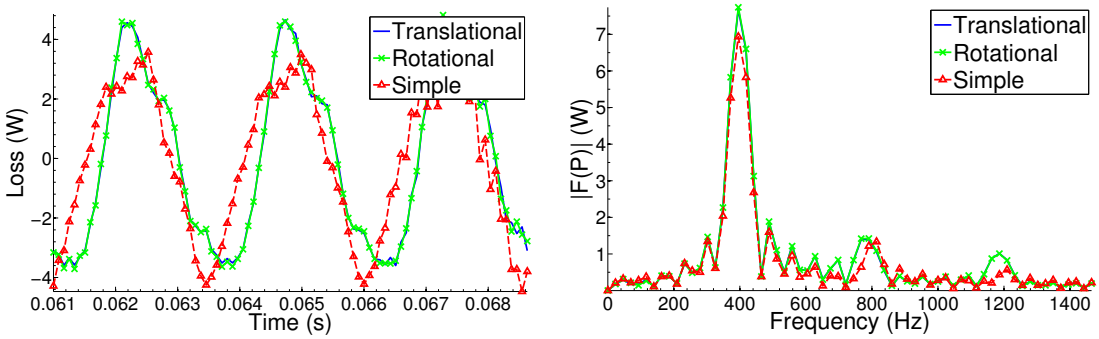

(a) Ripple waveform. (b) Frequency components of the ripple.

Figure 7.22: *Rotor losses ripple on the middle slice.*

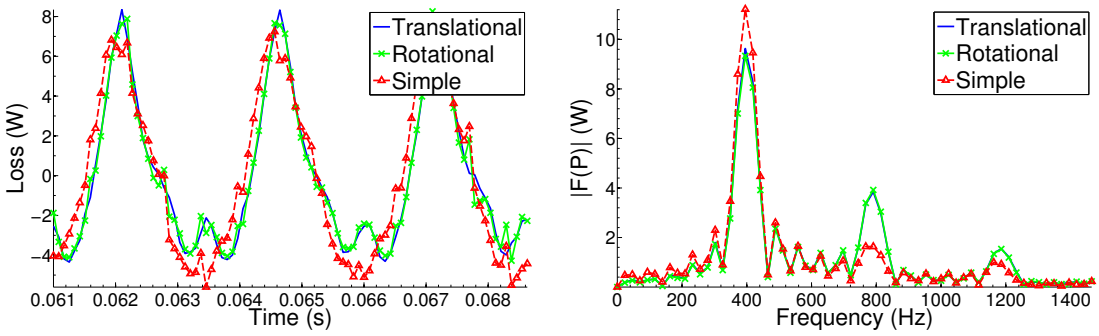

(a) Ripple waveform. (b) Frequency components of the ripple.

Figure 7.23: *Rotor losses ripple on the outer slice.*

As can be seen, the translational and rotational models show similar waveforms with respect to each other through all slices. The simple model deviates from these patterns for all computation quantities, as reflected in the harmonic content of the ripple. Thus, the difference between the ripple quantities is not only in the amplitude.

However, the effect of the distorted geometry in the simple model seems to diminish when the radius is increased; intuitively, the geometry of the simple model converges towards that of the translational and rotational models, and hence the geometric differences should play a smaller role in the results. Furthermore, it is known that the iron saturation diminishes towards the outer core boundary [46]. Therefore, the metric distortion should not affect the nonlinear magnetic materials to such extent as it does closer to the inner core boundary. This is a possible cause for the fact that the waveforms between the models are closer to each other on the outer slice than they are on the inner and middle slices.

7.4.2 Integration over the domain

The three slices can be further combined to mimic the 3D situation by taking their average and weighing the result with the core depth. The resulting values for the torque, axial force and rotor losses are given in Table 7.3.

Table 7.3: *Average values for the torque, axial force and rotor losses over complete domain.*

	Simple	Translational	Rotational
Torque $[Nm]$	352	349	348
Torque ripple $[Nm]$	1.65 (0.5%)	4.40 (1.3%)	4.44 (1.3%)
Force $[kN]$	11.1	11.2	11.3
Force ripple $[N]$	30.0 (0.3%)	63.5 (0.6%)	66.5 (0.6%)
Rotor losses $[W]$	183	191	192

Naturally, the translational and rotational models agree also over the complete domain. The results from the simple model fall well within 5% to that of the others—with the exception of the torque and force ripples, where the simple model yields significantly lower values. As an example, overall torque ripple and its harmonic content is depicted in Figure 7.24.

While the choice of using only three slices is probably not enough for any definite conclusions on the overall machine behaviour, it seems safe to assume that all three

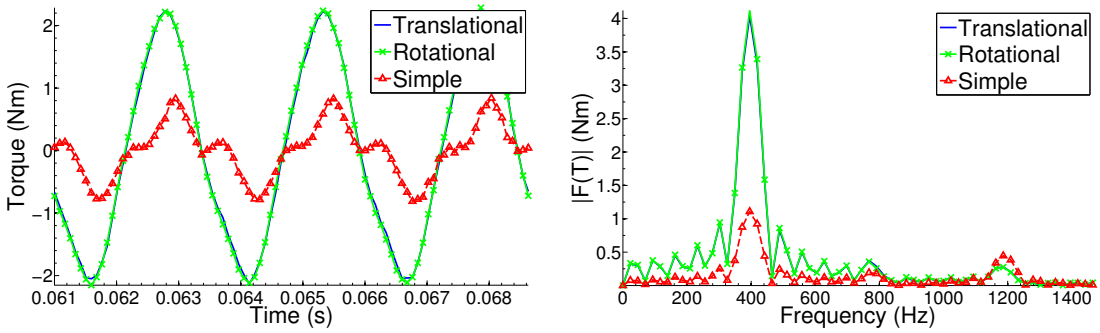

(a) Ripple waveform.

(b) Frequency components of the ripple.

Figure 7.24: *Torque ripple over the complete domain.*

models yield concurrent results over the complete domain in terms of the average values. The differences between the models are more apparent when single slices or harmonic content of the computation quantities are considered.

Open question 6. How would the models compare with a more realistic—in the sense of the demands in the actual machine design process—amount of slices?

8. CONCLUSION

The purpose of this study was to formalize the quasi 3D modelling method for axial flux machines and to test the possibly improved modelling tools with a computational implementation involving actual, industry-used machine models. The results are divided into three categories: the theoretical framework for the quasi 3D method, the definitions of the 2D models, and the implementation. We also gather here the questions that were raised during the work, yet left unanswered.

Quasi 3D method

We devoted Chapters 2 and 4 for fleshing out the more general mathematical framework on which the modelling application concerning axial flux machines was found. In Chapter 2, we presented the general mathematical background in terms of differential geometry. In Chapter 4, we introduced the concept of the observer structure as a tool for geometric decomposition and dimensional reduction. In particular, the derivation of the splitting of the Hodge operator for metric incompatible observer structure is a novel result.

The quasi 3D method was introduced in Chapter 3, and it was given a detailed treatment in the axial flux machine setting in Chapter 5. We based the method on the dimensional reduction, starting from a general 3D eddy currents problem formulation, which was then decomposed into coupled (2+1)D problems. We showed that the dimensional reduction needed to formulate independent 2D problems relied on two assumptions:

(1) the radial component of the magnetic flux in the machine domain is ignored, and

(2) the scalar potential arising from the eddy currents formulation vanishes.

The omission of the radial flux and the scalar potential gave rise to two residuals, which could be used as indicators of the modelling errors related to the assumptions.

2D modelling

The 2D cylindrical models intrinsic to the quasi 3D method were re-defined under two readily implementable geometries; namely, we introduced the translational

and the rotational models for posing the problem to a general purpose modelling software. This was done in Chapter 6.

The construction of the 2D models was based on the diffeomorphic mappings between coordinate charts, and their geometric properties were derived in detail. While both models are suitable for computations, it was shown that the construction of the translational model is significantly simpler. The non-standard metric representation employed in the rotational model may increase the complexity of the implementation, as the metric becomes dependent on the so-called conformal factor.

Implementation

In Chapter 7, the constructed 2D models were successfully tested against an already existing, industry-used model called the simple model. The software implementation made the complexity of the rotational model explicit.

Specifically, we investigated the overall electromagnetic torque of the machine, the axial force on the stator teeth, and the ohmic losses in the rotor core. The results of the computation showed good overall agreement, while the slice-wise analysis made the effect of the inaccurate geometry of the simple model apparent. The differences were most pronounced in ripple amplitudes and waveforms.

Based on the results, it was proposed that the effect of the exactness of the geometry becomes more pronounced on small radii, that is, on the computation slices closer to the machine axis. The inaccuracies of the simple model tend to diminish as the radius is extended; for machines of a greater scale, the results of the simple model should be closer to the models of more accurate geometries. Likewise, the effect of the conformal factor in the rotational model should diminish on greater radii, as long as the height of the machine axis is not increasing with the radius.

Open questions

Specifically mentioned open questions in the treatment were:

Open question 1. How to interpret the values of the residuals? Are there definite error bounds that could be related to the residuals? The residuals give error *indication*; however, a pre-computation error *estimation* would be ideal.

Open question 2. Would it be feasible to evaluate the residuals in the quasi 3D method by a proper alignment of the element meshes on the separate slices? In the present approach, the residuals are neglected, and could be evaluated only after solutions for several slices are known.

Open question 3. Could the currently equidistant slice positioning be improved with adaptive methods? Ideally, the number of the slices could be reduced, or the accuracy of the solution increased with the same number of the slices.

Open question 4. What is the accuracy of the quasi 3D method compared to the full 3D approach?

Open question 5. How to optimize the material discretization in the rotational model, if software limitations require it?

Open question 6. How would the models compare with a more realistic—in the sense of the demands in the actual machine design process—amount of slices? The three slices used in the computation can serve only as a starting point for detailed analysis of the machine.

BIBLIOGRAPHY

[1] P. Raumonen. 'Mathematical structures for dimensional reduction and equivalence classification of electromagnetic boundary value problems.' PhD thesis. Tampere University of Technology, June 2009.

[2] *Abstraction*. Wikipedia Foundation, Inc. URL: `http://en.wikipedia.org/wiki/Abstraction` (visited on 17/06/2011).

[3] T. Tarhasaari. Private communication. 12th June 2012.

[4] G.H. Hardy. *A Mathematician's Apology*. Cambridge, UK: University Press, 1940.

[5] K. Jänich. *Vector Analysis*. New York, USA: Springer–Verlag, 1993.

[6] J.R. Munkres. *Topology*. 2nd ed. Upper Saddle River, USA: Prentice Hall, 2000.

[7] J. Väisälä. *Topologia I*. Helsinki, Finland: Limes ry, 2007.

[8] M. Fecko. *Differential Geometry and Lie Groups for Physicists*. Cambridge, UK: Cambridge University Press, 2006.

[9] H. Flanders. *Differential Forms with Applications to the Physical Sciences*. New York, USA: Dover Publications, 1989.

[10] S. Kurz et al. *Dimensional reduction of field problems in a differential-forms framework—extended version*. 2008. URL: `http://cern.ch/stefankurz` (visited on 17/06/2011).

[11] W.L. Burke. *Applied Differential Geometry*. Cambridge, UK: Cambridge University Press, 1985.

[12] T. Tarhasaari. 'Mathematical structure of cochain in computational electromagnetics.' PhD thesis. Tampere University of Technology, Oct. 2002.

[13] E.J. Rothwell and M.J. Cloud. *Electromagnetics*. CRC Press, 2001.

[14] J.R. Reitz, F.J. Milford and R.W. Christy. *Foundations of Electromagnetic Theory*. 4th ed. Addison–Wesley, 1993.

[15] G. Lehner. 'Circulation'. In: *Electromagnetic Field Theory for Engineers and Physicists*. Berlin, Germany: Springer-Verlag, 2010, pp. 123–124.

[16] A.J. Hewitt. 'The effects of curvature on axial flux machine cores'. PhD thesis. The University of Southern Queensland, Mar. 2005.

[17] J.F. Gieras, R. Wang and M.J. Kamper. *Axial Flux Permanent Magnet Brushless Machines*. Kluwer Academic Publishers, 2004.

[18] A. Parviainen. 'Design of axial-flux permanent-magnet low-speed machines and performance comparison between radial-flux and axial-flux machines.' PhD thesis. Lappeenranta University of Technology, Apr. 2005.

[19] J.R. Bumby et al. 'Electromagnetic design of axial-flux permanent magnet machines'. In: *IEE Proc.-Electr. Power Appl.* 151.2 (Mar. 2004), pp. 151–160.

[20] G. Barakat et al. 'Analysis of the cogging torque behavior of a two-phase axial flux permanent magnet synchronous machine'. In: *IEEE Trans. Magn.* 37.4 (July 2001), pp. 2803–2805.

[21] D. Hanselman. *Brushless Permanent Magnet Motor Design*. 2nd ed. McGraw-Hill, 1994.

[22] Z.Q. Zhu et al. 'Analytical modelling and finite element computation of radial vibration force in fractional-slot permanent magnet brushless machines'. In: *IEEE Electric Machines and Drives Conf.* (May 2009), pp. 144–151.

[23] P. Gross and R. Kotiuga. *Electromagnetic Theory and Computation: A Topological Approach*. Cambridge, UK: Cambridge University Press, 2004.

[24] J. Fritz. *Partial Differential Equations*. 4th ed. New York, USA: Springer–Verlag, 1982.

[25] O. Bíró and K. Preis. 'On the use of the magnetic vector potential in the finite element analysis of three-dimensional eddy currents'. In: *IEEE Trans. Magn.* 25.4 (July 1984), pp. 3145–3159.

[26] J.V. Bladel. 'Lorenz or Lorentz?' In: *IEEE Antennas Propagat. Mag.* 33.2 (Apr. 1991), p. 69.

[27] G.A. Deschamps. 'Electromagnetics and differential geometry'. In: *IEEE Proc.* 69.6 (June 1981), pp. 676–696.

[28] M. Sadiku. *Numerical Techniques in Electromagnetics*. 2nd ed. New York: CRC Press, 2000.

[29] A. Azzouzi et al. 'Quasi-3-D analytical modelling of the magnetic field of an axial flux permanent-magnet synchronous machine'. In: *IEEE Trans. Energy Convers.* 20.4 (Dec. 2005), pp. 746–752.

[30] P. Virtič et al. 'Analytical analysis of magnetic field and back electromotive force calculation of an axial-flux permanent magnet synchronous generator with coreless stator'. In: *IEEE Trans. Magn.* 44.11 (Nov. 2008), pp. 4233–4236.

[31] J. Choi et al. 'Improved analytical model for electromagnetic analysis of axial flux machines with double-sided permanent magnet rotor and coreless stator windings'. In: *IEEE Trans. Magn.* 47.10 (Oct. 2011), pp. 2760–2763.

[32] H. Tiegna et al. 'Analytical modeling of the open-circuit magnetic field in axial flux permanent-magnet machines with semi-closed slots'. In: *IEEE Trans. Magn.* 48.3 (Mar. 2012), pp. 1212–1226.

[33] A. Parviainen et al. 'Modeling of axial flux permanent-magnet machines'. In: *IEEE Trans. Ind. Appl.* 40.5 (Oct. 2004), pp. 1333–1340.

[34] E.P. Furlani and M.A. Knewtson. 'A three-dimensional field solution for permanent magnet axial-field motors'. In: *IEEE Trans. Magn.* 33.3 (Mar. 1997), pp. 2322–2325.

[35] Y.N. Zhilichev. 'Three-dimensional analytic model of permanent magnet axial flux machine'. In: *IEEE Trans. Magn.* 34.6 (Nov. 1998), pp. 3897–3901.

[36] O. Axelsson and V.A. Barker. *Finite Element Solution of Boundary Value Problems*. Philadelphia, USA: SIAM, 2001.

[37] A. Bossavit. *Computational Electromagnetism*. Boston, USA: Academic Press, 1998. URL: `http://butler.cc.tut.fi/~bossavit/`.

[38] S. Gair et al. 'A new 2D FEM analysis of a disc machine with offset rotor'. In: *Power Electronics, Drives and Energy Systems for Industrial Growth Conf.* (Jan. 1996), pp. 617–621.

[39] G. Cvetkovski et al. 'Torque analysis of axial field PM synchronous motor for EV'. In: *Power Electronics, Electrical Drives, Automation and Motion Symp.* (May 2006), pp. 214–217.

[40] T. Korhonen and J. Huppunen. Private communication. Discussion at KONE. 11th June 2011.

[41] B. Auchmann et al. 'A discrete 2-D formulation for 3-D field problems with continuous symmetry'. In: *IEEE Trans. Magn.* 46.8 (2010), pp. 3508–3511.

[42] R. Dennemeyer. 'The Heat Equation'. In: *Introduction to Partial Differential Equations and Boundary Value Problems*. USA: McGraw–Hill, 1968, pp. 282–321.

[43] J. R. Rice. 'A metalgorithm for adaptive quadrature'. In: *Journal of the ACM* 22.1 (Jan. 1975), pp. 61–82.

[44] W.H. Press, S.A. Teukolsky and B.P. Flannery. 'Adaptive Quadrature'. In: *Numerical Recipes: The Art of Scientific Computing*. 3rd ed. New York: Cambridge University Press, 2007, pp. 194–196.

[45] S. Kurz. Private communication. 5th Dec. 2011.

[46] T. Korhonen and A. Burakov. Private communication. Discussion at KONE. 4th Apr. 2012.

Appendices

A. MATHEMATICAL DETAILS

Horizontal Hodge operator

In Chapter 4, we defined the horizontal Hodge operator as follows:

$$\hat{\star} = \frac{1}{\eta_s}\, \iota_{\vec{t}}\, j_{\mathrm{d}s} \star j_{\mathrm{d}s}.$$

Proposition. Let (u_i) be a positively oriented orthonormal basis of any given horizontal surface $\mathcal{T}_t$, and ω a horizontal k-form. Then,

$$\hat{\star}\omega(u_{k+1}, \ldots, u_{n-1}) = \omega(u_1, \ldots, u_k).$$

Proof. Let (v_i) be a positively oriented orthonormal basis of $T_p\mathcal{M}$. For the Hodge operator, it holds by definition that

$$\star\omega(v_{k+1}, \ldots, v_n) = \omega(v_1, \ldots, v_k).$$

The complementation

$$(\frac{1}{\eta_s}\sharp \mathrm{d}s, u_1, \ldots, u_{n-1})$$

of the basis (u_i) is a positively oriented orthonormal basis of $T_p\mathcal{M}$. By Equation (4.3.6),

$$\begin{aligned}
\hat{\star}\omega(u_{k+1}, \ldots, u_{n-1}) &= \left((-1)^k\, \frac{1}{\eta_s}\, \iota_{\vec{t}}\, j_{\mathrm{d}s}\, \iota_{\sharp \mathrm{d}s} \star\, \omega\right)(u_{k+1}, \ldots, u_{n-1}) \\
&= \left(\iota_{\vec{t}}\, j_{\mathrm{d}s}\, (-1)^k\, \frac{1}{\eta_s}\, \iota_{\sharp \mathrm{d}s} \star\, \omega\right)(u_{k+1}, \ldots, u_{n-1}) \\
&= \vartheta_{\parallel}(u_{k+1}, \ldots, u_{n-1}),
\end{aligned}$$

where

$$\vartheta = (-1)^k\, \frac{1}{\eta_s}\, \iota_{\sharp \mathrm{d}s} \star\, \omega.$$

But u_i are horizontal vectors, and it was shown in Chapter 4 that then

$$\vartheta_{\parallel}(u_{k+1}, \ldots, u_{n-1}) = \vartheta(u_{k+1}, \ldots, u_{n-1}).$$

Hence

$$\begin{aligned}\hat{\star}\omega(u_{k+1},\dots,u_{n-1}) &= \left((-1)^k \frac{1}{\eta_s}\, \iota_{\sharp \mathrm{d}s} \star\, \omega\right)(u_{k+1},\dots,u_{n-1}) \\ &= (-1)^k \star \omega(\frac{1}{\eta_s}\sharp \mathrm{d}s, u_{k+1},\dots,u_{n-1}).\end{aligned}$$

Now,

$$vol(\frac{1}{\eta_s}\sharp \mathrm{d}s, u_1,\dots,u_{n-1}) = (-1)^k vol(u_1,\dots,u_k, \frac{1}{\eta_s}\sharp \mathrm{d}s, u_{k+1},\dots,u_{n-1}),$$

and hence,

$$\hat{\star}\omega(u_{k+1},\dots,u_{n-1}) = (-1)^k \star \omega(\frac{1}{\eta_s}\sharp \mathrm{d}s, u_{k+1},\dots,u_{n-1}) = \omega(u_1,\dots,u_k).$$

□

Electromagnetic torque

In Chapter 6, we gave the formula for computing the electromagnetic torque density on a single slice at radius r as follows:

$$T_r = \frac{r^2}{\mu_0}\int_{\Phi} B^{\varphi} B^{z}\, \mathrm{d}\varphi.$$

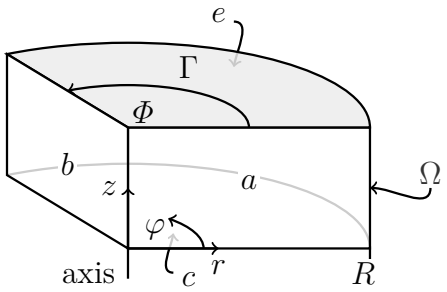

Figure A.1: *The rotor domain Ω under the cylindrical coordinates. The surface Γ is located in the air gap at $z = const$. Compare the geometry in Figure 3.2, of which the rotor domain constitutes the lower part.*

The formula for torque $\vec{T}$ on the rotor can be derived using the Maxwell stress tensor σ [13, p. 73–74]

$$\vec{T} = \int_{\partial\Omega} r\vec{e}_r \times (\sigma \cdot \vec{n})\mathrm{d}a,$$

where the rotor (and no parts of the stator) of the machine is enclosed by the volume Ω as in Figure A.1.

Under the assumptions of

(1) no radial flux,

(2) tangential boundary condition at the surface $z = 0$: $\vec{B} \cdot \vec{n} = 0$,

(3) periodic symmetry on the boundaries a and b,

the expression for the torque can be simplified. The relevant component

$$\vec{T}_z = T\vec{e}_z$$

is obtained from an integral over the surface Γ only. Under the cylindrical coordinates, this yields the formula

$$T = \int_0^R \frac{r^2}{\mu_0} \int_0^{\Phi} B^{\varphi} B^z \, \mathrm{d}\varphi \, \mathrm{d}r,$$

from which the density T_r at a fixed radius r follows by setting

$$T = \int_0^R T_r \, \mathrm{d}r.$$

B. IMPLEMENTATION

Test models

Herein one finds details of the example implementations in Section 7.1. The width of the domain was set to be $\Phi = \pi/2$ for the rotational models, and $L = r\Phi$ for the translational models. The angle Φ is the angle of assumed periodicity in the original 3D cylindrical model.

Source current

The source current K in [19] is defined as a sum of terms

$$K_n(x) = \hat{K}_n \sin(u_n x).$$

Taking into account the dimensional reduction behind the 2D model, we assume radial dependence:

$$K_n(x, r) = \hat{K}_n(r) \sin(u_n x),$$

where

$$u_n = \frac{2\pi n}{\ell} = \frac{2\pi n}{r\Phi}.$$

The transformation between the cylindrical and the translational charts defined the relations

$$x = r\varphi, \quad \mathrm{d}x = r\mathrm{d}\varphi,$$

and hence for the *current one-form* K_n it holds that

$$K_n = K_n(x, r)\mathrm{d}x = K_n(r\varphi, r)r\mathrm{d}\varphi = \hat{K}_n(r)r \sin(u_n r\varphi)\,\mathrm{d}\varphi.$$

Under the cylindrical coordinates, we then have

$$K_{\varphi,n} = K_n(r\varphi, r)r.$$

Following the continuity condition $\mathrm{d}K = 0$, this gives

$$\partial_r K_{\varphi,n} = \partial_r \left(\hat{K}_n(r)r \sin\left(\frac{2\pi n}{\Phi}\varphi\right)\right) = 0,$$

and therefore

$$\partial_r \hat{K}_n(r) r = 0,$$

rendering the term $\hat{K}_n(r)r$ constant. We then define

$$\hat{K}_{\varphi,n} = \hat{K}_n(r)r,$$

from which it follows that

$$K_n(x,r) = \frac{1}{r}\hat{K}_{\varphi,n} \sin(u_n x).$$

This makes the source current inversely proportional to the radius, as naturally should be for a solenoidal current sheet.

Solution formulas for the magnetic potential

General linear magnetic material

The solution formula for the problem including linear magnetic materials with permeabilities μ_1 and μ_2, given as

$$A^r(r,\varphi,z) = \begin{cases} \sum_n \dfrac{\mu_2(1+\eta)}{u_n} \dfrac{\cosh(u_n(z_2-z))\cosh(u_n z_1)}{\sinh(u_n z_2) + \eta \sinh(u_n(z_2-2z_1))} K_n(r\varphi, r), \; z_1 < z \leq z_2 \\ \sum_n \dfrac{\mu_2(1+\eta)}{u_n} \dfrac{\cosh(u_n(z_2-z_1))\cosh(u_n z)}{\sinh(u_n z_2) + \eta \sinh(u_n(z_2-2z_1))} K_n(r\varphi, r), \; 0 \leq z \leq z_1 \end{cases}$$

where

$$\eta = \frac{\mu_1 - \mu_2}{\mu_1 + \mu_2},$$

can be derived starting from the following expressions:

$$A_1^r(r,\varphi,z) = \sum_n \frac{\alpha_{1,n}}{u_n} \cosh(u_n z) K_n(r\varphi, r)$$

for the potential below the sheet, and

$$A_2^r(r,\varphi,z) = \sum_n \frac{\alpha_{2,n}}{u_n} \cosh(u_n(z_2-z)) K_n(r\varphi, r)$$

for the potential above the sheet.

It is straightforward to see that the solution fulfills the governing PDE

$$\Delta_{\varphi z}^{\nu} A^r = \partial_\varphi \nu \frac{1}{r} \partial_\varphi A^r + \partial_z \nu r \partial_z A^r = 0,$$

and the boundary and interface conditions

$$\begin{cases} H^{\varphi} = 0, & \text{if } z = 0 \text{ or } z = z_2, \\ H_2^{\varphi} - H_1^{\varphi} = -K,\ H_2^z = H_1^z, & \text{if } z = z_1, \end{cases}$$

where

$$H_i^{\varphi} = \frac{1}{\mu}\partial_z A_i^r \quad \text{and} \quad H_i^z = -\frac{1}{\mu r}\partial_{\varphi} A_i^r,\ i \in \{1, 2\}.$$

Details on the computation models

In the computations involving the magnetic potential, the term z refers to the position of the computation line, and the term z_n to position of the selected neutral line.

The current sheets were constructed such that a horizontal line was divided into 20 segments, for which an average value of the current was imposed. This additional discretization was done due to software limitations.

Basic model

The results depicted in Figure 7.2 were computed using the data given in Table B.1.

Table B.1: *Example dimensions and driving terms for the basic model.*

Dimensions	$[m]$	Currents	$[A]$
z	1.45	$\hat{K}_{\varphi,1}$	100
z_n	1.0		
z_1	1.0		
z_2	2.0		
r	1.0		

Different permeabilities

For different permeabilities, we imposed the relative permeabilities $\mu_{1,r} = 1$ and $\mu_{2,r} = 100$. The results depicted in Figure 7.3 were then computed using the data given in Table B.2.

Table B.2: *Example dimensions and driving terms for the basic model with different permeabilities.*

Dimensions	$[m]$	Currents	$[A]$
z	1.45	$\hat{K}_{\varphi,1}$	100
z_n	1.0		
z_1	1.0		
z_2	2.0		
r	1.5		

Nonlinear magnetic material

The translational model used in testing the nonlinear magnetic material is depicted in Figure B.1. The dashed line at y_{12} marks the division of the nonlinear region for the rotational model. For the nonlinear properties, we used the material data of the

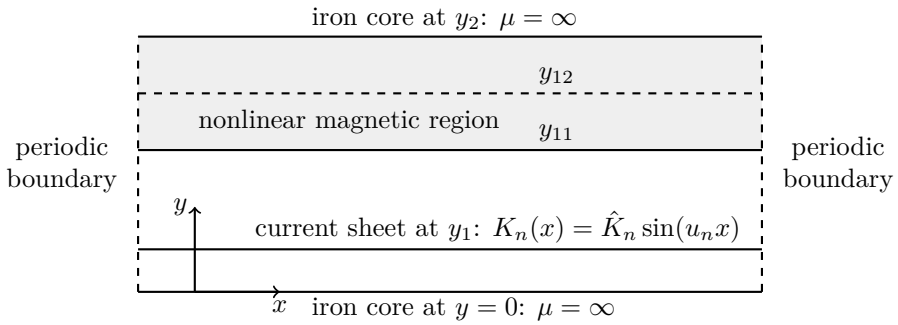

Figure B.1: *Test model for nonlinear magnetic materials based on the basic model.*

carbon steel 1010 SAE readily available in Flux® software. The results depicted in Figure 7.4 were then computed using the data given in Table B.3.

Table B.3: *Example dimensions and driving terms for the basic model including a nonlinear magnetic region.*

Dimensions	$[mm]$	Currents	$[A]$
z	2.5	$\hat{K}_{\varphi,1}$	100
z_n	1.0		
z_1	1.0		
z_{11}	2.0		
z_{12}	3.5		
z_2	5.0		
r	1.0		

Permanent magnets

For the permanent magnets, we imposed remanence flux density $M = 1.2\,T$ and relative permeability $\mu_r = 1.05$; the setting mimics neodymium magnets. The interface φ_1 between the magnets was posed on the middle of the domain, that is, $\varphi_1 = \pi/4$. The results depicted in Figure 7.6 were then computed using the data given in Table B.4.

Table B.4: *Example dimensions for the model including permanent magnets.*

Dimensions $[mm]$			
z	25	z_{11}	20
z_n	10	z_{12}	35
z_2	50	r	500

Torque

For the torque computation, the current sheets were divided into 40 segments instead of the 20 used for other computations. The results depicted in Table 7.1 were then computed using the data given in Table B.5.

The overall torque values were integrated by calculating the average of the torque density values; in this setting, the domain is given radial boundaries $r_0 = 0$ and $r_1 = 2.0$, and then the torque density values in Table 7.1 yield the average torque for radial intervals $(0, 1.0)$, $(0.5, 1.5)$ and $(1.0, 2.0)$. Similar approach is later employed in simulations concerning an actual KONE machine model.

Table B.5: *Example dimensions and driving terms for the torque computation.*

Dimensions	$[m]$	Currents	$[A]$
z_n	0.5	$\hat{K}_{\varphi,1}$	2000
z_{j1}	0.1	$\hat{J}_{\varphi,1}$	5000
z_{j2}	0.15		
z_2	0.2		

Ohmic losses

The model used to test conductive regions was similar to that of the nonlinear magnetic materials, as depicted in Figure B.1 for the translational geometry. The nonlinear magnetic region was replaced by a conductive region; the line at y_{12} marks the division for the rotational model. The conductive region was given the conductivity of 1.0×10^7 S/m, mimicking the conductive properties of iron. The current sheet was driven by a circuit similar to an actual KONE machine (see below), with the time step of 0.5×10^{-3} seconds. The results depicted in Figure 7.8 were then computed using the data given in Table B.6.

Table B.6: *Example dimensions for the basic model including a conductive region.*

Dimensions $[m]$			
z_n	0.5	z_{11}	0.15
z_1	0.1	z_{12}	0.175
z_2	0.2	r	1.0

The KONE model

All results of the KONE machine simulations reflect the behaviour of the computation quantities per one period of the source current, where the period was chosen such that the transient behaviour has sufficiently decreased. With the supply frequency of 65.53 Hz, the length of the period was approximately 0.0153 seconds with the time step being roughly 8.5×10^{-5} seconds.

The stator circuit comprises of a symmetric three-phase current-driven system. The equation of the rotor motion is not taken into account—the motion is modelled with a prescribed angular velocity of 20.6 rad/s, approximately. Newton-Rhapson method is employed for treating the nonlinearity of the magnetic materials.